

Building Integrated Photovoltaic/Thermal Collector for Arctic Residential Applications

Daniel Baril

A Thesis

in

The Department

of

Building, Civil and Environmental Engineering

Presented in Partial Fulfillment of the Requirements
for the Degree of Master of Applied Science (Building Engineering) at
Concordia University
Montreal, Quebec, Canada

December 2021

© Daniel Baril 2021

CONCORDIA UNIVERSITY
School of Graduate Studies

This is to certify that the thesis prepared

By: Daniel Baril

Entitled: Building Integrated Photovoltaic/Thermal Collector for Arctic Residential Applications

and submitted in partial fulfillment of the requirements for the degree of

Master of Applied Science (Building Engineering)

complies with the regulations of the University and meets the accepted standards with respect to the originality and quality.

Signed by the final Examining Committee:

_____ Chair
Dr. Radu Zmeureamu

_____ Examiner
Dr. Bruno Lee

_____ Thesis Co-Supervisor
Dr. Andreas Athienitis

_____ Thesis Co-Supervisor
Dr. Hua Ge

Approved by _____

Dr. Mazdak Nik-Bakht Graduate Program Director

December 07, 2021 _____

Dr. Mourad Debbabi, Dean

Gina Cody School of Engineering and Computer Science

Abstract

Building Integrated Photovoltaic/Thermal Collector for Arctic Residential Applications

Daniel Baril

This thesis investigated the performance of an open loop air-based building integrated photovoltaic/thermal collector (BIPV/T) designed to preheat ERV supply air and to generate electricity. Energy Recovery Ventilators (ERV) have proven successful in cold climates, but in the extreme cold of the Arctic, frequent frosting and defrosting cycles reduce their effectiveness and increase the energy consumption. Thus, by integrating with BIPV/T which preheats the ventilation air, this problem can be reduced while also generating electricity. A finite difference model of the BIPV/T system integrated in a typical potential application was simulated in MATLAB using local weather data and indoor fresh air requirements to obtain system outputs. BIPV/T design parameters such as the tilt angle, and cavity depth were varied, with consideration of using nominal lumber sizes and ease of construction for improved implementation for Arctic residential applications. It was seen that the BIPV/T was able to increase the fresh air temperature supplied to the ERV up to 16°C and helped to reduce the defrosting time up to 7 hours per day. The 40m² BIPV/T array also produced a considerable amount of electricity up to 33kWh/day and 7.5kWh/day of thermal energy was recovered.

Simulated electrical and thermal energy generated by the BIPV/T system are then compared with the measured energy usage data from a high-performance northern housing prototype located in Nunavik, Quebec. With this comparison the net energy usage is obtained along with the energy savings and was seen to reduce the annual electricity costs over 30% as well as approximately 5.5% of the total energy costs.

Acknowledgements

To start with I would like to thank the late Dr. Paul Fazio for encouraging me to pursue graduate studies when I was at that juncture in my engineering career. The opportunity to study under his tutelage was a great opportunity to learn from one of the pioneers in building engineering and helped provide a strong base, which I draw from on a regular basis. I would also like to thank Jeff Armstrong for getting my foot in the field monitoring door, Dr. Hua Ge for her help and support as well as Dr. Andreas Athienitis for the opportunity to study under his supervision. Thank you to Dr. Jiwu Rao for working on all the technical issues that no one else wants to, Dr. Ahmad “Rami” Kayello for being a wealth of knowledge, Yichao Chen for getting me interested in Arctic BIPV/T, Kativik Ilisarnilliriniq for their support, Shun-Hui Yang at Makivik Construction for introducing me to the Quaqtq pilot project, Marie-Pier Breton at SHQ for introducing me to the ULaval team, Dr. Louis Gosselin for allowing me to benefit from their extensive field monitoring project, Jean Rouleau for the data tables, Dr. Abhishek Gaur for the weather files, Dr. Jose Candanedo for getting me back up to speed after taking a break from academia, Dr. Stratos Rounis for his experience with BIPV/T, Collin Beattie for bringing HRV frosting to my awareness, Dr. Leon Wang & Dr. Radu Zmeureanu for their guidance during the Overheating project, my wife Tina for feeding me, and thank you for your camaraderie to the team in EV16.117 and EV1.625, Dr. Lin Wang, Mary Li Ma, Danlin Hou, Zihan Xie, Dr. Chang Shu, Fuad Baba, Jing Li, Kai Ye, Anna Maria Sigounis, John Hill, Erin Gaucher-Loksts, Dr. Costa Kapsis, NSERC, Jenny Drapeau, and anyone else that I cited in the references or have worked on developing BIPV/T helping to move the needle in the right direction.

Table of Contents

List of Figures	ix
List of Tables	xiii
Nomenclature	xiv
1. Introduction	1
1.1 Motivation.....	1
1.2 BIPV/T for Arctic Residential Applications.....	3
1.3 Objectives.....	4
1.4 Thesis Outline.....	4
2. Literature Review	6
2.1 Arctic Climate Change.....	6
2.2 Global Arctic Green Building Research	7
2.3 Canadian Arctic Green Building Research	11
2.4 Arctic Solar Application	11
2.4.1 Canadian Arctic Building Applied Photovoltaics (BAPV)	11
2.5 KOTT SIP House.....	15
2.6 Northern Quebec Building Studies	16
2.6.1 Northern Housing Prototype.....	16
2.6.1.1 Passive House Concepts.....	18
2.6.1.2 Building Envelope	18
2.6.1.3 Mechanical Systems.....	20
2.6.1.4 Initial Energy Analysis.....	21
2.6.1.5 Field Monitoring.....	22
2.6.1.6 Initial Data Analysis	23
2.6.1.7 Lessons Learned	24
2.6.2 Nunavik Clean Energy, BAPV & PV	25
2.7 BAPV vs PV.....	28
2.8 BIPV/T	29
2.8.1 BIPV/T Categories	30
2.8.2 Closed Loop Water/Glycol Based Systems vs Open Loop Air Systems	30

2.8.3 BIPV/T Projects	32
2.8.4 Arctic BIPV/T	35
2.9 Arctic ERV/HRV	36
3. Methodology	40
3.1 Design of an Integrated BIPV/T System.....	41
3.2 Thermal Network Model.....	43
3.2.1 Photovoltaic Specifications.....	46
3.2.2 Control Volumes	47
3.2.3 Air Properties	47
3.2.4 Convective Heat Transfer Coefficients	48
3.3 Model Validation.....	49
3.3.1 Model Calibration	52
3.3.1.1 Model Convective Heat Transfer Coefficients (CHTC).....	52
3.3.1.2 Sky Temperature.....	53
3.3.1.3 Emissivity Values	54
3.3.2 Model Validation Results	54
3.4 Weather Data.....	56
3.4.1 Dew Point Temperature, Dry Bulb Temperature, Wind Speed	56
3.4.2 Sky Temperature	59
3.4.3 Solar Irradiance	61
3.4.3.1 Clear Sky Irradiance	61
3.4.3.2 Cloud Cover.....	67
3.4.3.3 Canadian Weather Energy and Engineering Datasets	69
3.4.4 Ground Reflectance.....	74
3.4.4.1 Snow Cover Period	74
3.4.4.2 Reflectivity	75
3.4.5 Peak Surface Irradiance	76
3.5 Ventilation Rate Requirements.....	77
3.6 BIPV/T Configuration	78
3.6.1 Tilt Angle.....	78
3.6.2 Cavity Depth	79
3.7 Fan Energy Usage.....	81

3.7.1 Cavity Pressure Losses	82
3.7.2 Ducting Pressure Losses	83
3.7.3 Fan Power	85
3.7.4 Discussion	86
3.8 Methodology Conclusion	87
4. Simulation Results	89
4.1 BIPV/T Performance Analysis	89
4.1.1 Outlet Temperature	90
4.1.2 Maximum Outlet Temperatures with Extreme Ambient Temperatures	92
4.2 ERV Frosting Reductions	95
4.3 PV Efficiency Improvements	98
4.3.1 Electrical Efficiency	98
4.3.2 Thermal Efficiency	101
4.4 Energy Generation	104
4.4.1 Electrical Energy Generation	105
4.4.2 Thermal Energy Generation	106
4.4.3 Total Energy Generation	108
4.5 Discussion	109
5. Northern Housing Prototype Data Analysis	110
5.1 Hydro Quebec Domestic Rates for Off-Grid Systems	110
5.2 Daily Energy Usage	111
5.2.1 Electrical Energy	113
5.3 NHP Coupled with BIPV/T	116
5.3.1 Gross and Net Electrical Energy	116
5.3.2 Electrical Energy Costs and Savings	120
5.3.3 Thermal Energy	122
5.3.4 Gross and Net Thermal Energy	122
5.3.5 Total Energy	124
5.4 Indoor Air Quality CO ₂	125
6. Conclusions	127
6.1 Contributions	130
6.1.1 Publications	131

6.2 Future Additional Work.....	131
References.....	133
Appendix A Air Properties.....	139
Appendix B ASHRAE standard 62.2 Fresh Air Requirements Calculations.....	141
Appendix C MATLAB Code BIPV/T	142

List of Figures

Figure 1.1 Nunavik housing in 1950s & 60s	1
Figure 1.2 Fuel spills and leakage.....	2
Figure 2.1 Arctic floristic boundaries	6
Figure 2.2 Pilot project in Murmansk northern Russia 69°N	9
Figure 2.3 Low energy house in Sisimuit, Greenland.....	9
Figure 2.4 Sweden’s northern most passive house.	10
Figure 2.5 Kugluktuk’s diesel power plant to be replaced with new hybrid solar/diesel plant.....	12
Figure 2.6 Gjoa Haven solar and wind powered green house and research station	13
Figure 2.7 Solar array being applied to the façade of the Clyde River community center	14
Figure 2.8 Pond Inlet PV system install on roof of building to avoid vandalism.....	14
Figure 2.9 Kott SIP house located in Iqaluit, Nunavut	15
Figure 2.10 J2.2 Nunavik social housing duplex.....	17
Figure 2.11 Nunavik social housing built in 1980s & 90s	17
Figure 2.12 NHP south façade.....	19
Figure 2.13 NHP north façade	19
Figure 2.14 NHP floor plan.....	20
Figure 2.15 NHP subfloor ventilation ducts.....	21
Figure 2.16 NHP mechanical system could be difficult to maintain locally.....	24
Figure 2.17 Kuujjuaq, QC LEED certified airport with 6.3kW PV array.....	25
Figure 2.18 Laval University’s Centre for Northern Studies	26
Figure 2.19 Makivik head office and Nunavik research center PV pilot project	27
Figure 2.20 Quaqaq Hydro-Quebec solar project.....	27
Figure 2.21 Kuujjuaq solar/ geothermal pool heater.....	28

Figure 2.22 Unglazed transpired collector concept installed at Concordia University	33
Figure 2.23 Varennes Library.....	34
Figure 2.24 BIPV/T schematic	34
Figure 3.1 Vertical furring strips presently used on standard Nunavik housing construction.	41
Figure 3.2 South façade of duplex with 40m ² BIPV/T array.	42
Figure 3.4 Control volume of the BIPV/T cavity thermal network.....	44
Figure 3.5 Schematic of BIPV/T experimental setup	50
Figure 3.6 Experimental cavity dimensions and materials.....	51
Figure 3.7 Model calibration using 1.5m/s cavity air velocity with simulated & experimental data, with 20°C ambient temperature, 0.0228 m ³ /s air flow, and 1080W/m ² solar irradiance.	53
Figure 3.8 Outlet temperature using simulated & experimental data, with 0.26m/s cavity air velocity, 20°C ambient temperature, 0.0228 m ³ /s air flow, and 1080W/m ² solar irradiance.....	55
Figure 3.9 2017 Quaqtq monthly hourly average dew point temperature [°C]	57
Figure 3.10 2017 Quaqtq monthly hourly average dry bulb temperature [°C].....	58
Figure 3.11 2017 Quaqtq monthly hourly average wind speed [m/s].....	59
Figure 3.12 2017 Quaqtq monthly hourly average sky temperature [°C]	60
Figure 3.13 Quaqtq clear sky peak south facing surface irradiance for three surface tilt angles.	65
Figure 3.14 Quaqtq average monthly hourly clear sky 90° surface irradiance 0.7 ρ [W/m ²]	66
Figure 3.15 Quaqtq average monthly hourly 90° surface irradiance using clear sky with 0.7 snow reflectance with cloud cover values [W/m ²].....	68
Figure 3.16 Weather stations of Iqaluit 63°N, Quaqtq 61°N & Kuujjuaq 58°N	70
Figure 3.17 CWEEDS average hourly 90° south facing surface irradiance for Kuujjuaq [W/m ²]	71
Figure 3.18 CWEEDS average hourly 90° south facing surface irradiance for Iqaluit [W/m ²]....	72
Figure 3.19 2017 CWEEDS Quaqtq interpolated 90° south facing surface irradiance [W/m ²] with snow reflectance ρ=0.7.....	74

Figure 3.20 Peak south facing 90° surface irradiance for all irradiance calculation methods.	76
Figure 3.21 BIPV/T outlet air & ambient temperature at 150CFM with three tilt angles at clear sky daily peak irradiance for 21 st day each month, with corresponding ambient temperature.	79
Figure 3.22 Outlet temperature and channel air velocity vs. air flow rate for three cavity depths under outdoor condition: 960W/m ² irradiance, -15°C ambient temperature and 6m/s wind velocity.	80
Figure 3.23 Proposed ducting system to supply forced air to ERV. Elevation drawing.....	81
Figure 3.24 Proposed ducting system to supply forced air to ERV. Section drawing.....	82
Figure 3.25 Plan view of ducting system.	84
Figure 4.1 Maximum outlet temperature increase at peak irradiance using 0.70 and 0.95 snow reflectance values.	90
Figure 4.2 Outlet temperature at peak irradiance using 0.70 and 0.95 snow reflectance values along with the monthly average ambient temperature at peak irradiance.	92
Figure 4.3 Outlet temperatures for 20 year monthly maximum ambient temperature at monthly averaged peak irradiance.	93
Figure 4.4 Outlet temp. reduction & additional heat recovered with increased air flow compared to 150CFM flow rate, for 20 year monthly maximum ambient temperature at monthly averaged peak irradiance.	94
Figure 4.5 Hours/day outlet temperature higher than ambient temperature and volume of pre-heated fresh air per m ² of floor area.	97
Figure 4.6 Electrical efficiencies with range of air flow rates at peak irradiance with corresponding ambient temperature using averaged monthly weather data for each hour of day.	99
Figure 4.7 PV electrical efficiency improvements at peak irradiance with 2 air flow rates.	100
Figure 4.8 Thermal efficiency for range of flow rates with peak surface irradiance and corresponding ambient temperature.	101
Figure 4.9 BIPV/T efficiencies using 150 CFM air flow rate.	102
Figure 4.10 BIPV/T efficiency for range of flow rates.	104

Figure 4.11 Monthly average electrical energy generated per day using 150 CFM air flow rate.
105

Figure 4.12 Monthly average thermal energy recovered per day using 150 CFM air flow rate. 106

Figure 4.13 Monthly average thermal energy recovered per day using 150CFM and 1500CFM
airflow rates. 107

Figure 4.14 Total energy generated per day using 150 CFM air flow rate. 108

Figure 5.1 Daily energy usage normalized with living area and total usage. 112

Figure 5.2 Daily electrical energy breakdown by housing unit. 113

Figure 5.3 Daily electrical energy usage duration curves per housing unit. 115

Figure 5.4 2017 daily gross and net electrical loads using BIPV/T simulated electrical energy
generation. 117

Figure 5.5 Total building electrical load and simulated PV generation. 118

Figure 5.6 Gross and net electrical loads with BIPV/T generation. 119

Figure 5.7 Daily gross and net electrical energy duration curves. 120

Figure 5.8 Indoor air CO₂ levels duration curve. 125

List of Tables

Table 2.1 Nunavik housing exterior wall sections.....	18
Table 2.2 NHP parameters measured and sampling frequency.....	23
Table 3.1 Model calibration results & validation criteria	55
Table 3.2 Climate correction factor table.....	63
Table 3.3 Pressure losses and fan power for air flow range of 150-1500CFM.....	85
Table 4.1 Maximum Quaqtqaq ambient temperature [°C] over past 20 years.....	92
Table 4.2 ERV frosting reductions with BIPV/T pre-heated air.	96
Table 4.3 BIPV/T pre-heated fresh air supplied to ERV.	97
Table 5.1 Annual gross and net electrical loads with corresponding costs.....	121
Table 5.2 Gross and net thermal loads with correspond costs.....	123
Table 5.3 Breakdown of annual gross and net energy.	124

Nomenclature

List of Symbols

A -Altitude above sea level, km	\dot{m} -Mass flow rate, kg/s
$A_{BIPV/T}$ -BIPV/T collector surface area, m ²	m_i -Measured value
A_{CV} -Control volume surface area, m ²	n -Number of experimental data points
A_{pv} -PV surface area, m ²	Nu_b -Cavity back side Nusselt number
c -Fraction of time ground assumed over one inch snow cover, 0 or 1	Nu_f -Cavity front side Nusselt number
C_o -Loss coefficient	P_{elec} -Electrical energy generated, W
C_p -Specific heat at constant pressure, kJ/kgK	Pr -Prandtl number
C_{p_air} -Specific heat of air, kJ/kgK	P_v -Velocity head, Pa
D -Round duct cross sectional diameter, m	Q_{heat} - Heating load, kW
D_h -Hydraulic diameter, m	q_{sky} -Heat losses to sky, W/m ²
e -Emissivity	R_{hb} -BIPV/T back cavity surface convective boundary layer thermal resistance, m ² K/W
F - Fuel consumption, L	R_{hf} –PV inner surface convective boundary layer thermal resistance, m ² K/W
f -Friction factor	R_{ho} –Exterior convective boundary layer thermal resistance, m ² K/W
G – Incident irradiance, W/m ²	R_{hr} –Cavity air radiative heat transfer thermal resistance, m ² K/W
g -Gravitational acceleration, m/s ²	R_{ins} -Exterior wall thermal resistance, m ² K/W
H -Heating value of fuel, kWh/L	s_i -Simulated value
ha- Hour angle, °	
hb -Cavity back surface convective heat transfer coefficient, W/(m ² K)	

hf - Cavity front surface convective heat transfer coefficient, $W/(m^2K)$

I - Beam normal irradiance, W/m^2

I_0 - Clear sky beam normal irradiance, W/m^2

I_{bn} - Direct beam normal radiation, W/m^2

I_{bs} -Beam surface irradiance, W/m^2

I_{dh} - Diffused horizontal radiation, W/m^2

I_{ds} -Diffused surface irradiance, W/m^2

I_{on} - Extraterrestrial solar radiation, W/m^2

I_{rs} -Reflected surface irradiance, W/m^2

I_{sc} - Solar constant, W/m^2

I_{st} -Total surface irradiance, W/m^2

L -Duct section length, m

L_{CV} -Control volume length, m

l_f -Duct head loss, m

M - Volume flow rate, m^3/s

t -Hours from midnight, hour

T_a - Dry bulb temperature, $^{\circ}C$

T_B - Cavity back surface temperature, $^{\circ}C$

T_{Base} - Cavity back surface temperature, $^{\circ}C$

T_{dp} -Dew point temperature, $^{\circ}C$

T_{ext} - Outdoor Dry Bulb Temperature, $^{\circ}C$

T_{in} - Indoor temperature, $^{\circ}C$

T_{inlet} -Control volume inlet temperature, $^{\circ}C$

T_{ma} -Cavity air mass temperature, $^{\circ}C$

T_{outlet} -Control volume outlet temperature, $^{\circ}C$

T_{pv} -PV Module temperature, $^{\circ}C$

T_{sky} -Sky Temperature, $^{\circ}C$

T_{STC} -Standard test condition temperature, $^{\circ}C$

\bar{V} – Duct section average velocity, m/s

W_{ch} -Width of channel, m

z -Zenith angle, $^{\circ}$

Greek Letters

α - Solar altitude, °	η_{pv} - PV efficiency, %
α_{PV} –Absorptance of PV	η_{STC} -PV STC efficiency, %
β - Temperature coefficient, %/°C	$\eta_{thermal}$ -Thermal efficiency, %
β -Tilt angle, °	θ - Angle of incident, °
γ - Solar surface azimuth, °	k - Thermal conductivity, W/mK
ΔP - Pressure losses, Pa	ν - Kinematic viscosity, m ² /s
ΔP_o -Fittings dynamic losses, Pa	ξ_1 -Entrance loss friction factor
ΔP_{cavity} - Cavity straight portion pressure losses, Pa	ξ_2 -Exit loss friction factor
ΔP_{drive} -Total cavity pressure losses, Pa	ξ_{elbow} - Elbow friction loss factor
$\Delta P_{entrance}$ -Cavity entrance pressure losses, Pa	ρ - Air density, kg/m ³
ΔP_{exit} -Cavity exit pressure losses, Pa	ρ –Reflectance
δ -Declination angle, °	σ - Stefan-Boltzman constant, W/(m ² K ⁴)
η_{boiler} -Boiler efficiency, %	τ_b - Direct beam transmittance
η_{fan} - Fan efficiency, %	τ_{ah} -Horizontal diffused transmittance
	φ - Solar azimuth angle, °
	Ψ - Surface azimuth angle, °

List of Acronyms

AC-Alternating electrical current	IAQ- Indoor Air Quality
ACH50- Air Changes per Hour at 50 Pascals	JMSB-John Molson School of Business
AMAP-Arctic Monitoring and Assessment Program	LEED -Leadership in Energy and Environmental Design
ASHRAE-American Society for Heating Refrigeration and Air-Conditioning Engineering	LAT-latitude
AST- Apparent solar time	LFP- Lithium Iron Phosphate
BAPV- Building Applied Photovoltaics	LON- longitude
BIPV/T - Building Integrated Photovoltaic/Thermal Collector	Low-e – Low Emissivity
CanPhi- Canadian Passive House Institute	LST- local standard time
CFM-Cubic feet per minute	MATLAB- MATrix LABoratory
CHTC-Convective Heat Transfer Coefficient	NHP-Northern House Prototype
CO ₂ -Carbon Dioxide	N- North
COP- Coefficient of Performance	NMBE-Normalized Mean Bias Error
CV-RMSE - Coefficient of Variation- Root Mean Square Error	NRC-National Research Council of Canada
CWEC- Canadian Weather Year for Energy Calculations	NRCan-Natural Resources Canada
CWEEDS- Canadian Weather Energy and Engineering Datasets	NU-Nunavut
DC-Direct electrical current	NWT-Northwest Territories
DN-Domestic North	OSB- Orientated Strand Board
E-East	PHPP- Passive House Planning Package
ECCC- Environment and Climate Change Canada	PV- Photovoltaic
EPS-Extruded Polystyrene	QC – Québec
	RH/T – Relative Humidity and Temperature
	RSI- Resistance System International
	Re-Reynolds Number
	SHQ- Société de Habitation Québec
	SIP- Structurally Insulated Panel

ERV - Energy Recovery Ventilator

ET- Equation of time

FTP- File Transfer Protocol

GrAB- Green Arctic Buildings

HRV- Heat Recovery Ventilator

HVAC- heating, ventilation, and air conditioning

S-South

SPN- Société du Plan Nord

STC-Standard Test Conditions

SUNY- State University of New York

UV- Ultraviolet Radiation

W-West

XPS Extruded polystyrene

1. Introduction

1.1 Motivation

The northern villages of Canada have seen massive change over the last 60 years and even though substantial technological improvements have been made to the everyday life, lingering issues such as insufficient housing and energy dependence on fossil fuels remain as major challenges to overcome (Bolton, 2011) (Perreault et al., 2020).



(a) Nunavik igloo in 1950's (Knight, 1950s) (b) Nunavik housing in 1965 (Pearson, 1965)

Figure 1.1 Nunavik housing in 1950s & 60s

Nearly all the electrical and heating energy production in Nunavik is produced with fossil fuels, consuming over 170 million liters of petroleum each year (Plan Nunavik, 2011). This not only leads to high energy costs but also results in many environmental problems such as leaks from heating systems as seen in Figure 1.2 (a), leaks from storage containers as seen in Figure 1.2 (b) & 1.2 (c) and fuel spills during transportation, as well as the associated greenhouse gas emissions.



(a) Fuel leakage from home heating system. (Photo taken by author)



(b) Fuel spill from residential storage tank. (Photo taken by Edua Jones)



(c) Fuel leakage from storage drums. (Photo taken by author)

Figure 1.2 Fuel spills and leakage

With a lack of skilled labor and long lead times to receive repair material, heating system failures are also a common occurrence, increasing the risk of plumbing system freezing, leading to costly repairs and major disruptions to the occupants. With this energy dependence on fossil fuels in the northern villages of Canada it is vital to seek ways to reduce the fuel consumption to lower the environmental impacts, improve resiliency in emergency situations and to avoid high peak energy costs.

1.2 BIPV/T for Arctic Residential Applications

On top of the already long list of obstacles in the northern housing industry, the need for healthy indoor air quality is now more important than ever. With an increase in the amount of tele-working from home, quarantine periods and public gatherings being restricted, people are spending an even larger portion of their time indoors at home, further increasing the need for fresh air (Abouleish, 2020). As well, residential energy usage during daytime hours were seen by Rouleau et al., (2021) to have risen during the COVID-19 lockdown periods and are expected to remain at these levels with tele-working becoming more of the norm. Strategies to ensure a steady supply of fresh air while at the same time reducing the net energy usage are vital to a sustainable future in the North. In cold climates energy recovery ventilators (ERV) have been shown to provide adequate fresh air while reducing energy usage (Garber-Slaght & Stevens, 2016), but as seen from Beattie et al., (2018) in the extreme cold climate of the Arctic, frequent frosting/defrosting during the many cold months greatly reduces the effectiveness and reliability.

In this study the potential of using a building integrated photovoltaic/thermal collector (BIPV/T) to pre-heat fresh air before it enters an ERV to mitigate ERV frosting is studied through simulations.

As well, simulated electrical and thermal energy produced, with local weather data used as inputs, is analyzed, and compared with monitored energy data from a prototype high performance residential duplex located in the northern village of Quaqtaq, QC. From this, the improvements in fresh air provisions and net energy usage of a high-performance residential duplex are estimated.

1.3 Objectives

The following points are the main objectives of the thesis study:

- To adapt an air based BIPV/T systems designed for northern housing, keeping in mind the ease of construction and maintenance.
- To simulate the performance of a BIPV/T system using local weather data for an Arctic community, in order to obtain the outlet air temperature increase as well as the electrical and thermal energy generation.
- To analyze the effectiveness of the BIPV/T to pre-heated air to reduce the ERV core frosting and to increase the fresh air supply, while maximizing the electricity and thermal energy generation.
- To analyze the net electricity and thermal energy usage of an Arctic residential duplex when combining simulated energy generation with monitored energy usage data.

1.4 Thesis Outline

Chapter 2 provides a literature review starting with climate change effects in the Arctic. Followed by Arctic green building projects in northern Europe, Canada, and Quebec, along with recent solar projects in Canada. The next section presents a review of BIPV/T and concludes with HRV/ERV studies in extreme cold climates.

Chapter 3 presents the modeling methodology, including the PV building integration, simulation model numerical method, model calibration/validation, weather data preparation, multiple BIPV/T configurations to obtain the highest outlet temperature, and the fan power usage calculations.

Chapter 4 presents the simulation results for the BIPV/T, when using local weather data. Specifically, the performance of the BIPV/T to pre-heat air to mitigate ERV frosting, as well as the electricity and thermal energy generation. The chapter concludes with a simulation of an alternative BIPV/T configuration to recover an increased amount of heat while keeping a sufficiently high outlet temperature.

Chapter 5 provides the analysis of a northern housing prototype field monitored energy consumption. As well as an analysis of the building's net energy when the simulated energy generated from the BIPV/T is coupled with the monitored energy usage.

Chapter 6 provides the conclusions and contributions of the study, as well as suggested future research to further the study.

2. Literature Review

2.1 Arctic Climate Change

The Arctic is described as either the regions north of the 10°C July isotherm, areas above the 66°N latitude Arctic circle or above the treeline (AMAP, 1998). These regions can be seen in Figure 2.1, with the community of Quaqtqaq, QC, located in the Low Arctic region. Characteristics of Arctic regions usually consist of large seasonal variations in solar irradiance, solar altitude, precipitation, and temperatures. As well as having permanently frozen ground better known as permafrost. With an increase in global temperatures, the Arctic is particularly vulnerable due to the melting of the permafrost, which releases carbon dioxide and methane further adding to the temperature increase (AMAP, 2017). Siron, et al., (2016) highlighted that with the heightened effects of climate change in the Arctic, adaption to the impacts is important to mitigate the risks to this sensitive area.

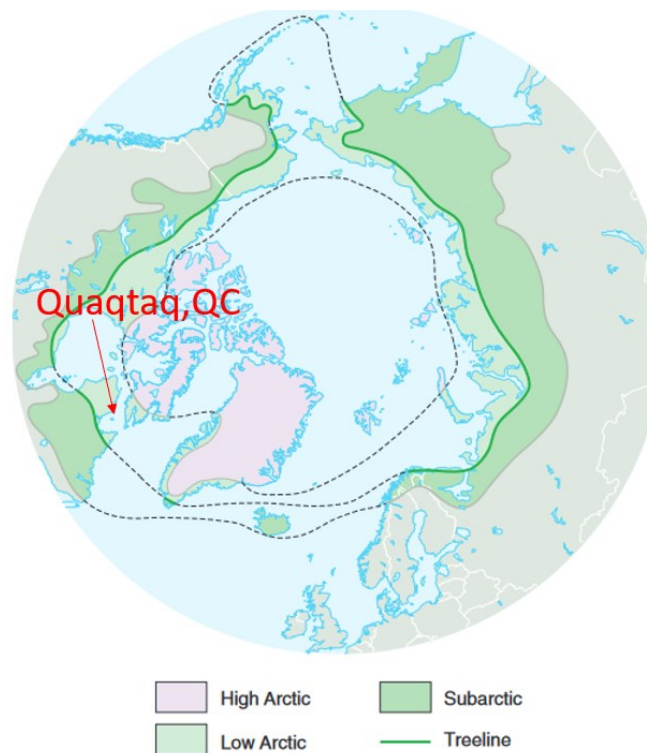


Figure 2.1 Arctic floristic boundaries (AMAP, 1998)

2.2 Global Arctic Green Building Research

Several countries have Arctic regions within their borders and have created the Arctic Council which consists of the countries of Canada, Russia, Finland, Denmark, Norway, Sweden, United States, and Iceland. The council works to maintain and create new initiatives to promote environmental protection in the Arctic and each country has set up guidelines and policies according to their needs.

Specific initiatives aim to improve the building construction industry and to create environmental, economic, and social benefits. Environmental benefits are obtained through conservation of energy, water, material, and land. By using natural ventilation and daylighting, coupled with renewable resources and high-performance building envelopes, energy usage and greenhouse gas emissions can be greatly reduced (Ding et al., 2013).

Economic benefits occur from the lowered energy usage resulting in lower operating and maintenance costs. However, there are generally higher initial material costs, certifications fees, and technological costs to meet the green building standards. Therefore, it is vital to optimize building material amounts to achieve long term costs savings. Incorporated with renewable energy usage, the environmental impacts can be greatly reduced.

The following key points mentioned in the literature review by Ravasio et al., (2020) were vital to green building design practices in Arctic climates:

- A high-performance building envelope to reduce air infiltration and heat loss.
- An energy efficient ventilation system, such as HRVs and ERVs.

- Renewable energy generation such as PV, and on-site generation such as heat pumps.
- Smart energy control systems, which can provide feed back to the users for improved management of room temperatures as well as water and energy usage.
- Locally produced environmentally friendly building products.

Some of the recent European projects include the Green Arctic Buildings (GrAB) pilot project consisting of collaborations from four Arctic countries, Sweden, Norway, Russia and Finland. With objectives to research sustainable construction to improve the buildings in the Arctic region with social, environmental, and economic issues at the forefront (Ravasio et al., 2020).

Some of their project included a pilot project in Murmansk northern Russia 69°N, and Petrozavodsk, Russia 61°N where two identical prototype houses have been constructed to compare green technologies in a sub-arctic climate versus a location below the sub-arctic, with the prototype seen in Figure 2.2. An alternative wall construction using locally produced wood chips sandwiched between layer of logs are being compared with a standard mineral wool insulated wall. Extensive field monitoring equipment was installed during construction to monitor the hygrothermal and energy performance. Initial studies have shown that that mineral wool wall was more effective than the double log wall at reducing energy usage (Buryachenko et al., 2020).



Figure 2.2 Pilot project in Murmansk northern Russia 69°N (Buryachenko et al., 2020).

In Sisimuit, Greenland 66°N, a low energy house, seen in Figure 2.3, uses a passive solar design with an HRV and solar domestic hot water heating and was able to obtain a normalized net energy consumption of 140kWh/m², which is well below the Greenlandic Building Code requirements of 230 kWh/m² (Vladykova et al., 2013).



Figure 2.3 Low energy house in Sisimuit, Greenland. (Vladykova et al., 2013).

In Kiruna, Sweden 67° N, the northern most house in Sweden to meet the passive house standard was built, as seen in Figure 2.4. It was designed to have an annual energy use of 64kWh/m²/year. The building uses a highly insulated air-tight envelope with an HRV, and a façade applied PV to take advantage of the reflected irradiance from the snow. Measured energy values of 56.7kWh/m²/year were below the passive house requirements and demonstrated that the passive house standard could be met in a sub-arctic climate (Dehlin et al., 2017).



Figure 2.4 Sweden's northern most passive house. (Dehlin et al., 2017).

Modeling of a dwelling in Longyearbyen, Svalbard 78°N, theoretically showed that it was possible to achieve the Passive House standard in this high Arctic location. However, some of the boundary conditions needed to be changed such as the simulated bathroom and closets room temperatures need to be lowered to 18°C instead of 20°C. As well, feasibility was not considered in the design, although the archetype was based on the Kiruna, Sweden passive house design with some modifications, such as reduced window areas and a rowhouse concept to reduce the ratio of exterior wall to floor area. It was also mentioned that the technical skills of the workers in Arctic region were not considered, therefore in reality it will be much harder to achieve the extremely high quality of workmanship needed to reach the targets. (Buijze & Wright, 2021).

2.3 Canadian Arctic Green Building Research

The government of Canada's latest Arctic policy (Arctic and Northern Policy Framework, 2019) contained three sections which mostly focused on international cooperation as well as collaborations with local northern communities.

One of the federal government's programs from Natural Resources Canada (NRCan), is presently supporting the Indigenous Off-Diesel Initiative. The initiative aims to support remote Canadian communities to seek innovative means to reduce the use of diesel for heating and electrical energy. This is accomplished by providing training programs, financing, and access to technical experts to implement clean energy projects (Impact Canada, 2021).

A more specific program focusing on clean energy includes the Indigenous 20/20 Catalyst, which is a mentor-based capacity building program, created from the Indigenous Clean Energy enterprise. The focus is on teaching individuals from aboriginal communities across Canada about clean energy, helping to improve community engagement, economic development, project management as well as the operation and maintenance aspects of renewable energy projects and partnerships (Indigenous Clean Energy, 2021).

2.4 Arctic Solar Application

2.4.1 Canadian Arctic Building Applied Photovoltaics (BAPV)

The following projects are recent clean energy projects carried out or planned in the new future across the Canadian Arctic.

A newly constructed 10kW PV array in the hamlet of Kugaaruk, Nunavut has been installed to help power the community freezer. The community's clean energy manager is a graduate of the

Indigenous Clean Energy 20/20 Catalysts program and the Indigenous Off-Diesel Initiative (Last, 2020).

The community of Kugluktuk, Nunavut started the initial construction of the first hybrid solar/diesel power plant in the circumpolar region (McKay, 2019). The plan was to replace the 50-year-old existing diesel power plant seen in Figure 2.5. As well, the 1.5km fuel line connecting the power plant to the diesel storage tanks no longer complies with the present petroleum code is a leakage risk. The new 2.6 MW plant will use higher efficiency diesel generators producing less emissions and will allow for integration with solar and wind systems. However due to COVID-19 the project completion date has been delayed until 2023 (George, 2020).

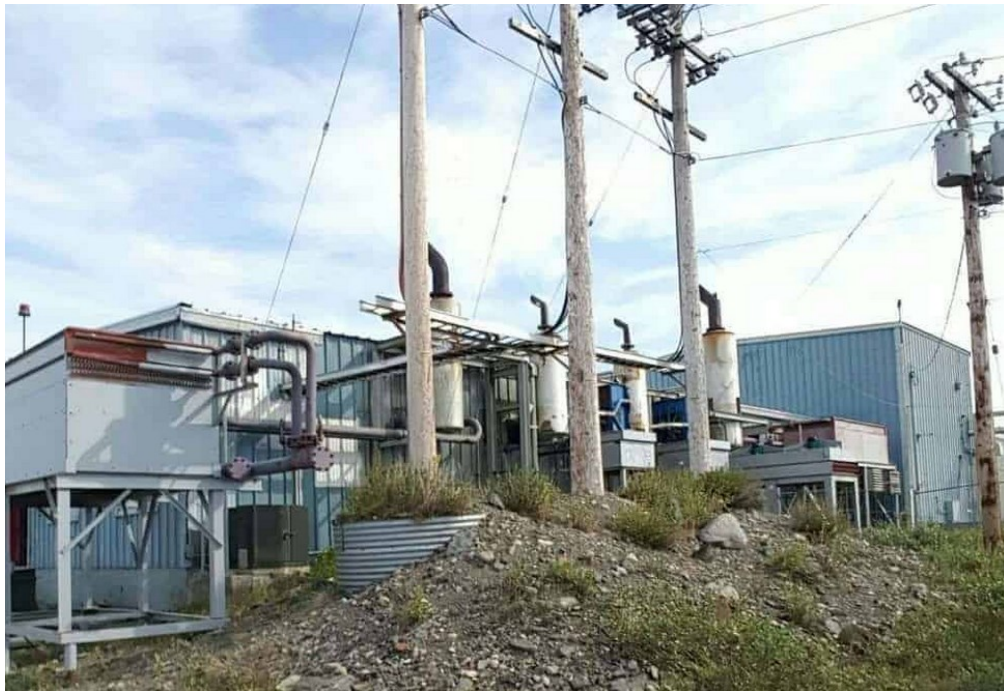


Figure 2.5 Kugluktuk's diesel power plant to be replaced with new hybrid solar/diesel plant (George, 2020).

A wind and solar powered greenhouse in Gjoa Haven is helping to supply fresh produce to the small northern village as seen in Figure 2.6. The initiative is part of a larger research project to

efficiently grow food in remote locations and is funded by several agencies including the Arctic Research Foundation, NRCan, and the Canadian Space Agency, with the project planned to continue until 2025 (Tranter, 2020).



Figure 2.6 Gjoa Haven solar and wind powered green house and research station (Tranter, 2020).

In 2017, a 27-panel solar array was installed on the community center in Clyde River, Nunavut 70° N 68°W as seen in Figure 2.7. The system has resulted in approximately \$5,000-\$10,000 in savings per year. It was reported that some panels were cracked from vandalism, however the system was confirmed to be still fully functional.



Figure 2.7 Solar array being applied to the façade of the Clyde River community center (Rogers, 2018).

The community of Pond Inlet, Nunavut has also installed a 9.27 kW PV system on the roof top of the community hall to reduce the chances of vandalism as seen in Figure 2.8. The system is also remotely monitored with real time data available on-line (Rogers, 2018).



Figure 2.8 Pond Inlet PV system install on roof of building to avoid vandalism (Rogers, 2018).

2.5 KOTT SIP House

Another notable high-performance residential building project in the Canadian North includes the Kott SIP House located in Iqaluit, Nunavut 63°N, shown in Figure 2.9.



Figure 2.9 Kott SIP house located in Iqaluit, Nunavut (Photo taken by author).

The duplex was constructed with structurally insulated panels (SIP) composed of expanded polystyrene (EPS) sandwiched between sheets of orientated strand board (OSB). The SIP envelope was chosen for its air tightness of less than 0.5 air changes per hour at 50Pa, and excellent thermal insulation values with an RSI-7.0 floor, RSI-8.8 walls and RSI-12.3 ceiling. Building with SIPs also provided the advantage of enclosing the building envelope within 5-6 days (Armstrong, 2011), which is an important factor, considering the short construction season in the Arctic. Building with SIPs also reduces the thermal bridging through structural components compared to the standard wood framed constructions and reduces the amount of skilled labor required on site, since the panels are prefabricated before shipping north. Some of the disadvantages of using SIPs are the

need for lifting equipment on site, higher marine shipping cost due to larger volume of the pre-assembled panels, as well care must be taken to install each panel tightly and the joints properly sealed to eliminate the risk of air leakage (Kayello et al., 2017b).

The building also used a passive solar design with larger south facing windows and a solar porch that acts as an air lock vestibule when entering the duplex. Advanced fenestration was used with low-e argon filled, triple pane windows, as well as a heat recovery ventilator (HRV) to recover heat from the exhausted air.

A standard truss framed roof was chosen instead of a SIP roof for ease of construction and to prevent possible air leakage issues previously mentioned. As well, using trusses to create an attic space compared to a sandwich panel cathedral ceiling allowed for an increased thickness of insulation. The performance of the unventilated attic space was monitored by Baril et al., (2013) in a remote hygrothermal field monitoring project and was studied through modeling and experimental testing by Kayello et al., (2017) & Ge et al., (2018).

2.6 Northern Quebec Building Studies

2.6.1 Northern Housing Prototype

Approximately 90% of the housing stock in the northern Quebec territory of Nunavik consists of social housing, of which, 50% are the J2.2 duplex built annually by Makivik's Construction Division since 2000, which can be seen in Figure 2.10 (SHQ, 2020). The other 50% of the social housing primarily consists of older Société de Habitation Québec (SHQ) wood framed detached and semi-detached housing designs built in the 1980s and 90s as seen in Figure 2.11 (SHQ, 2014).



Figure 2.10 J2.2 Nunavik social housing duplex (Photo taken by author).



Figure 2.11 Nunavik social housing built in 1980s & 90s (SHQ, 2014).

With such a large portion of the population residing in the J2.2 archetype it was seen as a good starting point for a pilot project to help solve local housing issues.

In 2015 a pilot project entitled Prototype D’Habitation Nordique, Northern Housing Prototype (NHP), was funded by the Société du Plan Nord (SPN), managed by the SHQ, and was created to improve the current Nunavik social housing design. A steering committee comprising of several Nunavik organizations, stakeholders, community members and SHQ took part in a design charrette with the following objectives:

- Improve the cultural appropriateness of the design.
- Increase the energy efficiency of the building.

- Adapting the foundation system to address issues from climate change, more specifically, preserving the permafrost and Arctic tundra landscape.

2.6.1.1 Passive House Concepts

To achieve the energy efficiency goals the design team worked with the Canadian Passive House Institute (CanPhi) to incorporate techniques inspired from their program. Passive Haus concepts were used to reduce the building’s energy consumption such as, a double stud building envelope, with RSI-10.0 walls, compared to the RSI-5.1 used in the J2.2, an ERV, passive solar design, and large triple pane, south facing windows, with a solar heat gain coefficient greater than 50% to take advantage of the solar heat gains and natural daylighting.

2.6.1.2 Building Envelope

Table 2.1 Nunavik housing exterior wall configuration

J2.2	NHP
Exterior siding	Exterior siding
Vertical wood strapping 19X64mm	Vertical wood strapping 19X64mm
Air barrier	Extruded polystyrene rigid insulation 50mm
Extruded polystyrene rigid insulation 50mm	Self-adhered air barrier
OSB 11mm	Plywood 13mm
Wood Stud 38X140mm	Wood Stud 38X140mm
Mineral wool insulation in stud cavity	Air space 50mm
Vapour barrier 0.15mm	Wood Stud 38X89mm
Wood Strapping 19X64mm	Blown in high density fiberglass wool insulation in 279mm cavity
Gypsum Board 13mm	Optima membrane vapour barrier
	Wood Strapping 19X64mm
	Gypsum Board 13mm
Total RSI 5.1	Total RSI 10.04

The site was selected in the Northern Village of Quaqtuq, QC, 61°N with the south facing façade seen in Figure 2.12 and north facing façade seen in Figure 2.13.



Figure 2.12 NHP south façade (SHQ, 2020)



Figure 2.13 NHP north façade (SHQ, 2020)

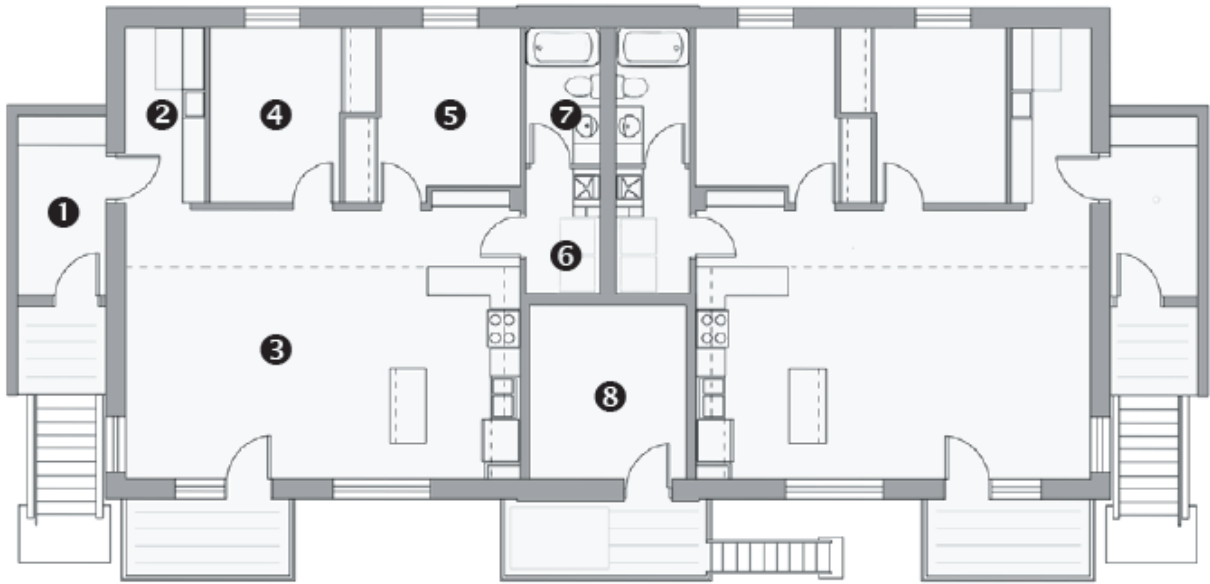


Figure 2.14 NHP floor plan (SHQ, 2020)

1: Cold Porch 2: Heated Vestibule 3: Living Room/Kitchen 4: Bedroom 1 5: Bedroom 2 6: Laundry Room 7: Bathroom 8: Mechanical Room

The NHP floor plan can be seen in Figure 2.14, with a floor area for both housing units and mechanical room of 209m².

2.6.1.3 Mechanical Systems

A 47kW (160,000 BTU/hr) oil fired boiler is used to heat a glycol water mixture which is transferred to a double heating coil hot water storage tank. One coil is used to heat the domestic hot water system while the other one heats the hydronic baseboards and the ventilation fresh air. This system replaces the two oil fired forced air furnaces from the J2.2 as well as the oil-fired burners for the domestic hot water heating.

North and south zones were set up for the fresh ventilation air which is preheated using an Energy Recovery Ventilator (ERV). The ventilation air is then ducted throughout the house in

the subfloor cavity with the outlets located at the bottom of the windows, which can be seen in Figure 2.15.



Figure 2.15 NHP subfloor ventilation ducts (SHQ, 2020)

An initial air leakage test was conducted during construction before the gypsum board was installed to find and seal air leakage locations in the building envelope. Another test was conducted after construction resulting in 3.05 ACH50. This was seen as an improvement from the 4.5 ACH50 obtained from the J2.2 house, since the same builder was used to construct both houses. It was not mentioned if all intentional openings were sealed, since the ACH50 was much higher than Passive House Standard target of 0.6 ACH50 (SHQ, 2020).

2.6.1.4 Initial Energy Analysis

The design team carried out an initial energy analysis using the Passive House Planning Package (PHPP) to compare the performance of the J2.2 and the Northern House Prototype and was validated with EnergyPlus. Due to the extreme cold conditions, the exterior exposure of the bottom floor surface, and the energy losses from daily cold potable water delivery to the interior storage

tanks, it was concluded that the Passive house standard was not feasibly obtained for the NHP. However, a new design to reduce the thermal energy usage of the J2.2 duplex by 60% from 310 kWh/m² to 128 kWh/m² was proposed along with a maximum heating load reduction from 122 W/m² to 42 W/m² (SHQ, 2020).

2.6.1.5 Field Monitoring

The SHQ, (2020) and an automation firm planned the field monitoring system during the design phase, to be integrated into the building, allowing for expandability while at the same time being non-intrusive to the occupants. The main objectives were to monitor and compare the energy usage of the two housing units and mechanical room, as well as verifications of mechanical equipment design choices, by monitoring the indoor air conditions.

The data loggers installed collect information from 29 sensors and communicate the data to an on-site web connected computer which sends the information to an online FTP site. Some issues have arisen with the dependability of the internet connection, power outages in the village and the data reception at the FTP site. However, over time the issues have been corrected allowing for a more stable data collection. Logging intervals range from 15 minutes, 60 minutes and 24 hours depending on the parameter. As well some sensors collect the operating or opening times such as the bathroom fan usage or window openings.

Table 2.2 NHP parameters measured and sampling frequency

15 minutes	60 minutes	24hours
CO ₂ levels for Unit 1 &2	Water levels:	Electrical energy
Relative humidity & temperature for ventilation air return	<ul style="list-style-type: none"> ● Potable water ● Wastewater 	Heating oil usage
Air temperature:	Water temperatures:	Usage times:
<ul style="list-style-type: none"> ● Bedrooms 1 & 2 ● Cold porch ● Kitchen/living room ● ERV exhaust 	<ul style="list-style-type: none"> ● Potable water ● Wastewater ● Domestic hot water 	<ul style="list-style-type: none"> ● Kitchen range hood ● Bathroom ventilation fan ● Clothes dryer ● ERV
		Total opening times:
		<ul style="list-style-type: none"> ● Exterior door ● Porch door ● Vestibule door ● Mechanical room door ● Bedroom 1&2 windows

2.6.1.6 Initial Data Analysis

From the initial data collected it was found that the actual energy consumption was much higher than previously simulated, especially from one of the two housing units. For example, the thermal energy consumption was 237 kWh/m² compared to the estimated value of 170 kWh/m², the same can be said for the electricity usage. This illustrates the difficulties in modeling occupant behaviors in simulations programs. It was also noted that the occupants opened the windows frequently during the heating season, increasing the air exchange rate of the condition space, decreasing RH, and increasing the heating loads significantly (SHQ, 2020).

2.6.1.7 Lessons Learned

Some difficulties and delays occurred during construction due to the worker's unfamiliarity with the dual coil hot water tank, used to heat the hydronic baseboards, pre-heat the ventilation air and the domestic hot water. As well the workers were not accustomed installing the triple pane windows, metal roofing and the large scaffolding required to work on the back side of the house. The increased ceiling height of the prototype also added additional volume to the conditioned space compared to the J2.2 volume of 14,019 ft³ compared to 22,685 ft³ for the prototype. Concerns have also been raised about the complexity of the heating and control systems, as seen in Figure 2.16, that could lead to difficulties repairing and maintaining the system by the local workers (SHQ, 2020). As was mentioned in SHQ (2018) it is important that the mechanical systems of the residential buildings in the Nunavik are kept simple and at a minimum to allow for regular maintenance and performance tests by local maintenance personnel.



Figure 2.16 NHP mechanical system could be difficult to maintain locally (SHQ, 2020).

2.6.2 Nunavik Clean Energy, BAPV & PV

There has been local interest over the past 15 years in Nunavik concerning renewable energy, including photovoltaic technologies. Successful projects include the Kuujjuaq airport terminal, which is the first LEED certified building in Nunavik, and was constructed in 2008. A 6.3kWp grid connected monocrystalline PV array, as seen in Figure 2.17, was installed on the south façade to reduce the electrical load and provide an estimated 5040 to 5670 kWh of electrical energy generation annually (Matrix Energy, 2007).



Figure 2.17 Kuujjuaq, QC LEED certified airport with 6.3kW PV array (Matrix Energy, 2007).



Figure 2.18 Laval University's Centre for Northern Studies Whapmagoostui, QC (Matrix Energy, 2011).

In 2011, a 4.2kWp monocrystalline PV system was installed on the Laval University's Centre for Northern Studies in Whapmagoosui-Kuujuarapik, QC 55°N, as seen in Figure 2.18, and uses low voltage DC appliances (Matrix Energy, 2011).

In 2017, a BAPV pilot project to study the solar potential in Kuujjuaq, QC took place where a 20kWp solar PV system was installed on the Makivik Corporation head office as well as a 45kWp solar PV system was installed on the Nunavik Research Center building, as seen in Figure 2.19. The project is the largest local grid connected net metering PV system in Nunavik (Gordon, 2017).



Figure 2.19 Makivik head office and Nunavik research center PV pilot project (Gordon, 2017).

In 2018, Hydro-Quebec installed 69 PV panels as seen in Figure 2.20, in the community of Quaqtaq, QC with two 500kWh Lithium iron phosphate (LFP) batteries installed in an Arctic electrical energy storage systems that has an operating range of -40°C to 30°C (EVLO, 2018).



Figure 2.20 Quaqtaq Hydro-Quebec solar project (EVLO, 2018)

A 100 kWp PV system is planned to be installed on the Kuujjuaq Forum to provide electricity for two 6-ton ground source heat pumps installed in 2020, that will be used to heat the water at the local swimming pool, as seen in Figure 2.21 (Giordano & Raymond, 2020).



Figure 2.21 Kuujjuaq solar/ geothermal pool heater (Giordano & Raymond, 2020).

2.7 BAPV vs PV

When using stand alone ground mounted PV systems as seen in Figure 2.20 there is a requirement for the preparation of the land to securely erect the structural framing, as well as the need for the installation of a service road will be required in most cases. Both construction processes require the removal of the natural landscape, that can years to grow back in Arctic climates. The occupying of this space also takes away natural habitat that could other wise be used for wildlife and traditional activities. Building applied photovoltaic (BAPV) systems on the other hand help to conserve the landscape by installing the PV system on existing buildings that have already had the lot developed for the structural foundation of the building. As well, having the PV system near the loads reduces transmission losses (IEA, 2019). These conventional BAPV systems typically

convert the incoming solar radiation to electricity with an efficiency in the range of 6-20% depending on the composition of the PV modules, with the remainder of the solar radiation either being reflected or converted to heat (Candanedo, 2010). Typical designs promote the heat loss to the environment to improve the electrical energy generation efficiency and to prolong the panel life span.

2.8 BIPV/T

Building incorporated photovoltaics/ thermal collectors (BIPV/T) aim to improve on BAPV systems, generating electrical energy, while recovering the heat that would otherwise be lost, for pre-heating fresh air or supplying a heat pump, as seen in the simulation study by (Ma et al., 2021). Helping to improve the total solar radiation conversion to useful energy efficiency up to 55% (Bambara et al., 2011).

As with BAPV, BIPV/T system can help to reduce electrical loads, avoiding high peak electrical energy rates common in Arctic regions. Since total heating loads, including domestic hot water (DHW), in the Canadian residential sector are in the 80% range of the total building's energy usage (NRCan, 2011), it makes sense to recover heat from solar systems that would otherwise be lost (Pinel et al., 2011). This useful sensible heat can lead to a reduction in the maximum thermal energy loads, allowing for a downsizing in the home heating system sizing, resulting in increased heating system efficiency by allowing the heating system to operate at full load for longer periods of time, reducing cycling. Heat recovery also reduces the fossil fuels used by the heating systems and improves energy security in emergency situations. While at the same time achieving the objective of cooling the PV modules for increased electrical efficiency and increased service life.

2.8.1 BIPV/T Categories

There are several variations of BIPV/T collectors which use different configurations and heat transfer fluids. The major categories can be divided into concentrating or flat plate systems each of which can be installed on the façade and/or roof. While concentrating systems have proven successful in certain situations as seen by Daigle & O'Brien, (2020) and Chemisana et al., (2013), the complexity of the systems can lead to high installation and maintenance costs in the Arctic communities (Chen et al., 2012). Therefore, this study will focus solely on flat plate collectors.

The flat plate systems typically uses either air, water/glycol or a phase changing substance such as a refrigerant as the heat transfer fluid. Air based systems can be further divided into active system where air is forced by a fan or passive systems that use natural convection. Water based systems use circulators or thermosyphon action to transport the liquid.

2.8.2 Closed Loop Water/Glycol Based Systems vs Open Loop Air Systems

Using water/glycol as the heat transfer fluid as opposed to an air-based system does have its advantages as the specific heat of air is approximately 1 kJ/kg·K compared to 3.6 kJ/kg·K for a 50/50 water/polypropylene glycol mixture (Dow, 2021). This higher specific heat increases the useful heat transfer available from the PV to the building for increased thermal efficiency (Joshi & Dhoble, 2018). However, there are several disadvantages of using a water/glycol-based system in the northern communities. Having outdoor air flowing in the cavity behind the PV modules and exterior wall has no risks of freezing or leaking when compared to a water/glycol system which will inevitably leak over its service life and can be difficult to access for repairs. As well, there is a risk of freezing if the extreme cold winter temperatures drop below the freezing point of -33°C

for a 50/50 water/polypropylene glycol mixture, or if water is added to a leaking system diluting the mixture increasing the freezing point to -21°C for a 60/40 water/polypropylene glycol mixture (Dow, 2021).

Using an air based, open loop, flat plate, façade integrated system has many benefits for use in Arctic regions. Air as a heat transfer fluid is extremely light making it easy to integrate on a façade or roof compared water/glycol that also requires a piping system. Air on the on the hand can be transported through pre-existing cladding wall cavities and eventually enters the building through light weight sheet metal ducts where the air flow is easily modulated with a low power fan.

The use of a 90° sloped façade takes advantage of the low solar incident angle in high latitude locations, especially during the winter months, helping to match the energy generation with the higher loads during these times. The 90° tilt angle also allows for maximum surface irradiance gains, taking advantage of the highly reflective snow cover for several months of the year that would other wise be greatly reduced with a system installed on the typical low sloped roofs (Chen et al., 2012) (Dehlin et al., 2017).

Having the BIPV/T system incorporated into the design of the building allows the PV panels to serve multiple purposes for the building other than solely energy generation. BIPV/T can replace a portion of the cladding or roofing material acting as the rain and UV barrier of the building envelope, reducing the material costs that would otherwise require having both PV and cladding material installed. At the same time the esthetics of the PV module integration can be considered, blending in the modules with the standard cladding or roofing materials keeping the architectural concept consistent (Reijenga, 2000).

It is also worth mentioning that heat losses through the building envelope from the interior conditioned spaces can be recovered in the cavities and brought back inside, changing the U-value of the envelope helping to compensate for low thermal resistance of the insulation or air leakage from workmanship errors (Yang & Athienitis, 2016).

A simple design that does not pose additional risks to the building operation and maintenance are important for the northern communities, where there are long lead times to receive parts and materials through expensive air transport, as well as the shortage of skilled labor to carry out maintenance and repair work. For these reasons mentioned the study will focus on an air based flat plate BIPV/T system.

2.8.3 BIPV/T Projects

Building incorporated photovoltaics/ thermal collectors BIPV/T play an important role in the implementation of renewable energy in the building sector, with several studies and prototypes demonstrating the benefits (Sultan & Efzan, 2018).

Several full scale BIPV/T projects have been implemented such as a 288m² unglazed transpired BIPV/T collector installed on the John Molson School of Business building at Concordia University located in Montreal, Quebec, with the concept seen in Figure 2.22. Experimental testing conducted by (Bambara et al., 2011) demonstrated that the system was able to pre-heat ventilation air up to 20°C, while obtaining a combined electrical and thermal efficiency in the range of 37-55%. It was mentioned that essential items for an optimal design were the south facing orientation, and the proximity to the mechanical room to reduce ducting requirements, thus minimizing material costs and the fan power, as well as to facilitate the electrical connections.

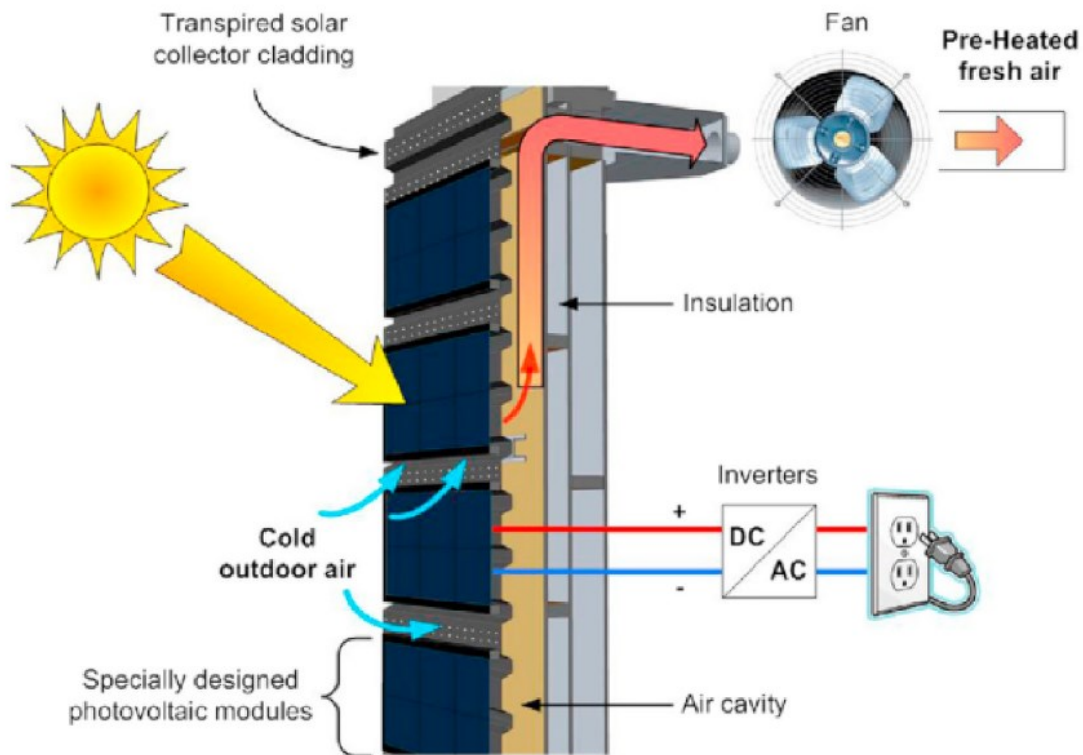


Figure 2.22 Unglazed transpired collector concept installed at Concordia University (Bambara et al, 2011).

Dermardiros et al., (2019) studied the performance of the BIPV, and BIPV/T systems installed at the new Library in Varennes, QC, which were installed as part of the design to achieve net-zero energy building usage, as seen in Figure 2.23. Other features of the building design include optimal shape and orientation of the building to maximize daylighting and surface irradiance on the PV system. As well, the building takes advantage of natural ventilation for free cooling of the building and uses the BIPV/T to pre-heat fresh air. The first year normalized gross energy consumption of the building was 78kWh/m^2 and was further reduced to 70kWh/m^2 . With the BIPV & BIPV/T energy generation the normalized net energy usage of the building was reduced to 15kWh/m^2 . Further commissioning and optimization of the building's mechanical system controls are being studied to further reduce the net energy usage (Sigounis et al., 2021).



Figure 2.23 Varennes Library (Rounis et. al., 2020)

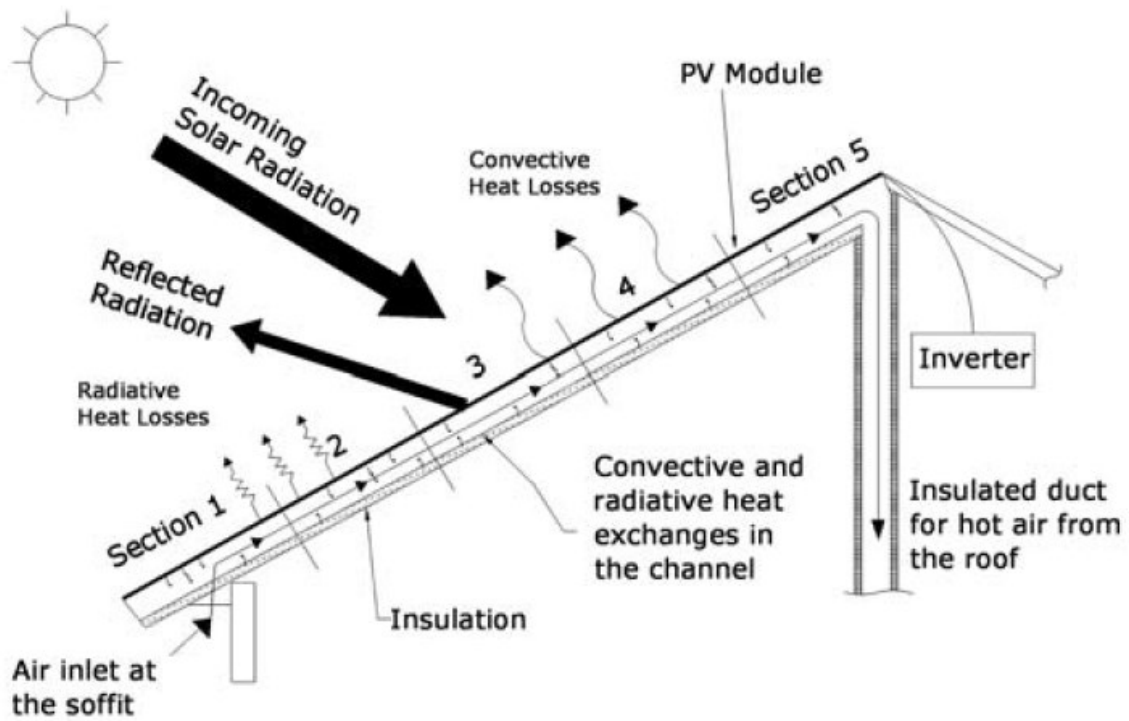


Figure 2.24 BIPV/T schematic (Candanedo et al., 2011)

Candanedo et al., (2011) modeled and performed experimental studies with an open-loop air based BIPV/T system based on the system that was installed on the sloped roof of the EcoTerra™ demonstration house in Eastman, QC. A schematic of the system can be seen in Figure 2.24. From the study, convective heat transfer correlations (CHTCs) were developed for the asymmetric top and bottom surfaces of the cavity for forced convection.

2.8.4 Arctic BIPV/T

With the year-round heating loads in Nunavik, it makes sense to take advantage of thermal energy that would otherwise be lost to the environment. Experimental studies have been conducted for Arctic BIPV/T applications by Chen et al., (2012a) and have shown that the BIPV/T thermal efficiency can be improved by reducing the heat losses to the environment by the addition of transpired glazing to the exterior surface of the system.

Kayello et al., (2016) performed a simulation study using BIPV/T to lower humidity levels in residential attic spaces in Arctic climates while at the same time providing a substantial amount of the heating and electrical energy for the house.

Toffinin et al., (2019) demonstrated through simulations that BIPV/T could be successful at pre-heating air for HRVs to reduce the defrosting cycles for a residential application in Iqaluit, Nunavut.

Ma et al., (2019) concluded that an optimized passive solar design of a house in Yellowknife, NWT could bring the normalized energy demand below 77 kWh/m². As well, a BIPV/T could be used with an HRV to help reduce the frosting risk time or coupled with a heat pump to improve the efficiency and the working period.

2.9 Arctic ERV/HRV

To achieve an energy efficient building envelope, it is vital to minimize outdoor air infiltration and the exfiltration of conditioned air through unintentional openings. As construction processes are becoming increasingly effective at reducing unintended air passage in and out of the building, the need for controlled fresh air ventilation systems are vital to ensure high quality air for the occupant's comfort and health as concluded in the Nunavik residential indoor air quality (IAQ) study from Aubin et al., (2019). As well controlled humidity levels are important for preservation of the building materials (Ge et al., 2018).

Air to air heat exchangers also know as Heat Recovery Ventilators (HRVs) have been an effective method to efficiently meet the fresh air needs of the building, while recovering sensible thermal energy from the exhausted air. During the regular operation of an HRV, condensation can occur in the heat exchanger core of the unit, where the warm moist indoor air and the cold outdoor air streams pass. In warmer seasons the condensate is designed to be drained as part of the process. However, in cold climates the condensate begins freezing when the inlet supply air is below -5°C . In the extreme cold climate of the Arctic, core freezing occurs on a much higher frequency as ambient temperatures are below -5°C for a large portion of the year. As seen from the experimental study conducted by Beattie et al., (2018), this can be problematic since, the heat transfer effectiveness is reduced from the core frosting and can eventually lead to system failure and more importantly, the fresh air supply is reduced.

Various strategies exist to mitigate the core frosting. The most common technique is the recirculation of the warm indoor air inside of the unit, stopping the supply of fresh outdoor air during the defrost period. As mentioned in the HVAC best practices in Arctic climates (Winfield

et al., 2021), cutting off the fresh air supply to commercial buildings is not acceptable and is not recommended for residential buildings as well.

Another method is to pre-heat the outdoor air supply with a heating coil before it enters the heat-exchanger as well as having a second heating coil after the HRV to increase the supply air temperature to the room, to a comfortable level. This method is seen to be effective, however large amounts of energy are consumed by the heating coils in the process. However, as seen in the experimental study conducted by Berquist et al., (2021) in the Canadian Arctic, which compared the two defrosting techniques, pre-heated air versus recirculation, it was seen that the pre-heated air was the more energy efficient method to reduce core frosting and ensured the designed fresh air supply to the occupants. The system that was reliant on the recirculation method, without air preheating by heating coils, had air supplied to the living space at times cooler than the indoor air, requiring the home heating system to warm the air, increasing the overall energy usage of the building. As well, this was seen to create discomfort to the occupants, from the cool draft of air being supplied, which led to the ventilation system being turned off all together in some cases.

Another successful defrost mitigation method used in Greenland and studied by Vlaykova et al., (2012) uses a dual core system that alternates airflow between cores to keep a continuous fresh air flow while the other core is defrosting. In a study conducted by B Ouazia et al., (2019) it was also shown that dual core systems were able to perform well in northern settings.

A similar device to the HRV is an Energy Recovery Ventilator (ERV), which uses a vapor permeable heat exchanger core that allows for sensible as well as latent heat transfer between the conditioned indoor air being exhausted, and the cold dry outdoor air entering the building. This process helps humidify the cold dry outdoor air being brought into the building, while at the same time helping to mitigate the condensation occurrence inside the core and lowers the core frosting

threshold to approximately -10°C (Beattie et al., 2018). In a simulation study conducted by Li et al., (2021) significant reduction was found in the heating energy usage for northern housing.

In conclusion, ERVs are an attractive option to be used in the extreme cold climate of the Arctic as the frosting risk thresholds are reduced while at the same time increasing the occupant's comfort by increasing the indoor relative humidity during the cold, dry, heating season. It is worth noting that in the conclusion discussed in the study of Aubin et al., (2019), it was seen in Nunavik that regular preventative maintenance on the HRV/ERV systems was lacking, however once properly maintained they were able to provide effective IAQ and energy saving benefits.

2.10 Literature Review Summary

As was seen in the sections of the literature review presented, there is a desire to improve the construction practices of the buildings in the Arctic regions of the world, for the environmental, social, and economical benefits that are a consequence of the green building concepts. Several projects have focused on green building and passive house concepts to improve the thermal performance of the building envelope, and the energy efficiency of the mechanical systems. As well, it was seen that there has been an increased amount of interest in renewable energy generation, specifically solar power in the northern villages of Canada, with the community members taking part in training initiatives and programs to be able to actively participate in the clean solar energy projects.

From the studies reviewed it was seen that BIPV/T has several advantages over stand alone PV, BAPV and BIPV, with the most important benefit being the recovery of heat, which is of even greater significance in the extreme cold climate of the Arctic. It was seen that HRVs and ERVs are a key component to provide fresh air to the occupants in tightly sealed, energy efficient building

envelopes. However, in the cold Arctic conditions the frosting of the heat exchanger core reduces the effectiveness of the units and lowers the amount of fresh air supplied to the occupants. It was demonstrated from previous studies that coupling BIPV/T with HRVs have been effective at reducing the frosting times however, there have been limited implementation of such systems in the Arctic.

This study aims to build on the promising studies reviewed and will focus on adapting the BIPV/T system for wood framed Arctic residential applications while keeping in mind the ease of construction and maintenance that are vital to accomplish successful projects in the small Arctic communities with limited skilled labor and materials.

3. Methodology

The methodology section presents the steps taken to meet the objectives set out in Chapter 1 of adapting an air-based BIPV/T for northern housing to maximize the outlet air temperature to mitigate ERV core frosting while generating electricity and thermal energy.

The first step in meeting the objectives of adapting a BIPV/T design for northern housing, was to propose an integration of the BIPV/T system onto a typical housing duplex presently being constructed in northern Quebec. The envelope design was kept the same, except the cladding was replaced by PV modules which serve as the rain and UV barriers while generating heat and electricity.

To analyze the effectiveness of the BIPV/T to pre-heat fresh air and obtain electricity and thermal energy, a finite difference simulation model of an air based open loop system has been developed. Model validation was conducted using BIPV/T experimental data from Concordia University's solar simulator lab.

Local weather data has been gathered from multiple sources and was used to prepare the inputs of ambient temperature, solar irradiance, wind speed, and sky temperature. Indoor fresh air requirements for a typical overcrowded duplex were determined and used to supply an ERV.

Possible configurations of the BIPV/T tilt angle and cavity depth were evaluated to obtain the highest outlet temperatures during the coldest months to mitigate ERV core frosting.

A ducting system was then designed to supply the pre-heated fresh air to an ERV and the associated pressure losses were determined in the ducting and cavities to obtain the fan power required to overcome the losses.

3.1 Design of an Integrated BIPV/T System

To improve implementation of BIPV/T in Arctic regions, a simple, cost effective, pragmatic design is required, for ease of construction and maintenance. Keeping changes to the building design to a minimum are important to reduce any additional time required to install the BIPV/T system, and to minimize the chances of workmanship error in the process.

A typical J2.2 two-bedroom duplex built in Nunavik can be seen under construction in Figure 3.1. Vertical 1X3 (19 X 57mm) wood furring strips are installed to create cavities behind the cladding to provide drainage and ventilation, for drying of the envelope materials.



Figure 3.1 Vertical furring strips presently used on standard Nunavik housing construction. (Photo taken by author)

For the integration of the PV modules the building envelope design will be kept the same as Figure 3.1, except, instead of the standard cladding, PV panels will be installed on the south face of the

building. Creating a BIPV/T façade that not only produces electrical and thermal energy but also serves as rain and UV barrier of the building envelope.

To have a proper integration of the PV, the installation must be designed from the beginning of the project, and not added on latter in the process. For this study, the integration is assumed onto the south facing façade of a new iteration of the original Northern Housing Prototype (NHP) design, seen in section 2.6.1. However, the south facing windows have been shifted and the mechanical room access is assumed on the north face. The same south facing window to wall ratio is kept to have similar solar heat gains and daylighting, when analyzing the energy usage. This allows for 4m of vertical length for the cavities, and 10m of horizontal width of exterior wall to install 20- 2 X 1m PV panels, creating 5- 4m X 2m cavities as seen in Figure 3.2. Maximizing the available façade space for BIPV/T energy generation.

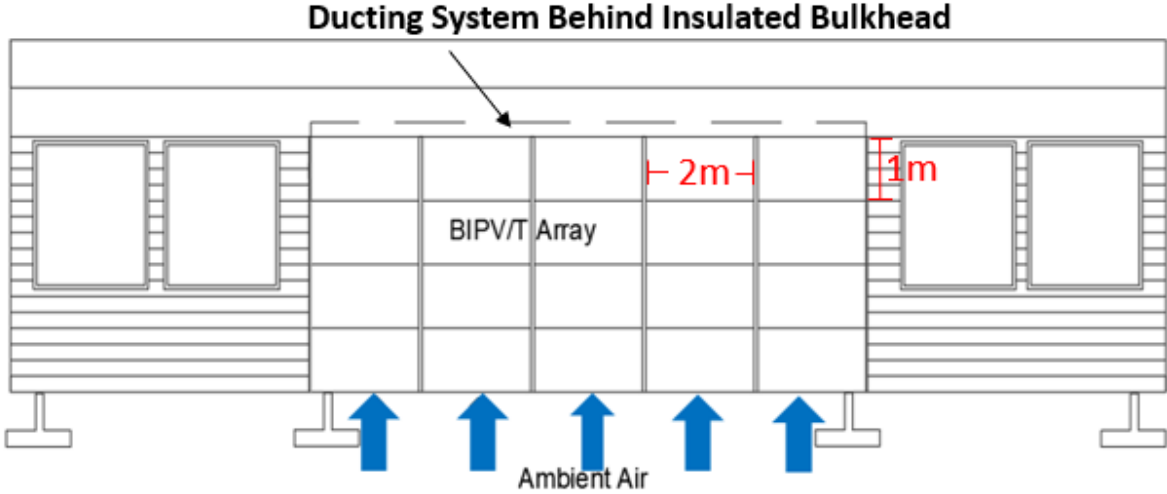


Figure 3.2 South façade of duplex with 40m² BIPV/T array.

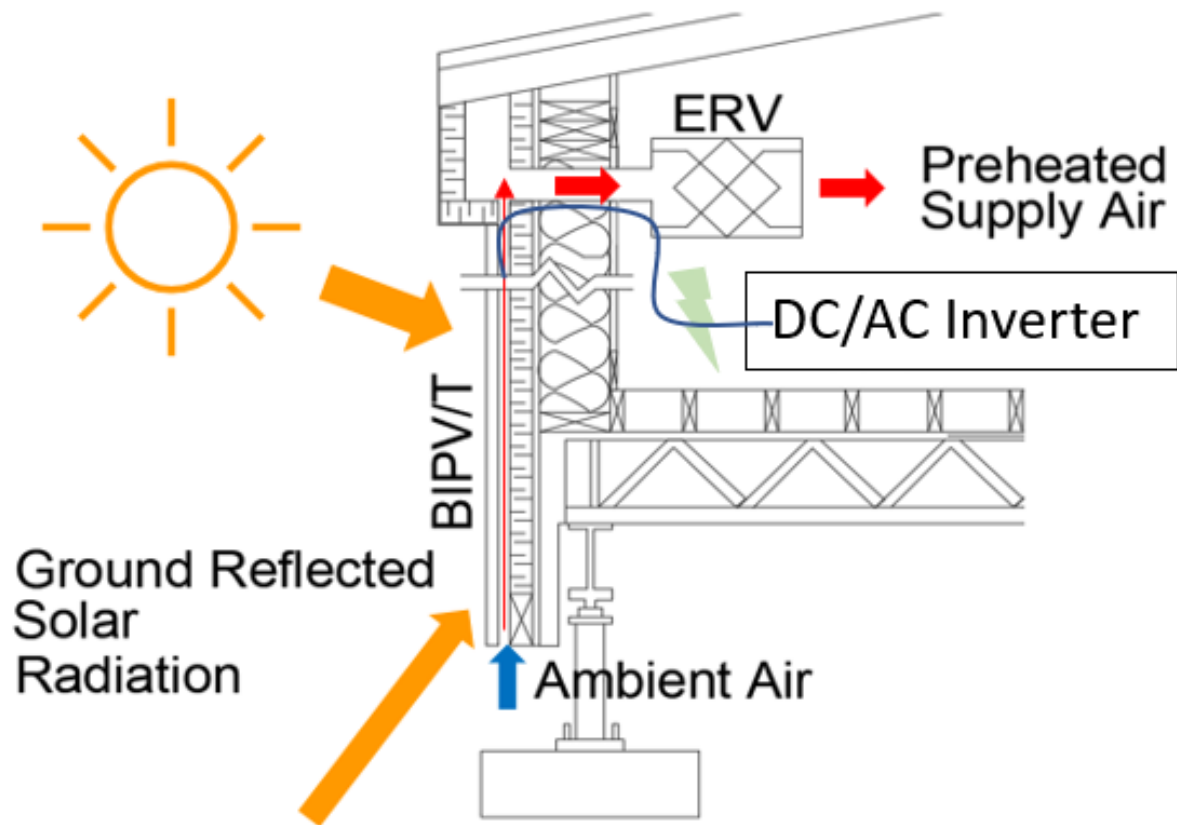


Figure 3.3 BIPV/T wall section drawing.

An annotated wall section drawing of the BIPV/T system can be seen in Figure 3.3.

3.2 Thermal Network Model

As was seen in section 2.8 of the literature review, an open loop BIPV/T system was chosen, with air as the heat transfer fluid since it is light weight, easily transferred, and has no risk of freezing, or leaking, compared to similar water/glycol systems (Yang & Athienitis, 2016).

The BIPV/T system was modeled in MATLAB, by using the finite difference control volume scheme. Where the cavity cross section is discretized into the thermal network shown in Figure

3.4. By establishing this thermal network, an energy balance was able to be performed at the principal nodes of the PV, cavity back surface and cavity air, to obtain a set of algebraic equations. These equations were then solved using the fully explicit Euler method. The list of parameters solved and corresponding equations 3.1-3.10 can be seen below.

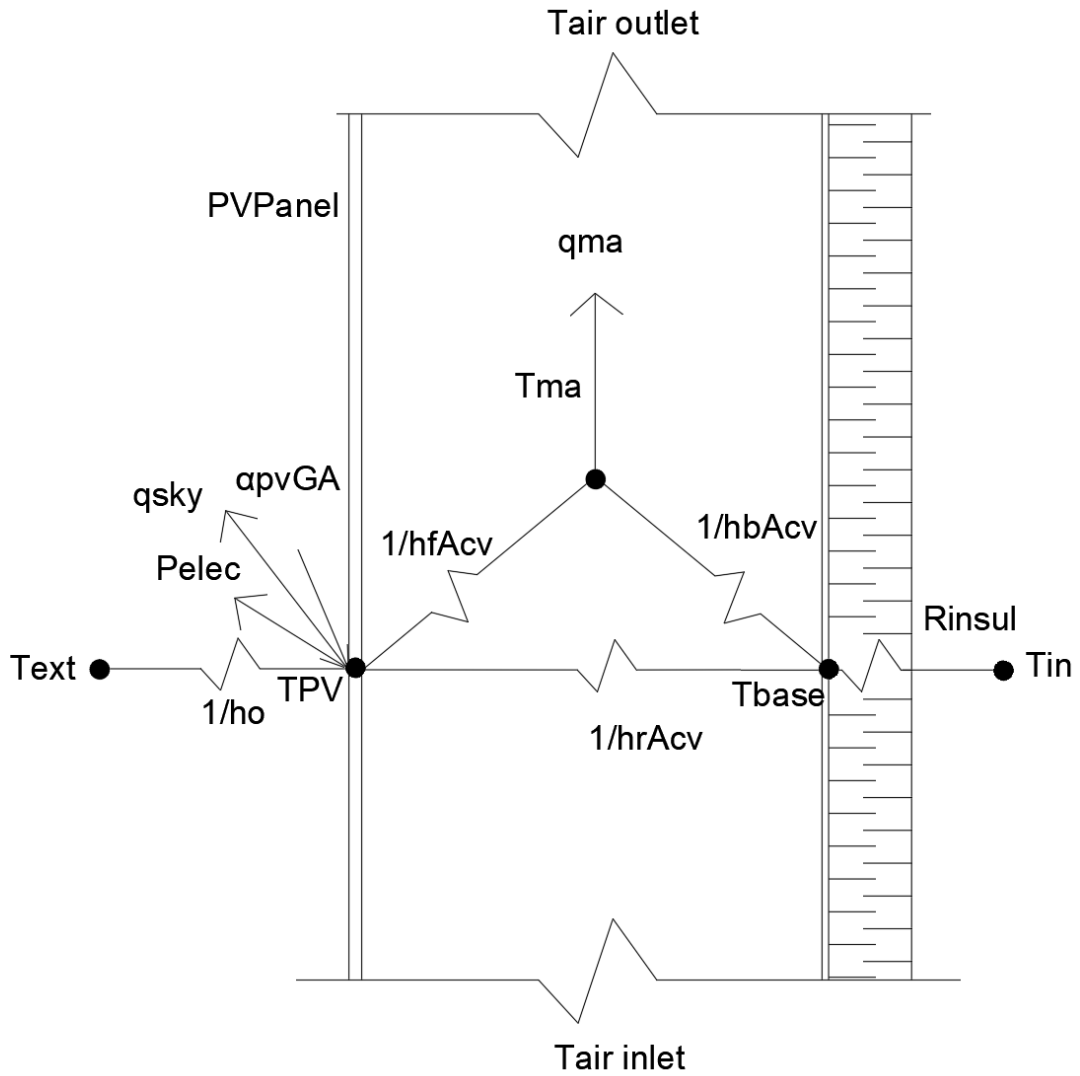


Figure 3.4 Control volume of the BIPV/T cavity thermal network.

$$T_{pv} = \frac{\frac{T_{ext}}{R_{ho}} + \alpha_{pv} * G * A_{cv} - P_{elec} - q_{sky} * A_{cv} + \frac{T_{ma}}{R_{hf}} + \frac{T_B}{R_{hr}}}{\frac{1}{R_{hr}} + \frac{1}{R_{ho}} + \frac{1}{R_{hf}}} \quad (3.1)$$

$$T_B = \frac{\frac{T_{PV}}{R_{ho}} + \frac{T_{in}}{R_{ins}} + \frac{T_{ma}}{R_{hb}}}{\frac{1}{R_{hr}} + \frac{1}{R_{ins}} + \frac{1}{R_{hb}}} \quad (3.2)$$

$$T_{ma} = \frac{T_{inlet} + T_{outlet}}{2} \quad (3.3)$$

$$T_{outlet} = \frac{T_{PV} + T_B}{2} + \left(T_{inlet} - \frac{T_{PV} + T_B}{2} \right) * e^{\frac{-2L_{CV}}{A}} \quad (\text{Athienitis et al., 2004}) \quad (3.4)$$

$$A = \frac{M * C_{p_air} * \rho}{W_{ch} * \frac{(hb+hf)}{2}} \quad (3.5)$$

M=volume flow rate in $\frac{m^3}{s}$

$$Q_{rec} = \dot{m} * C_{p_air} * (T_{outlet} - T_{extr}) \quad (3.6)$$

The average values of the mass flow rate \dot{m} , and specific heat of air C_{p_air} for the entire cavity were used when calculating the total heat recovered Q_{rec} .

$$P_{elec} = \eta_{pv} * \alpha_{pv} * G * A_{pv} \quad (3.7)$$

$$q_{sky} = e_1 * \sigma * (T_{PV} + 273.15)^4 - (T_{sky} + 273.15)^4 \quad (3.8)$$

The following linearized radiative heat conduction equation was used.

$$hr = 4\sigma * \frac{\left[\frac{(T_{PV} + 273.15) + (T_B + 273.15)}{2} \right]^3}{\frac{1}{e_2} + \frac{1}{e_3} - 1} \quad (3.9)$$

The top surface of the PV is assumed to be glass which has an assumed emissivity e_1 of 0.95.

The back surface of the PV panel is assumed to be steel plate with an emissivity e_2 of 0.95. The

back surface of the channel is assumed to be XPS insulation with an emissivity e_3 of 0.2.

The inlet temperature is considered the ambient temperature for the first control volume. For all other control volumes, the outlet temperature from the previous control volume was used as the next inlet temperature.

Each parameter was solved by using the values from the initial conditions or previous results. Equations are solved several times with the same hourly weather conditions, (outdoor temperature, solar irradiance, sky temperature and wind speed), to have the results converge to within 0.1% of the previous iteration.

3.2.1 Photovoltaic Specifications

$$\eta_{PV} = \eta_{STC} * (1 - \beta * (T_{PV} - T_{STC})) \quad (3.10)$$

$$\eta_{STC} = 15\% \text{ (Pike Research, 2012).}$$

$$T_{STC} = 20^\circ\text{C}$$

$$\beta = 0.0045$$

3.2.2 Control Volumes

The length of the channel was divided into several control volumes to accurately calculate the increasing bulk mean air temperature and its corresponding properties. As the number of control volumes were increased the results started to converge and were found to be within 0.1% of convergence when using 200 control volumes. It was of concern that using such a high number of control volumes could become computationally expensive and if necessary, the number of control volumes could be reduced to increase the program efficiency, while sacrificing some of the calculation accuracy, however this was not the case during the simulations.

3.2.3 Air Properties

As the properties of air change with temperature, correlations were established to use an accurate value for each control volume. Values for the following air properties, kinematic viscosity, Prandtl number, thermal conductivity, air density, and specific heat, at 1 atm pressure for a range between -50°C and +60°C were obtained from the properties tables of Cengel & Ghajar, (2011) and were plotted in MATLAB. Basic fitting was used to produce the correlations for each property as a function of the bulk mean temperature (T_{ma}) in the cavity. The curves for each property can be seen in the appendix.

The kinematic viscosity was determined with a linear approximation function.

$$\nu = 8.7 * 10^{-8} * T_{ma} + 1.338 * 10^{-5} \quad (3.11)$$

The Prandtl number was determined with a cubic approximation function.

$$Pr = 1.5 * 10^{-8} * T_{ma}^3 - 1.2 * 10^{-6} * T_{ma}^2 - 0.00025 * T_{ma} + 0.7362 \quad (3.12)$$

The thermal conductivity was determined with a linear approximation function.

$$k = 7.5 * 10^{-5} * T_{ma} + 0.02364 \quad (3.13)$$

The air density was determined with a cubic approximation function.

$$\rho = 6.6 * 10^{-8} * T_{ma}^3 + 1.8 * 10^{-5} * T_{ma}^2 - 0.00473 * T_{ma} + 1.292 \quad (3.14)$$

The specific heat at constant pressure was determined with a cubic approximation function.

$$c_p = 1.4 * 10^{-5} * T_{ma}^3 - 0.0013 * T_{ma}^2 + 0.42 * T_{ma} + 1006 \quad (3.15)$$

3.2.4 Convective Heat Transfer Coefficients

The Reynolds Number which is ratio of inertia forces to viscous forces was determined using the air velocity in the cavity multiplied by the hydraulic diameter (D_h) divided by the kinematic viscosity.

$$D_h = 4 \cdot \frac{\text{Cavity Cross Sectional Area}}{\text{Cavity Perimeter}} \quad (3.16)$$

$$Re = \text{Air Velocity} \cdot \frac{\text{Hydraulic Diameter}}{\text{Kinematic Viscosity}} \quad (3.17)$$

The Nusselt numbers used were taken from the experimental correlations for an air based, wood framed BIPV/T determined by (Candanedo et al., 2011).

For the front side of the cavity the following correlation was used.

$$Nu_f = 0.052 * Re^{0.78} * Pr^{0.4} \quad (3.18)$$

For the back side of the cavity the following correlation was used.

$$Nu_b = 1.017 * Re^{0.471} * Pr^{0.4} \quad (3.19)$$

From the Nusselt Number the convective heat transfer coefficients for the front side of the cavity

h_f and back side of the cavity h_b were calculated as follows.

$$h_f = \frac{Nu_f * k}{D_h} \quad (3.20)$$

$$h_b = \frac{Nu_b * k}{D_h} \quad (3.21)$$

3.3 Model Validation

The criteria from ASHRAE Guideline 14-2014 Measurement of Energy and Demand Savings (ASHRAE,2014), using the Coefficient of Variation- Root Mean Square Error (CV-RMSE) and the Normalized Mean Bias Error (NMBE), were utilized to validate and measure the model accuracy with regards to experimental data. The experimental data was obtained from the results of BIPV/T tests conducted at Concordia University's solar simulator lab by Yang & Athienitis, (2014), with a schematic of the experimental set up seen in Figure 3.5.

$$CV(RMSE) = \frac{1}{\bar{m}} \sqrt{\frac{\sum_{i=1}^n (m_i - s_i)^2}{n}} \times 100(\%) \quad (3.22)$$

$$NMBE = \frac{1}{\bar{m}} \cdot \frac{\sum_{i=1}^n m_i - s_i}{n} \times 100(\%) \quad (3.23)$$

m_i = measured value

s_i = simulated value

n = number of data points

\bar{m} = mean of measured values

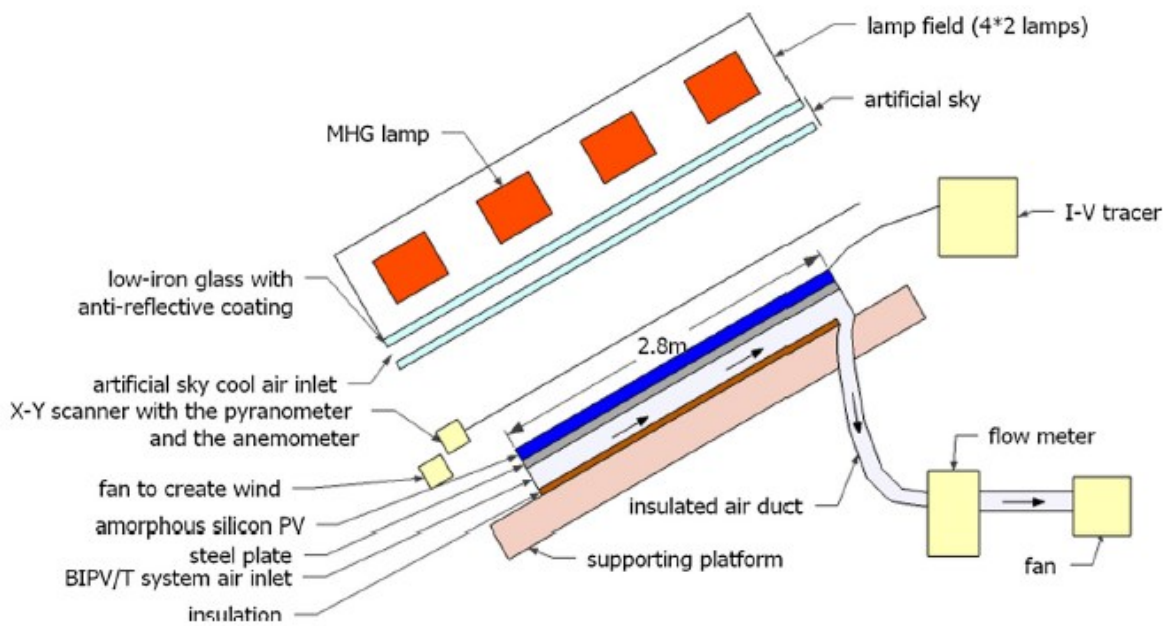


Figure 3.5 Schematic of BIPV/T experimental setup (Yang & Athienitis, 2014).

The following experimental parameters were used in the simulation model:

- Wind Speed: 1.6 m/s
- Ambient Temperature: 20°C
- Solar Irradiance: 1080W/m²

The experimental cavity dimensions were matched in the simulation model and can be seen in Figure 3.6.

- Height 0.04m,
- Width 0.38m,
- Length 2.89m

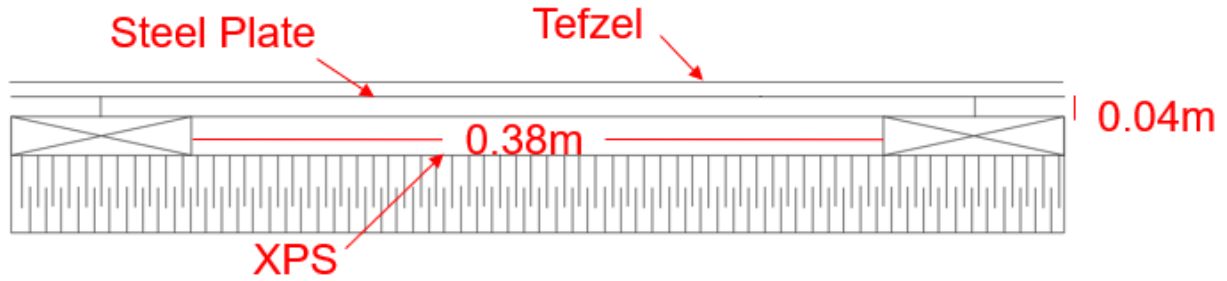


Figure 3.6 Experimental cavity dimensions and materials.

Measured experimental outlet temperature values taken at 14 points from the inlet, were compared with 14 simulated outlet temperature values taken at the same distance from the inlet, with the values seen in Table 3.1.

Table 3.1 Experimental measured and simulated values

Point	Distance from inlet (m)	Measured Outlet Temperature °C for 0.26m/s test	Calibrated Simulated Outlet Temperature °C for 0.26m/s test	Measured Outlet Temperature °C for 1.5m/s test	Calibrated Simulated Outlet Temperature °C for 1.5m/s test
1	0	20	20	20	20
2	0.06	27	21	24	20.3
3	0.29	27.5	24.7	23	21.6
4	0.52	29	28.1	23	22.7
5	0.75	31	31.1	24	23.9
6	0.98	33	33.8	24.5	25
7	1.21	36	36.3	26	26.1
8	1.44	38	38.5	26.5	27.1
9	1.67	39	40.4	27	28.2
10	1.9	40.5	42.2	28	29.2
11	2.13	41	43.8	29.5	30.1
12	2.36	43	45.2	31	31
13	2.59	44	46.4	31	31.9
14	2.74	45	47.2	30	32.5

3.3.1 Model Calibration

Iterations of the simulation were run using the experimental BIPV/T cavity dimensions along with the environmental conditions. The convective heat transfer coefficients, sky temperature assumption, and emissivity values were varied, with the objective of having the simulated outlet temperature approach the experimental outlet temperature values.

3.3.1.1 Model Convective Heat Transfer Coefficients (CHTC)

Nusselt numbers developed from BIPV/T experimental correlations from Candanedo et al., (2011) were used in the model to determine the convective heat transfer from the cavity surfaces.

Cavity front side

$$Nu_f = 0.052 * Re^{0.78} * Pr^{0.4} \quad (3.24)$$

Cavity back side

$$Nu_b = 1.017 * Re^{0.471} * Pr^{0.4} \quad (3.25)$$

Iterations were performed with three different exterior convective heat transfer coefficients to find the closest fit to the experimental data.

- $h_o = 5.7 + 3.8 \cdot V_{wind}$ (McAdams, 2006) (3.26)

- $h_o = 8.55 + 2.56 \cdot V_{wind}$ (Test et al., 1981) (3.27)

- $h_o = 11.99 + 2.2 \cdot V_{wind}$ (Sharples & Charlesworth, 1998) (3.28)

The outlet temperatures of the simulation model, as well as the experimental data, with both using a 1.5m/s cavity air velocity, are shown in Figure 3.7. It was found that the Sharples and Charlesworth CHTC correlation provided the most accurate results compared to the McAdams and Test et al., CHTC correlations.

3.3.1.2 Sky Temperature

Original simulations were also run assuming the sky temperature was the same as the 20°C ambient lab temperature. However, after reviewing the experimental details, the Solar Simulator artificial sky usage was noted. Therefore, the sky temperature correlation from (Duffie & Beckman, 2013) was used which resulted in closer results to the measured values when used with the Sharples & Charlesworth CHTC.

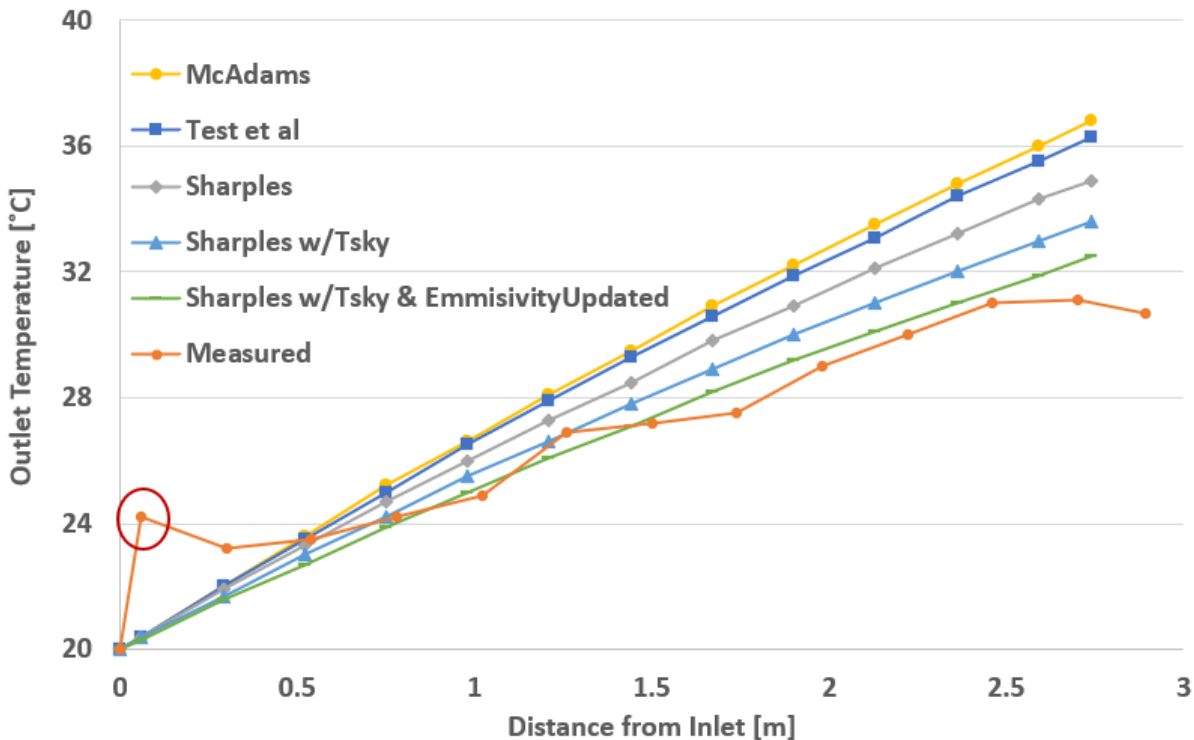


Figure 3.7 Model calibration using 1.5m/s cavity air velocity with simulated & experimental data, with 20°C ambient temperature, 0.0228 m³/s air flow, and 1080W/m² solar irradiance.

3.3.1.3 Emissivity Values

For further improvements, the emissivity values were changed to match the values used by (Candanedo et al., 2011) with the exterior surface of the PV module assumed to be made from Tefzel with an emissivity ε_1 of 0.95. The interior surface of the PV module was assumed to be made from a steel plate with an emissivity ε_2 of 0.80. The back surface of the cavity was assumed to be made from XPS insulation with an emissivity ε_3 of 0.20.

3.3.2 Model Validation Results

Using these parameters, the CV-RMSE was determined to be 5.3% and the NMBE was determined to be -1.8% when using the measured experimental data from Yang & Athienitis, (2014) as seen in Table 3.1, for the cavity air velocity of 1.5m/s test. The differences in the results are seen to be greatest at point two of the measured data, where the entrance effects had an influence on the cavity air temperature. If this point is removed from the CV-RMSE calculation, the percentage is improved to 3.9%. The (ASHRAE, 2014) criteria for a validated model is <30% for CV-RSME and <+/-10% for NMBE. Both CV-RMSE and NMBE determined were within the validated model range.

As well, the measured experimental results using a 0.26m/s cavity air velocity, were compared with the simulated values as seen in Figure 3.8. Using equations 3.22 & 3.23 resulted in a CV-RMSE of 6.6%, and a NMBE of -2.4%. The same entrance effect can be seen to occur at point two of the measured data, and when removed from the calculation the CV-RMSE improved to 4.8%. Both CV-RSME and NMBE percentages were also within the validated model range.

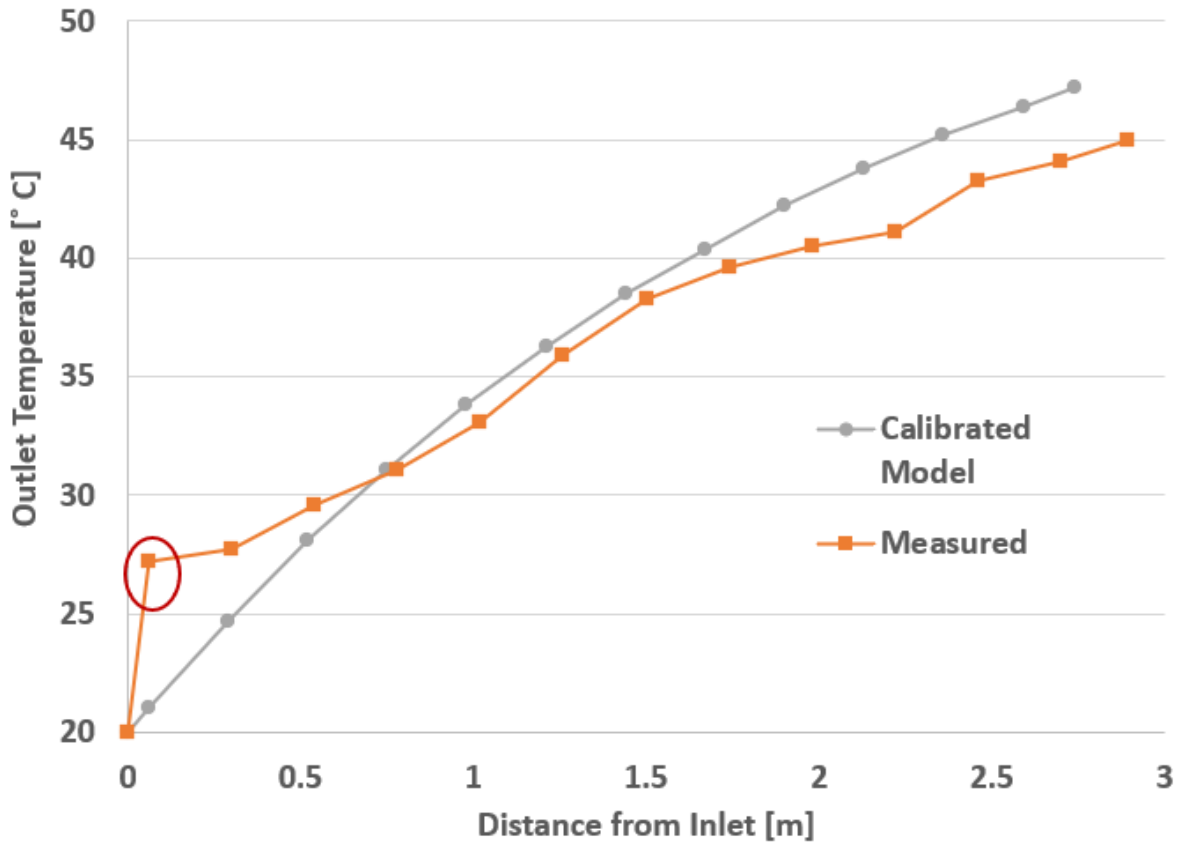


Figure 3.8 Outlet temperature using simulated & experimental data, with 0.26m/s cavity air velocity, 20°C ambient temperature, 0.0228 m³/s air flow, and 1080W/m²solar irradiance.

Table 3.2 Model calibration results & validation criteria

Index	ASHRAE-14 2014 Validation Criteria	1.5 m/s Experiment	0.26m/s Experiment
NMBE	<+/-10%	-1.8%	-2.4%
CV-RMSE	<30%	5.3%	6.6%

3.4 Weather Data

To obtain the BIPV/T system outputs for a specific location, hourly weather data was required to be input into the calibrated model. Local weather data for dew point temperature, dry bulb temperature, and wind speed for the community of Quaqtaq, QC were obtained from Environment and Climate Change Canada's (ECCC 2020) historical weather files which are based on the local weather station operated by NAV Canada at the Quaqtaq airport.

- Climate ID 7116273
- Latitude 61°02'47.000" N
- Longitude 69°37'04.00" W
- Elevation 32.30m

3.4.1 Dew Point Temperature, Dry Bulb Temperature, Wind Speed

The hourly values of the dew point temperature, dry bulb temperature and wind speed were averaged for each month based on the 2017 ECCC Quaqtaq, QC weather file and can be seen in Figures 3.9, 3.10 & 3.11. Color scales were added to the tables to facilitate analysis of the monthly trends. July and August were the warmest months with the average hourly ambient temperature remaining below 10°C for the entire year. The coldest month was seen to be in February with the lowest hourly average temperature of -22.8°C obtained. It was noticed that the average hourly monthly temperatures were only above zero for the entire day in June, July, August, and September.

	Jan	Feb	Mar	Apr	May	Jun	Jul	Aug	Sep	Oct	Nov	Dec
0	-20.5	-25.6	-21.6	-15.5	-5.5	-0.5	4.0	4.1	1.4	-2.9	-10.3	-15.5
1	-20.4	-25.5	-21.7	-15.7	-5.7	-0.6	4.0	3.9	1.3	-2.9	-10.1	-15.5
2	-20.7	-25.7	-21.9	-16.0	-5.9	-0.5	4.0	3.9	1.5	-2.7	-10.3	-15.6
3	-20.5	-25.4	-22.0	-16.1	-5.7	-0.5	4.0	3.9	1.4	-2.8	-10.1	-15.5
4	-20.6	-25.5	-21.9	-16.4	-5.6	-0.4	3.6	3.9	1.7	-2.5	-9.2	-15.5
5	-20.4	-25.6	-21.7	-16.5	-5.5	-0.2	4.2	4.1	1.4	-2.7	-8.8	-11.5
6	-20.5	-25.7	-21.6	-16.1	-5.3	0.0	4.3	4.6	1.4	-2.8	-9.9	-14.6
7	-20.2	-25.9	-21.5	-15.5	-5.0	0.1	4.5	5.0	1.8	-2.7	-9.8	-14.5
8	-20.5	-25.7	-20.8	-14.6	-4.7	0.2	4.6	5.1	2.0	-2.6	-9.9	-15.5
9	-20.4	-25.5	-20.3	-14.4	-4.6	0.3	4.6	5.1	1.9	-2.3	-9.4	-15.4
10	-20.2	-25.1	-19.9	-14.0	-4.5	0.3	4.4	5.3	2.0	-2.5	-9.5	-15.7
11	-20.1	-24.6	-19.4	-13.6	-4.4	0.6	4.2	5.3	2.0	-2.5	-9.7	-14.1
12	-20.0	-23.9	-18.7	-13.3	-4.3	0.7	4.3	5.4	2.0	-2.5	-9.4	-15.8
13	-19.9	-23.4	-18.7	-13.2	-4.1	0.8	4.3	5.3	1.7	-2.3	-9.9	-15.8
14	-20.1	-23.3	-18.7	-13.1	-3.9	0.7	4.2	5.1	1.6	-2.2	-10.0	-16.1
15	-20.2	-23.5	-18.6	-12.8	-4.0	0.8	4.0	4.9	1.5	-2.3	-10.1	-16.1
16	-20.3	-23.9	-18.9	-13.1	-4.0	0.8	4.1	4.8	1.5	-2.4	-10.2	-12.3
17	-20.6	-24.3	-19.1	-13.2	-4.1	0.5	4.1	4.6	1.4	-2.6	-10.4	-16.5
18	-20.2	-24.5	-19.7	-13.5	-4.1	0.5	3.9	4.4	1.5	-2.6	-10.5	-15.5
19	-20.7	-24.8	-20.0	-13.0	-4.3	0.3	4.1	4.3	1.5	-2.6	-10.4	-13.5
20	-20.8	-25.0	-20.3	-14.0	-4.3	0.1	4.2	4.1	1.4	-2.6	-10.2	-16.2
21	-20.8	-25.0	-20.6	-13.8	-4.5	0.0	3.9	4.1	1.4	-2.7	-10.5	-13.5
22	-20.8	-25.1	-20.9	-13.8	-4.8	-0.1	4.1	4.2	1.4	-2.8	-10.2	-14.8
23	-20.6	-25.2	-21.0	-14.8	-4.9	-0.3	4.1	4.2	1.4	-2.8	-9.7	-15.9

Figure 3.9 2017 Quaqtaq monthly hourly average dew point temperature [°C]

	Jan	Feb	Mar	Apr	May	Jun	Jul	Aug	Sep	Oct	Nov	Dec
0	-17.4	-22.5	-18.6	-12.8	-3.5	1.0	6.0	5.7	3.6	-0.5	-6.9	-12.0
1	-17.3	-22.5	-18.8	-13.1	-3.7	0.8	6.0	5.5	3.5	-0.4	-6.8	-12.1
2	-17.6	-22.6	-19.0	-13.3	-4.1	0.8	5.8	5.6	3.4	-0.4	-6.8	-12.2
3	-17.5	-22.4	-19.1	-13.5	-4.0	0.9	5.7	5.6	3.4	-0.5	-6.7	-12.1
4	-17.5	-22.4	-19.1	-13.8	-3.8	1.0	5.0	5.2	3.0	-0.4	-6.1	-12.2
5	-17.3	-22.7	-19.0	-13.8	-3.3	1.4	6.1	5.6	3.3	-0.4	-5.7	-9.0
6	-17.4	-22.7	-18.9	-13.3	-2.9	2.0	6.3	6.1	3.4	-0.3	-6.5	-11.5
7	-17.1	-22.8	-18.6	-12.6	-2.4	2.4	7.2	6.7	3.9	-0.2	-6.5	-11.5
8	-17.4	-22.6	-17.9	-11.8	-1.9	2.8	7.7	7.2	4.3	-0.1	-6.6	-12.3
9	-17.4	-22.2	-17.3	-11.2	-1.3	3.2	8.5	7.6	4.6	0.2	-6.1	-12.1
10	-17.2	-21.9	-16.6	-10.5	-0.8	3.5	9.0	7.9	4.8	0.5	-6.3	-12.3
11	-17.0	-21.2	-16.1	-10.1	-0.3	4.1	8.9	8.1	5.0	0.6	-6.2	-11.0
12	-16.9	-20.6	-15.5	-9.8	-0.1	4.5	9.2	8.3	5.4	0.6	-5.9	-12.3
13	-16.8	-20.2	-15.3	-9.6	0.0	4.5	9.2	8.3	5.3	0.7	-6.1	-12.3
14	-16.9	-20.1	-15.1	-9.3	0.1	4.5	9.3	8.1	5.3	0.7	-6.3	-12.7
15	-17.1	-20.4	-15.2	-9.2	0.0	4.5	9.2	8.0	5.2	0.6	-6.4	-12.9
16	-17.3	-20.9	-15.6	-9.5	-0.3	4.5	8.8	7.6	5.0	0.4	-6.3	-9.8
17	-17.5	-21.4	-16.0	-9.8	-0.6	4.0	8.1	7.3	4.6	0.1	-6.5	-13.1
18	-17.1	-21.7	-16.7	-10.5	-1.0	3.5	7.8	6.9	4.3	-0.1	-6.7	-12.4
19	-17.6	-21.9	-17.0	-10.3	-1.6	3.1	7.5	6.5	4.0	-0.3	-6.5	-10.8
20	-17.7	-22.1	-17.4	-11.2	-2.1	2.6	7.0	6.2	3.9	-0.1	-6.4	-12.9
21	-17.7	-22.1	-17.7	-11.1	-2.5	1.9	6.3	5.9	3.8	-0.2	-6.7	-10.7
22	-17.8	-22.2	-18.0	-11.2	-2.9	1.5	6.3	5.9	3.7	-0.3	-6.7	-11.7
23	-17.4	-22.3	-18.1	-12.1	-3.0	1.4	6.1	5.8	3.6	-0.4	-6.4	-12.6

Figure 3.10 2017 Quaqtq monthly hourly average dry bulb temperature [°C]

The monthly wind speed trends for Quaqtq as seen in Figure 3.11, show that the windiest months are October and November, with the highest average hourly speed of 9.0 m/s obtained. The calmest months were seen to be in February, May, June, July, and August with the lowest average hourly wind speed of 3.8 m/s obtained.

	Jan	Feb	Mar	Apr	May	Jun	Jul	Aug	Sep	Oct	Nov	Dec
0	6.6	4.2	5.5	5.0	4.6	4.1	4.4	4.2	6.0	7.9	7.8	6.1
1	6.0	3.9	5.8	5.2	4.3	4.6	4.9	4.3	6.1	8.0	7.3	6.4
2	6.2	4.1	5.6	5.2	4.4	4.6	4.9	4.0	5.8	8.0	7.1	6.3
3	6.2	4.2	5.6	5.2	4.0	4.7	4.8	4.0	5.9	8.5	7.1	6.4
4	6.6	4.5	6.0	5.0	4.1	4.0	3.8	4.0	4.5	7.7	7.0	6.4
5	6.2	4.6	5.8	4.7	4.3	4.6	4.7	4.3	6.4	9.0	6.9	5.1
6	6.7	4.4	5.9	5.2	4.4	4.8	4.8	4.3	6.6	8.7	7.6	6.3
7	6.5	4.9	5.9	5.1	4.2	5.1	5.5	4.7	6.1	9.0	7.5	6.7
8	6.7	4.6	5.9	6.0	4.3	5.3	5.3	4.8	6.9	8.3	7.8	6.7
9	6.7	4.5	6.1	5.8	4.7	5.6	5.5	4.6	6.5	8.8	7.3	6.7
10	6.9	4.3	6.3	6.4	4.6	5.3	5.3	4.9	6.6	8.6	6.5	6.5
11	7.5	4.5	6.2	6.4	5.2	5.6	5.4	5.2	7.0	8.6	7.4	5.2
12	7.1	4.6	6.5	6.8	5.4	5.4	5.4	5.0	6.9	8.5	7.5	6.6
13	7.2	4.9	6.7	6.6	5.5	5.4	5.8	5.1	7.2	8.4	8.3	6.7
14	6.9	4.8	6.6	7.1	5.6	5.7	6.0	5.1	7.3	7.4	8.1	6.4
15	7.3	4.8	6.5	6.6	5.2	5.5	5.8	4.9	7.0	7.0	8.0	6.0
16	6.1	4.2	6.6	6.5	5.2	5.7	5.5	4.7	6.9	7.1	8.3	5.2
17	6.3	4.0	6.3	6.6	4.9	5.5	5.5	4.7	6.6	7.3	8.0	6.0
18	5.9	4.2	6.3	6.0	4.8	5.3	5.4	4.3	6.1	7.4	7.9	5.9
19	6.9	3.8	5.8	6.1	4.7	5.4	5.7	4.0	5.6	7.5	8.1	5.5
20	6.2	3.9	6.2	5.7	4.4	5.0	5.7	4.4	6.1	8.0	7.6	5.9
21	7.0	3.9	6.0	5.3	4.4	4.5	5.0	4.3	6.1	8.0	7.9	5.2
22	6.5	3.9	6.2	5.5	4.3	4.1	5.0	3.9	6.2	7.9	6.8	6.0
23	6.9	4.0	5.9	5.4	4.4	3.8	4.8	4.1	6.5	8.2	6.8	6.1

Figure 3.11 2017 Quaqtq monthly hourly average wind speed [m/s]

3.4.2 Sky Temperature

The following correlation has been used to determine the sky temperature T_{sky} for Quaqtq.

$$T_{sky} = T_a \cdot [0.711 + 0.0056 \cdot T_{dp} + 0.000073 \cdot T_{dp}^2 + 0.013 \cos(15t)]^{1/4} \quad (3.29)$$

(Duffie and Beckman, 2013)

Dew point temperatures (T_{dp}) and the dry bulb temperature (T_a) are taken from ECCC historical data. Where t is the hours from midnight.

The following sky temperature correlation from (Anderson et al., 2009), was also used.

$$T_{sky} = 0.037536 \cdot (T_a)^{1.5} + 0.32 \cdot T_a \quad (3.30)$$

(Anderson et al., 2009)

However, the sky temperatures obtained using (3.30) were higher than the ambient temperatures for ambient temperatures below 0°C, therefore the Duffie & Beckman, (2013) equation was used for the simulation data tables shown in Figure 3.12. The sky temperature reaches its minimum value of -51.8°C in February and maximum value of -12.5°C in July.

	Jan	Feb	Mar	Apr	May	Jun	Jul	Aug	Sep	Oct	Nov	Dec
0	-44.4	-50.0	-45.7	-39.0	-26.9	-20.5	-13.5	-13.8	-17.2	-23.0	-31.9	-38.3
1	-44.3	-50.0	-45.9	-39.4	-27.3	-20.8	-13.7	-14.1	-17.3	-23.0	-31.8	-38.4
2	-44.8	-50.3	-46.3	-39.7	-27.8	-20.9	-13.9	-14.2	-17.5	-23.0	-31.9	-38.6
3	-44.8	-50.2	-46.6	-40.1	-27.8	-20.9	-14.2	-14.4	-17.6	-23.3	-32.0	-38.6
4	-45.1	-50.4	-46.8	-40.7	-27.8	-21.1	-15.3	-15.0	-18.1	-23.3	-31.4	-39.0
5	-45.2	-51.0	-46.9	-41.0	-27.6	-20.8	-14.2	-14.8	-18.4	-23.7	-31.1	-35.1
6	-45.6	-51.3	-47.1	-40.8	-27.4	-20.5	-14.3	-14.3	-18.5	-23.9	-32.6	-38.7
7	-45.5	-51.7	-47.2	-40.2	-27.1	-20.3	-13.6	-13.9	-18.2	-24.1	-32.9	-39.0
8	-46.2	-51.8	-46.7	-39.5	-26.8	-20.2	-13.4	-13.6	-18.0	-24.2	-33.2	-40.2
9	-46.4	-51.7	-46.3	-39.1	-26.5	-20.0	-12.9	-13.4	-17.9	-24.1	-32.8	-40.3
10	-46.4	-51.5	-45.8	-38.7	-26.2	-20.0	-12.7	-13.2	-17.9	-24.1	-33.2	-40.8
11	-46.3	-51.0	-45.3	-38.3	-25.8	-19.4	-13.0	-13.2	-17.8	-24.1	-33.3	-39.2
12	-46.2	-50.3	-44.6	-37.9	-25.6	-19.1	-12.7	-13.0	-17.5	-24.1	-33.0	-41.0
13	-46.1	-49.8	-44.4	-37.6	-25.4	-19.0	-12.8	-13.0	-17.7	-23.9	-33.4	-40.9
14	-46.1	-49.6	-44.1	-37.3	-25.1	-18.8	-12.5	-13.2	-17.6	-23.8	-33.5	-41.3
15	-46.1	-49.8	-44.0	-36.9	-25.1	-18.6	-12.6	-13.2	-17.6	-23.7	-33.4	-41.2
16	-46.0	-50.0	-44.2	-37.0	-25.1	-18.4	-12.7	-13.4	-17.6	-23.7	-33.1	-37.0
17	-46.0	-50.2	-44.3	-37.0	-25.1	-18.6	-13.0	-13.4	-17.7	-23.8	-33.1	-41.0
18	-45.3	-50.2	-44.7	-37.4	-25.1	-18.9	-13.0	-13.7	-17.6	-23.7	-32.9	-39.8
19	-45.5	-50.2	-44.8	-36.8	-25.5	-19.1	-13.0	-13.8	-17.6	-23.6	-32.4	-37.4
20	-45.3	-50.1	-44.9	-37.7	-25.7	-19.4	-13.2	-13.9	-17.5	-23.2	-32.0	-39.8
21	-45.1	-49.9	-45.0	-37.3	-25.9	-19.8	-13.7	-13.9	-17.4	-23.0	-32.1	-36.8
22	-44.9	-49.8	-45.2	-37.2	-26.2	-20.0	-13.4	-13.7	-17.2	-22.9	-31.8	-37.9
23	-44.5	-49.8	-45.2	-38.1	-26.3	-20.1	-13.5	-13.7	-17.2	-23.0	-31.2	-38.9

Figure 3.12 2017 Quaqtq monthly hourly average sky temperature [°C]

3.4.3 Solar Irradiance

Solar irradiance data for Quaqtac was not collected by ECCC therefore alternative methods were required to approximate the hourly total surface irradiance. The first method uses a Clear Sky Model with Cloudiness values recorded by ECCC. The second method uses satellite derived weather data obtained from Canadian Weather Energy and Engineering Datasets CWEEDS from the weather stations of Iqaluit, NU and Kuujjuaq, QC interpolated for Quaqtac, QC.

3.4.3.1 Clear Sky Irradiance

Hottel's clear sky model (Hottel, 1976) and correlations from (Liu & Jordan, 1960), were used to estimate the total clear sky solar radiation for a surface azimuth of 0° due south and tilt angles of 90°, 80° and 10°. Where the 10° tilt angle is based on the roof slope of the NHP.

The similar geographic coordinates as the Quaqtac airport were used in the clear sky model.

- 61° 02'N
- 69 °37' W
- Elevation: 32m
- Local Standard Meridian 75

The beam surface radiation I_{bs} , diffused surface radiation I_{ds} and ground reflected surface radiation I_{rs} were calculated using the correlations from (Liu & Jordan, 1960). These three components were then added to provide the total surface radiation I_{st} .

$$I_{st} = I_{bs} + I_{ds} + I_{rs} \quad (3.31)$$

I_{on} is the extraterrestrial solar radiation which is a function of I_{sc} the solar constant and day of the year. The value ranges by +/- 3% depending on the earth's distance to the sun. Where the value for January 02 is 1412 W/m² and July 02 is 1321.9 W/m².

$$I_{on} = I_{sc} \left(1 + 0.033 \cos \left(2\pi \frac{n}{365} \right) \right) \quad (3.32)$$

$$I_{sc} = 1367 \text{ W/m}^2$$

The apparent solar time AST is used to give the exact sun position in the sky and is a function of the local standard time LST, geographic longitude of the specific location LON and the equation of time ET.

$$AST = LST + 4 \left(\frac{\text{min}}{\text{deg}} \right) (LSM - LOM) + ET \quad (3.33)$$

The equation of time ET is a correction factor used to account for irregularities in Earth's orbit and is a function of the day of the year n .

$$ET(n) = 9.87 \sin \left(4\pi \cdot \frac{n - 81}{364} \right) - 7.53 \cdot \cos \left(2\pi \cdot \frac{n - 81}{364} \right) - 1.5 \cdot \sin \left(2\pi \cdot \frac{n - 81}{364} \right) \quad (3.34)$$

The solar altitude α is the angle between the horizon and the sun rays. It is a function of the hour angle ha which gives the angle of the sun rays before or after solar noon. As well the ha depends on the declination angle δ which is account for Earth's axis tilt of 23.5° and its effect on the sun path. The third factor in the ha equation is the geographic latitude LAT of the location.

$$\alpha = \text{asin} [\cos(LAT) \cdot \cos(\delta) \cdot \cos(ha) + \sin(LAT) \cdot \sin(\delta)] \quad (3.35)$$

$$ha = 15 \frac{deg}{hr} (LST - 12hr) \quad (3.36)$$

$$\delta = 23.45 \cdot \sin\left(2\pi \cdot \frac{284 + n}{365}\right) \text{deg} \quad (3.37)$$

The solar azimuth angle φ is the angle of the sun's rays from a south facing surface.

$$\varphi = \text{acos}\left(\frac{\sin(\alpha) \cdot \sin(LAT) - \sin(\delta)}{\cos(\alpha) \cdot \cos(LAT)}\right) \cdot \frac{ha}{[ha]} \quad (3.38)$$

The zenith angle z is the complement of the solar altitude.

$$z = 90 - \alpha \quad (3.39)$$

The direct beam normal radiation I_{bn} is the irradiance on surface perpendicular to the sun's rays.

$$I_{bn} = \tau_b \cdot I_{on} \quad (3.40)$$

Hotel's Clear Sky model was used to determine the transmittance of the direct beam τ_b radiation through Earth's atmosphere.

$$\tau_b = a_0 + a_1 \cdot e^{-\frac{k}{\cos(z)}} \quad (3.41)$$

Table 3.3 Climate correction factor table

	r_0	r_1	r_k
Sub-Arctic Average	1.02	1	1
Sub-Arctic Summer	0.97	0.99	1.02
Sub-Arctic Winter	1.05	1.01	0.99

Using Hottel's Correction Factors for Climate Types seen in Table 3.3, from Duffie & Beckman, (2013), coefficients for the Subarctic winter were determined by using the summer values for Midlatitude and Subarctic then interpolating with the Midlatitude winter values. The average Subarctic values were then used to calculate the beam transmittance τ_b for each hour of the year. The location's altitude A is measured in km above sea level.

$$a_0 = r_0(0.4237 - 0.00821 \cdot (6 - A)^2) \quad (3.42)$$

$$a_1 = r_1(0.5055 + 0.00595 \cdot (6.5 - A)^2) \quad (3.43)$$

$$k = r_k(0.2711 + 0.01858 \cdot (2.5 - A)^2) \quad (3.44)$$

The horizontal diffuse transmittance τ_{dh} has been determined using the correlations from Liu and Jordan, (1960) which uses the beam transmittance previously determined. From this the diffused horizontal radiation I_{dh} is determined using the extraterrestrial solar radiation I_{on} and the solar altitude α .

$$\tau_{dh} = 0.2710 - 0.2939 \cdot \tau_b \quad (3.45)$$

$$I_{dh} = \tau_{dh} \cdot I_{on} \cdot \sin(\alpha) \quad (3.46)$$

The beam direct radiation component on the surface I_{bs} is determined using the angle of incident θ , the solar azimuth φ , the surface azimuth ψ , and the solar surface azimuth γ .

$$\gamma = \varphi - \psi \quad (3.47)$$

$$\theta = \text{acos} [\cos(\alpha) \cdot \cos([\gamma]) \cdot \sin(\beta) + \sin(\alpha) \cdot \cos(\beta)] \quad (3.48)$$

$$I_{bs} = I_{bn} \cdot \cos(\theta) \quad (3.49)$$

The diffused surface radiation I_{ds} is then determined, assuming isotropic distribution of the diffused radiation, using the surface tilt angle β , in this case the BIPV/T surface and the diffused horizontal radiation I_{dh} .

$$I_{ds} = I_{dh} \cdot \frac{1 + \cos(\beta)}{2} \quad (3.50)$$

The reflected ground radiation I_{rs} from a horizontal surface was determined using both the horizontal diffuse transmittance τ_{dh} and the transmittance of the direct beam τ_b along with the solar altitude α and the surface tilt angle β using equation (3.47). As well as the reflectance ρ of the ground surface, which is of importance and will be discussed in more detail in section 3.4.4.

$$I_{rs} = [I_{on} \cdot \sin(\alpha) \cdot (\tau_{dh} + \tau_b)] \cdot \rho \cdot \frac{1 - \cos(\beta)}{2} \quad (3.51)$$

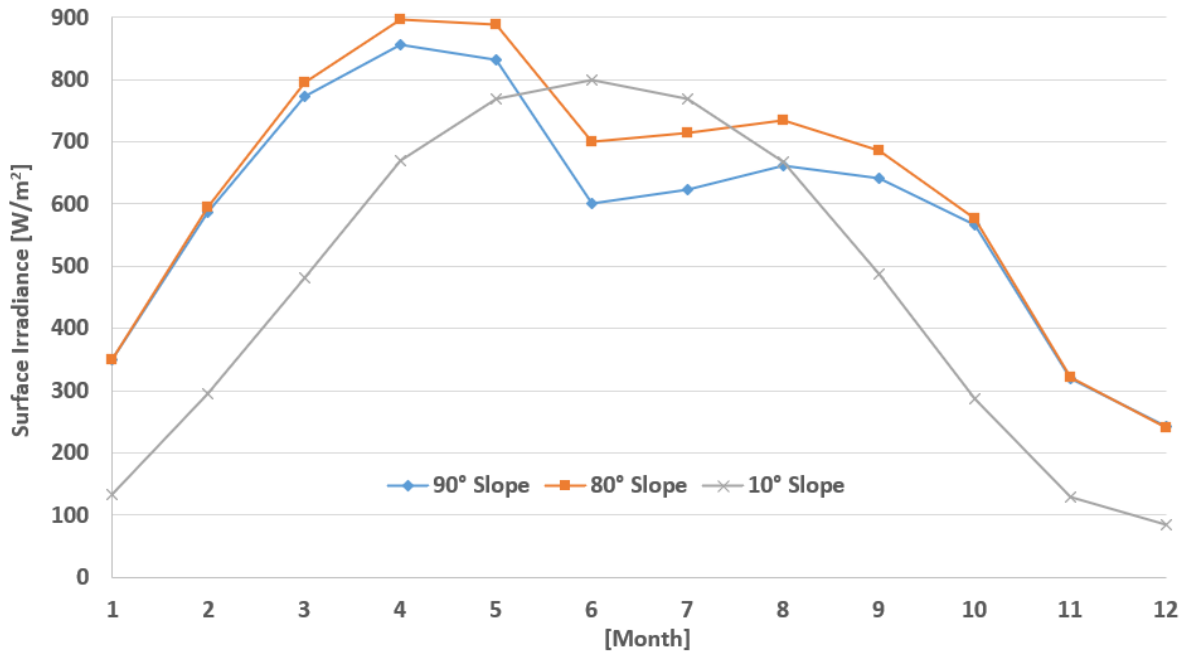


Figure 3.13 Quaqtq clear sky peak south facing surface irradiance for three surface tilt angles.

The total surface radiation I_{st} was then determined for every hour, for each day of the year for three tilt angles of 10°, 80° and 90°. The peak clear sky surface irradiance for three tilt angles can be seen in Figure 3.13. The 80° tilt provides an increased amount of peak irradiance between the months of February to October. As well the 90° and 80° slopes provide higher surface irradiance for all months except for June and July where the 10° slope peaked with its highest values. The peak values for the 90° and 80° tilt angles are seen to be in April where the large tilt angles take advantage of the lower solar altitude and snow reflectance.

	Jan	Feb	Mar	Apr	May	Jun	Jul	Aug	Sep	Oct	Nov	Dec
0	0	0	0	0	0	0	0	0	0	0	0	0
1	0	0	0	0	0	0	0	0	0	0	0	0
2	0	0	0	0	0	0	0	0	0	0	0	0
3	0	0	0	0	4	13	5	0	0	0	0	0
4	0	0	0	1	31	35	24	4	0	0	0	0
5	0	0	0	22	72	59	43	24	1	0	0	0
6	0	0	10	67	118	83	62	46	36	2	0	0
7	0	8	106	215	253	163	135	153	145	80	0	0
8	0	112	262	401	435	321	286	309	304	213	71	0
9	137	251	447	579	602	464	429	458	460	370	203	88
10	220	396	602	717	728	575	540	575	579	498	294	201
11	286	498	697	796	797	637	606	644	644	563	353	241
12	305	527	719	806	802	645	618	655	646	554	346	245
13	263	478	666	746	742	597	576	608	585	473	274	207
14	193	361	544	623	624	499	483	508	469	335	183	164
15	55	215	372	454	463	363	352	369	315	182	40	0
16	0	74	189	266	281	207	202	212	156	52	0	0
17	0	0	54	99	126	89	69	70	40	0	0	0
18	0	0	0	34	79	65	51	32	3	0	0	0
19	0	0	0	4	38	41	32	10	0	0	0	0
20	0	0	0	0	7	19	12	0	0	0	0	0
21	0	0	0	0	0	1	0	0	0	0	0	0
22	0	0	0	0	0	0	0	0	0	0	0	0
23	0	0	0	0	0	0	0	0	0	0	0	0

Figure 3.14 Quaqtq average monthly hourly clear sky 90° surface irradiance 0.7ρ [W/m²]

The complete table of the hourly average surface irradiance values for the 90° tilt for each month can be seen in Figure 3.14. Large seasonal variations in the amount of surface irradiance can be

seen with December having approximately 6 hours of solar irradiance while in June there was approximately 18 hours.

3.4.3.2 Cloud Cover

The 2017 hourly cloud cover data from ECCC was used in combination with the Hotel clear sky irradiance to determine the approximated surface irradiance for Quaqtaq. The measurement of cloud cover was performed by the observational method at the Quaqtaq airport using an oktas scale which assigns a value between 0 and 8 depending on the sky condition, with 0 representing a clear sky and 8 being overcast with a sky cloud coverage greater than 90%. The oktas values were then divided by 8 to obtain a decimal percent which was used as the value of C in the correlation (3.49) from Davies et al., (1984) to determine the beam normal irradiance with the observed cloud cover.

$$I = I_0(1 - C) \quad (3.52)$$

Where I_0 is the clear sky beam normal irradiance and I is the approximated actual beam normal irradiance.

Missing hourly cloud cover values in the ECCC data set during daylight hours were substituted with the daily average cloud cover values obtained from Canada Weather Stats which is based on ECCC's collected data. For days that were missing both hourly and daily average values, an average value of the previous and proceeding days was used.

From the Hotel clear sky calculated beam normal irradiance I_{bn} the new beam surface irradiance I_{bs} , and a portion of the ground reflected irradiance I_{rs} were calculated incorporating the cloud cover data. The original clear sky horizontal diffused irradiance I_{dh} was still used and was also

utilized in the second portion of the alternative ground reflected irradiance I_{rs} correlation (3.50) and total surface irradiance I_{st} calculations (3.28).

$$I_{rs} = (I_{bn} \cdot \sin(\alpha) + I_{ah}) \cdot \rho \cdot \frac{1 - \cos(\beta)}{2} \quad (3.53)$$

	Jan	Feb	March	April	May	June	July	August	Sep	Oct	Nov	Dec
0	0	0	0	0	0	0	0	0	0	0	0	0
1	0	0	0	0	0	0	0	0	0	0	0	0
2	0	0	0	0	0	0	0	0	0	0	0	0
3	0	0	0	0	3	12	5	0	0	0	0	0
4	0	0	0	1	26	30	22	4	0	0	0	0
5	0	0	0	18	52	45	37	21	1	0	0	0
6	0	0	8	51	73	57	48	38	20	1	0	0
7	0	5	70	112	112	80	70	70	54	25	0	0
8	0	45	151	199	137	121	104	86	84	58	17	0
9	38	102	260	246	169	158	125	126	111	90	61	26
10	64	148	316	314	177	181	157	143	120	108	78	69
11	90	173	337	306	239	192	179	147	155	123	116	79
12	89	196	384	301	254	185	190	140	138	118	117	86
13	76	156	350	247	238	183	173	142	139	113	85	70
14	50	131	319	240	209	175	141	104	113	88	50	49
15	15	84	228	192	168	128	111	94	89	54	4	0
16	0	29	118	128	124	88	86	80	50	15	0	0
17	0	0	33	66	78	59	51	47	20	0	0	0
18	0	0	11	28	56	49	42	28	3	0	0	0
19	0	0	0	3	30	35	29	9	0	0	0	0
20	0	0	0	0	5	17	11	0	0	0	0	0
21	0	0	0	0	0	1	0	0	0	0	0	0
22	0	0	0	0	0	0	0	0	0	0	0	0
23	0	0	0	0	0	0	0	0	0	0	0	0

Figure 3.15 Quaqtaq average monthly hourly 90° surface irradiance using clear sky with 0.7 snow reflectance with cloud cover values [W/m²]

Figure 3.15 shows the average monthly hourly surface irradiance values for a clear sky combined with cloud cover values. Average values for each month were used to smooth out the fluctuations caused from the variable sky clearness from day to day and allows for more accurate irradiance

data to be used for energy modeling. Peak clear sky values can be seen to occur in April from Figure 3.14 while the peak values for the cloud cover irradiances occur in March, which is due to the increased cloud cover during April and May.

3.4.3.3 Canadian Weather Energy and Engineering Datasets

The second method used to estimate surface irradiance was based on satellite-derived data from the Canadian Weather Energy and Engineering Datasets (CWEEDS), which has been established by satellite-derived estimates from the State University of New York (SUNY) methods. 2017 CWEEDS beam normal I_{bn} and horizontal diffused I_{dh} datasets for the two closest stations to Quaqtac were obtained for the cities of Iqaluit, NU 63°N, and Kuujjuaq, QC 58°N as seen in Figure 3.16.

The beam normal I_{bn} and horizontal diffused I_{dh} datasets were then used to determine the hourly beam surface irradiance I_{bs} with equation (3.48), surface diffused irradiance I_{ds} with equation (3.49), and ground reflected surface solar irradiance I_{rs} with equation (3.53).

$$I_{bs} = I_{bn} \cdot \cos(\theta) \quad (3.49)$$

$$I_{ds} = I_{dh} \cdot \frac{1 + \cos(\beta)}{2} \quad (3.50)$$

$$I_{rs} = (I_{bn} \cdot \sin(\alpha) + I_{dh}) \cdot \rho \cdot \frac{1 - \cos(\beta)}{2} \quad (3.53)$$

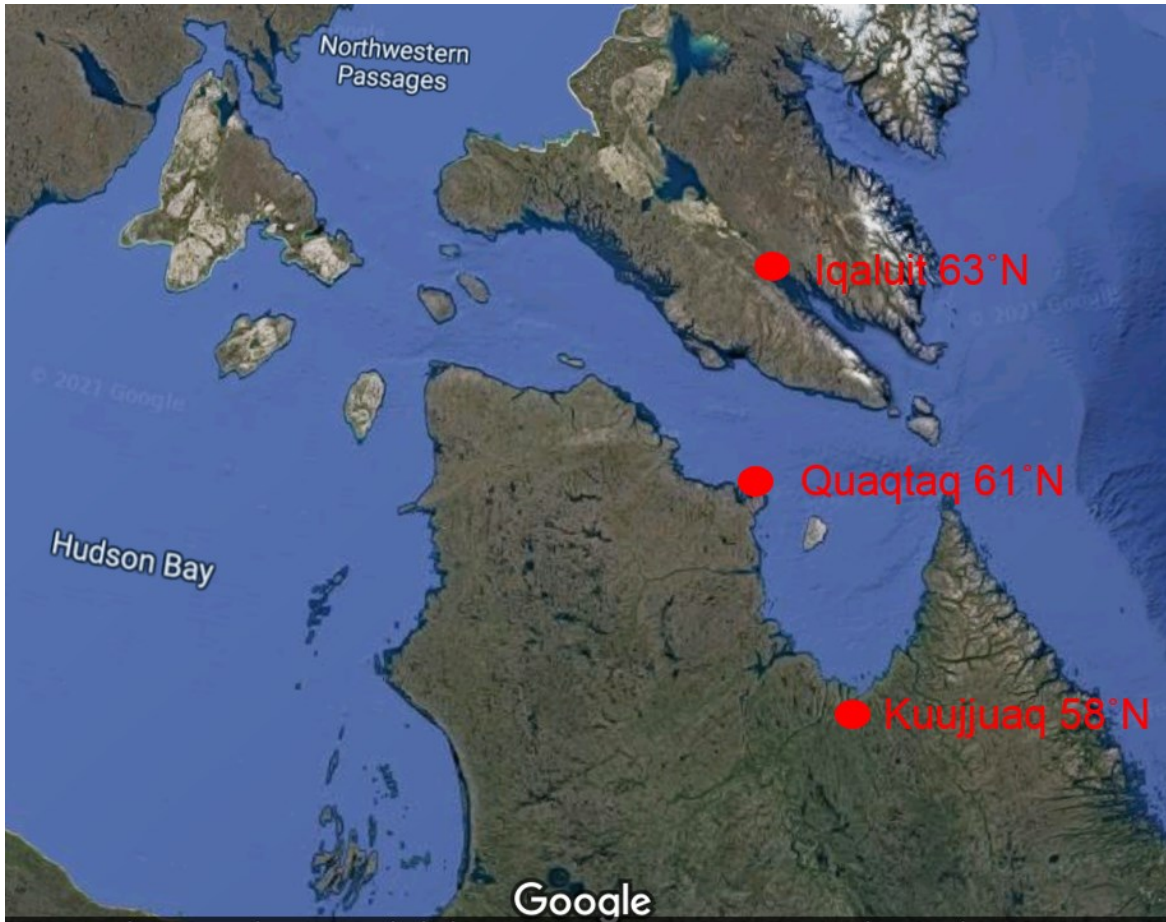


Figure 3.16 Weather stations of Iqaluit 63°N, Quaqtuaq 61°N & Kuujjuaq 58°N (Google, 2021)

	Jan	Feb	Marc	April	May	June	July	Augu	Sep	Oct	Nov	Dec
0	0	0	0	0	0	0	0	0	0	0	0	0
1	0	0	0	0	0	0	0	0	0	0	0	0
2	0	0	0	0	0	0	0	0	0	0	0	0
3	0	0	0	0	0	0	0	0	0	0	0	0
4	0	0	0	0	9.7	16	8	0	0	0	0	0
5	0	0	0	7.4	56	41	30	9.9	0	0	0	0
6	0	0	2.3	54	115	73	62	36	8.3	0	0	0
7	0	25	72	163	239	120	108	98	42	18	5	0
8	13	221	249	304	401	204	183	188	107	104	87	3.5
9	124	398	436	427	541	287	260	277	176	226	193	154
10	232	489	554	547	638	359	324	350	228	272	261	208
11	294	514	655	611	691	406	371	395	264	299	283	266
12	278	498	658	637	677	417	387	413	287	301	242	241
13	225	454	639	598	641	407	357	404	300	255	182	161
14	113	288	567	522	563	353	314	349	261	198	78	5.7
15	2.9	137	442	380	430	273	243	268	194	130	1.2	0
16	0	8.9	281	258	292	174	171	166	104	55	0	0
17	0	0	106	135	169	105	106	80	40	5	0	0
18	0	0	11	64	105	74	72	45	8.8	0	0	0
19	0	0	0	14	55	44	41	19	0.1	0	0	0
20	0	0	0	0	14	21	16	1.6	0	0	0	0
21	0	0	0	0	0	2.4	0.5	0	0	0	0	0
22	0	0	0	0	0	0	0	0	0	0	0	0
23	0	0	0	0	0	0	0	0	0	0	0	0

Figure 3.17 CWEEDS average hourly 90° south facing surface irradiance for Kuujjuaq [W/m²]

	Jan	Feb	Marc	April	May	June	July	Augu	Sep	Oct	Nov	Dec
0	0	0	0	0	0	0	0	0	0	0	0	0
1	0	0	0	0	0	0	0	0	0	0	0	0
2	0	0	0	0	0	0	0	0	0	0	0	0
3	0	0	0	0	2.9	10	3.5	0	0	0	0	0
4	0	0	0	0.3	28	28	19	1.7	0	0	0	0
5	0	0	0	17	73	55	42	16	0.1	0	0	0
6	0	0	3.4	71	127	85	71	41	8.6	0	0	0
7	0	7.7	74	216	249	141	122	116	53	3.9	0.2	0
8	0.2	142	262	408	390	224	194	208	119	55	12	0
9	20	313	459	581	518	318	274	293	179	124	65	1.7
10	75	401	619	697	631	404	350	359	215	180	111	24
11	110	441	689	738	710	455	407	406	257	219	128	46
12	117	474	649	728	720	440	413	413	267	226	115	29
13	76	426	654	724	692	423	383	389	277	222	68	2.3
14	7.4	288	605	647	609	374	343	334	241	173	5.3	0
15	0	91	457	506	467	280	267	256	180	107	0	0
16	0	2.1	270	330	311	190	186	169	107	32	0	0
17	0	0	93	145	167	115	112	83	41	2	0	0
18	0	0	10	66	116	85	83	47	9.1	0	0	0
19	0	0	0	21	69	58	53	22	0.3	0	0	0
20	0	0	0	1.1	30	33	27	4.9	0	0	0	0
21	0	0	0	0	5.7	14	9	0	0	0	0	0
22	0	0	0	0	0	1.3	0.1	0	0	0	0	0
23	0	0	0	0	0	0	0	0	0	0	0	0

Figure 3.18 CWEEEDS average hourly 90° south facing surface irradiance for Iqaluit [W/m²]

The average hourly south facing surface irradiance values for Kuujjuaq, and Iqaluit can be seen in Figures 3.17 and 3.18 for the 90° tilt angle. Both locations can be seen to have peak values in May, however Iqaluit has higher surface irradiance values in from March until August with Kuujjuaq having the higher values for the remainder of the year. It can also be seen that there are seasonal variation differences between Kuujjuaq and Iqaluit where Iqaluit has 19 hours of irradiance in June, while Kuujjuaq has 17. As well in the winter Kuujjuaq has approximately 5 hours of irradiance in December, while Iqaluit has approximately 3 hours. This shows that there can be substantial differences in the irradiance values for locations at different latitudes, even for the 5° difference between Kuujjuaq and Iqaluit.

To improve the approximated irradiance values, the surface irradiance values for Kuujjuaq and Iqaluit were interpolated for the location of Quaqaq, QC 61°N using equation (3.54).

$$y = y_1 + (x - x_1) \left(\frac{y_2 - y_1}{x_2 - x_1} \right) \quad (3.54)$$

Iqaluit latitude $x_1 = 63$

Kuujjuaq latitude $x_2 = 58$

Quaqaq latitude $x = 61$

$y =$ Quaqaq Irradiance

$y_1 =$ Iqaluit Irradiance

$y_2 =$ Kuujjuaq Irradiance

In Figure 3.19 the CWEEDS average hourly data for Kuujjuaq and Iqaluit were interpolated to produce the estimated hourly total south facing surface irradiance. The same trend as what was produced using the Hotel's Clear Sky in Figure 3.14 is obtained where the peak values occur around mid day and in the months of March, April, and May. As well, the seasonal irradiance variations of 18 hours per day in June and 5 hours per day of irradiance in December is similar to the clear sky amounts seen in Figure 3.14.

	Jan	Feb	Mar	Apr	May	Jun	Jul	Aug	Sep	Oct	Nov	Dec
0	0	0	0	0	0	0	0	0	0	0	0	0
1	0	0	0	0	0	0	0	0	0	0	0	0
2	0	0	0	0	0	0	0	0	0	0	0	0
3	0	0	0	0	2	7	2	0	0	0	0	0
4	0	0	0	0	20	25	14	1	0	0	0	0
5	0	0	0	13	63	54	37	14	0	0	0	0
6	0	0	3	60	115	90	67	39	8	0	0	0
7	0	32	70	185	233	147	116	109	48	9	2	0
8	5	194	246	348	379	238	190	200	114	72	39	1
9	60	365	432	493	508	334	268	286	183	159	110	61
10	134	449	570	604	612	419	340	356	222	209	161	95
11	178	474	649	652	679	473	392	402	262	241	181	131
12	176	492	626	653	679	469	402	413	279	246	157	111
13	132	447	622	639	649	452	373	395	289	226	109	65
14	48	303	567	564	569	398	331	340	251	176	32	2
15	1	125	434	428	434	305	257	261	188	112	0	0
16	0	9	263	281	289	204	180	168	108	39	0	0
17	0	0	93	129	158	126	110	82	40	3	0	0
18	0	0	10	60	105	91	79	46	9	0	0	0
19	0	0	0	18	60	58	48	21	0	0	0	0
20	0	0	0	1	23	31	23	4	0	0	0	0
21	0	0	0	0	3	10	6	0	0	0	0	0
22	0	0	0	0	0	1	0	0	0	0	0	0
23	0	0	0	0	0	0	0	0	0	0	0	0

Figure 3.19 2017 CWEEDS Quaqtq interpolated 90° south facing surface irradiance [W/m²] with snow reflectance $\rho=0.7$

3.4.4 Ground Reflectance

3.4.4.1 Snow Cover Period

To determine the snow ground cover period, the 2017 CWEEDS ground snow cover data was used from the two closest stations of Iqaluit, NU 63°N and Kuujjuaq, QC 58°N. In these data sets the snow cover is indicated as a value of 1 for snow cover or 0 for no snow cover. For Iqaluit, snow cover is indicated as 1 from January 01 until June 24 and indicated as 0 from June 25 until September 30 and is indicated as 1 from October 01 until December 31. For Kuujjuaq, the snow

cover is indicated as 1 from January 01 until May 12, is indicated as 0 until May 19 where it is 1 for one day then is 0 until October 07, where it fluctuates between 1 and 0 until October 28 then remains 1 for the remainder of the year. When the snow cover period is interpolated between Kuujjuaq and Iqaluit for Quaqtac the non-snow cover period begins at approximately June 08 and ends October 11, with the days in between considered as snow covered.

3.4.4.2 Reflectivity

The ground reflectivity coefficient ρ has been approximated by two different methods. The first method derived from (Liu & Jordan, 1963) uses the following correlation.

$$\rho = 0.2 \cdot (1 - c) + 0.7c \quad (\text{Liu \& Jordan, 1963}) \quad (3.55)$$

Where c is the fraction of time that the ground is assumed to have over one inch of snow cover. From the CWEEDS weather data the value of c is given as either a 1 or a 0 therefore the Liu & Jordan correlation will provide a ground reflectivity coefficient ρ of 0.7 for periods assumed to have ground snow cover.

The second method uses the typical surface albedo table from (Stull, 2000) that has a range of ρ values of 0.75 to 0.95 for fresh snow. For periods with out snow cover the value of ρ is assumed to be 0.2 which represents the reflectivity of tundra or sandy soil which is the typical ground surface material found in Quaqtac.

Based on these two sources, the value of ρ was set to 0.7 and 0.95 during the snow cover period to obtain a range of values that could be expected during this period to provide a more realistic approximation of the range of snow reflectivity encountered throughout the year.

3.4.5 Peak Surface Irradiance

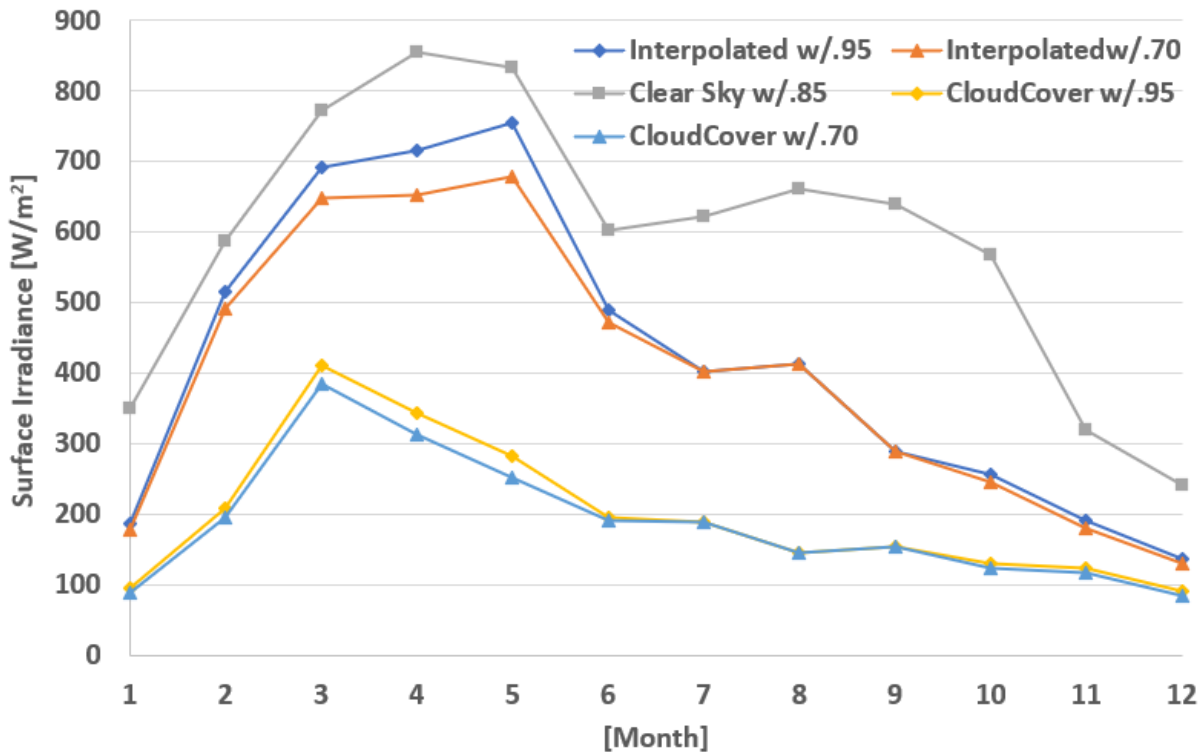


Figure 3.20 Peak south facing 90° surface irradiance for all irradiance calculation methods.

The peak 90° surface irradiances for the clear sky with a ρ of 0.85, clear sky with cloud cover with a ρ of 0.7 and a ρ of 0.95 and the interpolated CWEEDS values between Kuujuaq and Iqaluit with a ρ of 0.7 and a ρ of 0.95 can be seen in Figure 3.20. It is noted that the clear sky irradiance is the highest as expected, with the interpolated irradiance between Kuujuaq and Iqaluit being lower.

The clear sky with cloud cover irradiance is seen to be much lower than the interpolated values. The clear sky diffused surface irradiance correlation (3.47) was intended to be used with clear sky irradiance, however when used to determine the diffused irradiance component during overcast periods, demonstrated to underestimate the diffused irradiance when there was cloud cover.

Therefore, to accurately calculate the irradiance values with this method, a diffused irradiance model must be used.

As a result, due to the uncertainties mentioned using the clear sky combined with the cloud cover data, the interpolated CWEEDS surface irradiance data will be used in the BIPV/T simulations.

3.5 Ventilation Rate Requirements

To determine the volumetric air flow supplied to the ERV, and thus air flow used in the BIPV/T cavities, the minimum fresh air ventilation rates have been determined based on calculations from ASHRAE standard 62.2. It has been assumed that housing units are a typical overcrowded living space, of 5 occupants per two-bedroom housing unit, found in Nunavik.

An infiltration credit has been included to consider for fresh air infiltration from unintended openings. As well, additional flow rate has been added for an increased number of occupants.

It was found that using the 3.05ACH and 1,152CFM of air leakage @50Pa mentioned in SHQ passive house pilot project (SHQ 2020) that the ventilation system would need to provide 7.6CFM per dwelling unit. However, using the Passive House ACH rate of 0.6 would result in 50.5CFM required for acceptable IAQ for a family of 4. For the entire duplex with two housing units the minimum fresh air requirements would be 101CFM. The air requirement was rounded up to 150 CFM (70.8 L/s) to include a safety factor and to accommodate for more readily available ERVs on the market.

3.6 BIPV/T Configuration

The validated BIPV/T model, fresh air flow rate of 150CFM and integration concept will now be used to configure the BIPV/T system to maximize the outlet temperature for supplying pre-heated air to the ERV.

The BIPV/T tilt angle and the height of the cavity created from the vertical furring strips will be varied to obtain the highest outlet temperatures to be used for ERV pre-heating.

3.6.1 Tilt Angle

The outlet temperatures of the BIPV/T system for three PV tilt angles, with an air flow of 150CFM (70.8 L/s), are shown in Figure 3.21 at peak clear sky daily irradiance, for the 21st day each month, along with the corresponding ambient temperature at peak irradiance, for the 21st day each month. It can be seen that the outlet temperature was higher for the 90° and 80° façades compared to the 10° roof during the winter, spring and fall, when heating loads and ERV defrosting needs are highest, with the 80° tilt angle providing a slightly higher outlet temperature during this period.

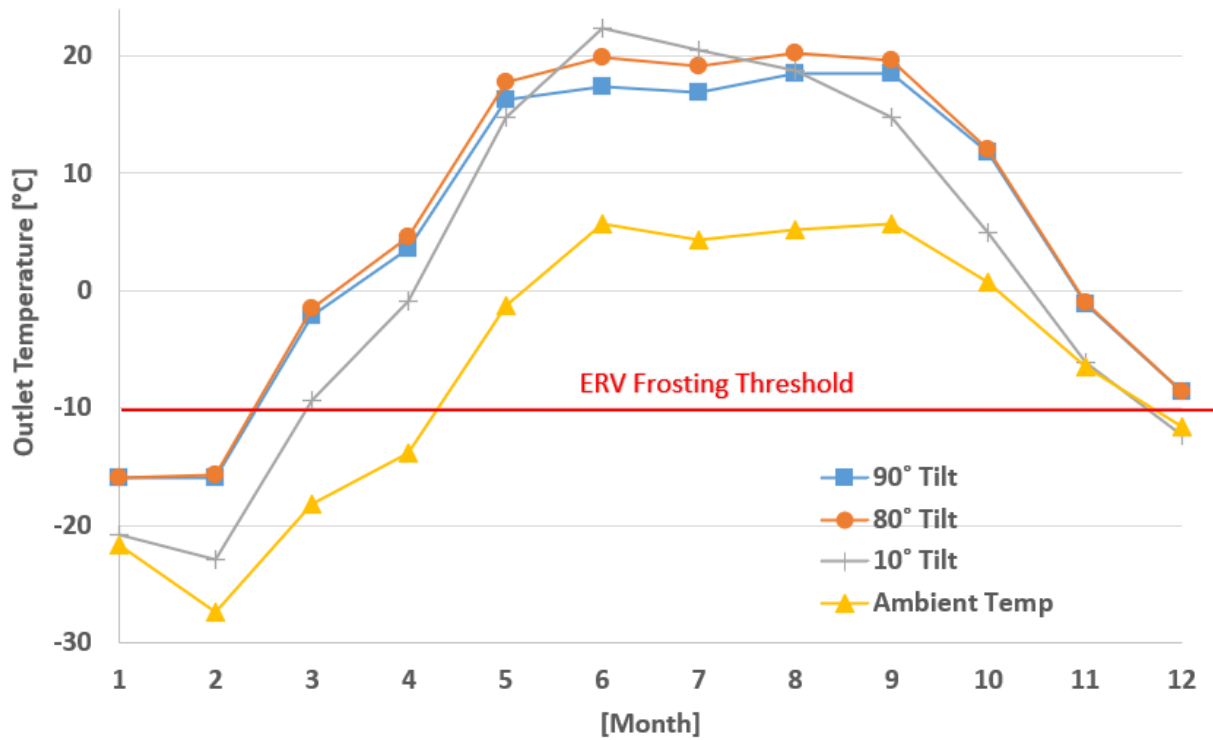


Figure 3.21 BIPV/T outlet air & ambient temperature at 150CFM with three tilt angles at clear sky daily peak irradiance for 21st day each month, with corresponding ambient temperature.

However, it can be assumed that the 90° façade would be more straightforward to construct than an 80° façade, by being able to keep the same vertical cavity method seen in Figure 3.1. Therefore, to keep the design as simple as possible for proper implementation in the northern communities a small amount of performance is sacrificed to increase the buildability.

3.6.2 Cavity Depth

Three different nominal lumber sizes have been used as the furring strips to create the cavity depth.

- 1X3- (19mm X 64mm)
- 2X3- (38mm X 64mm)
- 3X3- (57mm X 64mm)

Simulations were run for cavity depths of 19mm, 38mm and 57mm, using the 90° tilt angle. An arbitrary day was selected, in this case, April clear sky weather data at peak irradiance of 960W/m² and an ambient temperature of -15°C, with a wind speed of 6m/s was selected to be used for all three cases, with the results seen in Figure 3.22. Air volume flow rates were varied between 10 to 600CFM. The outlet temperatures were similar for all three depths at the low air flow rates until around the 25 CFM point, where the 19mm cavity provides the highest outlet temperatures for the remainder of the range. The channel air velocity is also seen to remain the highest for the 19mm channel, which results in higher Reynolds numbers, Nusselt numbers (Nu_f, Nu_b), and thus higher convective heat transfer coefficients for the front and back surfaces of the channel, providing the greatest heat transfer from the cavity surfaces to the air throughout the flow range.

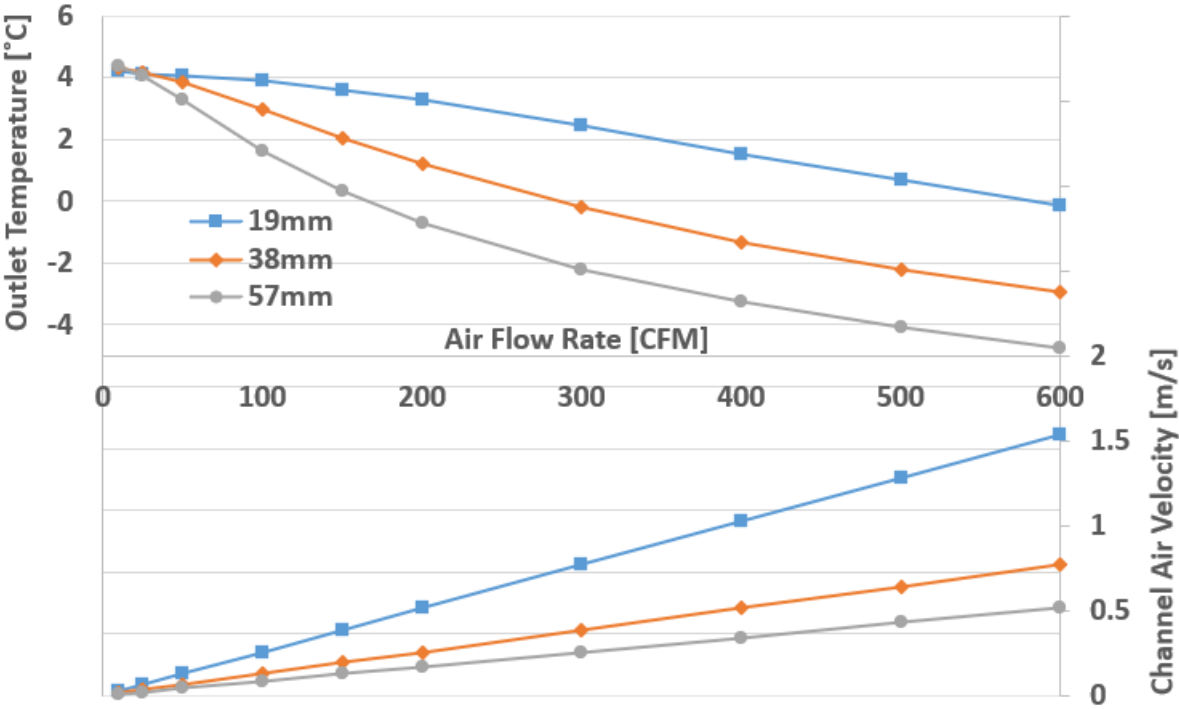


Figure 3.22 Outlet temperature and channel air velocity vs. air flow rate for three cavity depths under outdoor condition: 960W/m² irradiance, -15°C ambient temperature and 6m/s wind velocity.

In conclusion, when keeping in mind the ease of construction using readily available building materials, it was found that the ideal configuration of the BIPV/T used a south facing 90° façade tilt angle, with a 19mm cavity depth.

3.7 Fan Energy Usage

To force air movement in the cavities an electrically powered fan is required in the system. The electrical energy consumed by the fan is of importance to determine the net energy production of the entire BIPV/T system, and if it is advantageous to have the system operating during periods of low irradiance. The dynamic pressure losses have been determined for the critical path of the airflow assuming a cavity/ duct system as seen in Figures 3.23, 3.24 & 3.25.

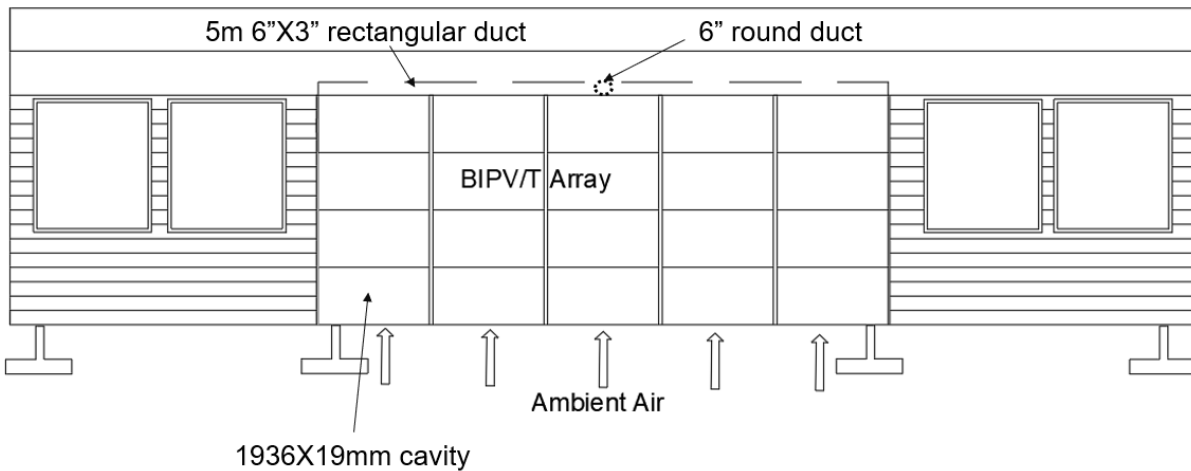


Figure 3.23 Proposed ducting system to supply forced air to ERV. Elevation drawing

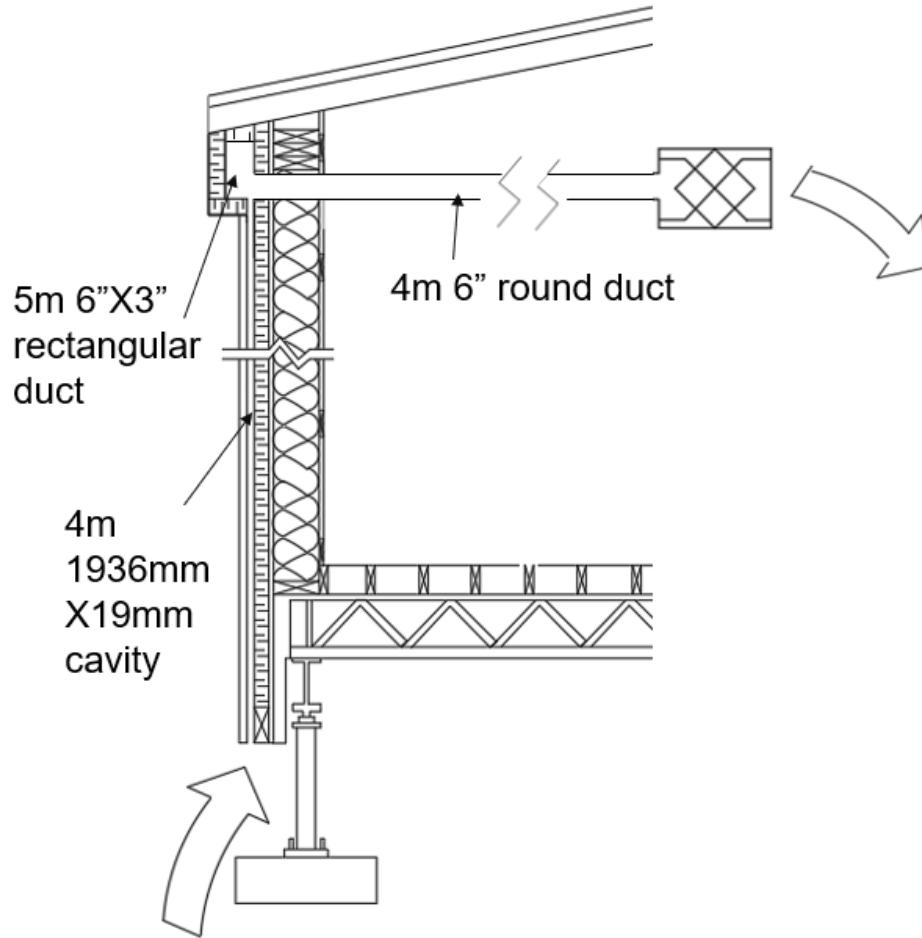


Figure 3.24 Proposed ducting system to supply forced air to ERV. Section drawing

3.7.1 Cavity Pressure Losses

Air enters the system through five 2m x 19mm wood framed cavities 4 meters in length.

Correlations used by (Ge &Ye, 2007) have been used to determine the pressure losses at the cavity entrance $\Delta P_{entrance}$, cavity straight portion ΔP_{cavity} , and cavity exit ΔP_{exit} .

$$\Delta P_{entrance} = (\xi_1 + \xi_{elbow}) * \frac{\rho}{2} * \left(\frac{Q}{A_{entrance}} \right)^2 \quad (3.56)$$

$$\Delta P_{cavity} = \frac{Q * h}{4611 * \gamma * w * l} \quad (3.57)$$

$$\Delta P_{exit} = (\xi_2 + \xi_{elbow}) * \frac{\rho}{2} * \left(\frac{Q}{A_{entrance}} \right)^2 \quad (3.58)$$

$$\Delta P_{drive} = \Delta P_{entrance} + \Delta P_{cavity} + \Delta P_{exit} \quad (3.59)$$

For air flows less than 1,200 CFM the Reynolds numbers remain under 10,000 and can be assumed as laminar/transitional for the purpose of determining the friction loss factors.

$\xi_1 =$ entrance friction loss factor

$$\xi_1 = 6.5 \cdot Re^{-0.4} + 0.5 \cdot (0.066 \ln(Re) + 0.16) \quad (3.60)$$

$\xi_2 =$ exit friction loss factor

$$\xi_2 = 6.5 \cdot Re^{-0.4} + 0.066 \ln(Re) + 0.16 \quad (3.61)$$

$\xi_{elbow} =$ rectangular elbow friction loss factor

$$\xi_{elbow} = 0.885 \cdot \left(\frac{d_1}{d_2} \right)^{-0.86} \quad (3.62)$$

3.7.2 Ducting Pressure Losses

The top of the cavities is assumed to be connected to a 5 meter long rectangular 6”X3” galvanized steel duct, which runs horizontally under the roof overhang in an insulated bulkhead. At the mid horizontal point of the façade, the 6”X3” duct is connected to a converging Tee to a 6” round duct which runs straight for 4 m to the ERV located centrally in the mechanical room, as seen in Figure 3.25.

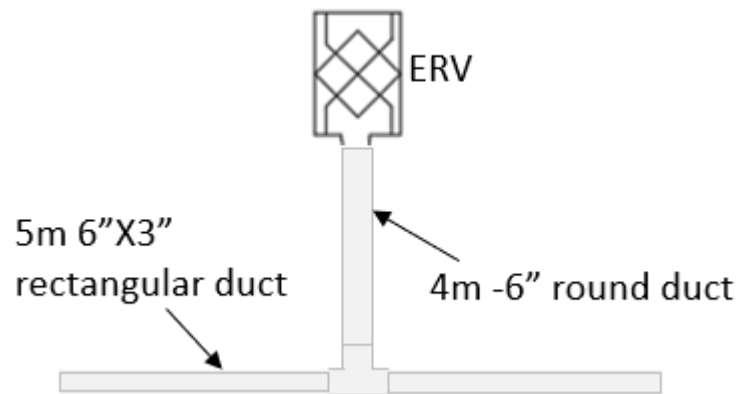


Figure 3.25 Plan view of ducting system.

The dynamic pressure loss calculations for the ducting system are determined using the Darcy-Weisbach equations which are based on the first law of thermodynamics. The pressure losses in the straight portions of galvanized steel ducts have been determined using the following correlation:

$$l_f = f \cdot \frac{L}{D} \cdot \frac{\bar{V}^2}{2g} \quad (3.63)$$

$l_f =$ duct head loss

$g =$ gravitation acceleration

$\bar{V} =$ average air velocity in duct section

$L =$ duct section length

$f =$ friction factor

$D =$ round duct cross sectional diameter

The pressure losses from the fittings, and directional changes have been determined by the following correlations:

$$\Delta P_o = C_o \cdot (P_v) \quad (3.64)$$

$$P_v = \left(\frac{\bar{V}}{4005}\right)^2 \text{ in. wg} \quad (3.65)$$

$P_v = \text{Velocity Head}$

$\Delta P_o = \text{Dynamic Losses in fittings}$

$C_o = \text{loss coefficient}$, determined from the ASHRAE Duct Fitting Database, 1992 for a converging tee, and 90°elbow (McQuiston et al., 2000).

3.7.3 Fan Power

$$\text{Fan Power} = \frac{\text{Volume flow rate} * \Delta P}{\eta_{fan}} \quad (3.66)$$

$$\eta_{fan} = 0.8$$

Table 3.4 Pressure losses and fan power for air flow range of 150-1500CFM

Volume Flow Rate [CFM]	150	300	600	1500
ΔP Cavity [Pa]	0.3	0.7	2	9.5
ΔP Duct [Pa]	21.4	85.4	342	2136
Total ΔP System [Pa]	21.7	86.1	344	2145
Fan Power [W]	1.9	15.2	122	1900
Re	250	500	992	2481
Cavity Air Velocity [m/s]	0.38	0.77	1.5	3.8
Main Duct Air Velocity [m/s]	3.9	7.8	15.5	38.8
Branch Duct Air Velocity [m/s]	3.5	6.9	13.8	34.5

3.7.4 Discussion

The ducting system was designed to be used with a volume flow rate of 150 CFM up to 300 CFM to account for a boosting of the fresh air if required. System air velocities were kept under 8 m/s to prevent vibrations and to reduce noise. As well, a shallow duct size was selected to be able to fit under the overhang, inside of an insulated bulkhead.

The results of the pressure losses for the cavity, ducts, total system, and fan power can be seen in Table 3.4. As well, the Reynolds Number, cavity air velocity, main 6" round duct air velocity and branch 6"X3" rectangular duct air velocity are presented.

It can be seen in Table 3.4 that the total system pressure losses are 21.7 Pa for the 150 CFM flow rate and 86.1 Pa for the 300 CFM flow rate. This corresponds to 1.9W and 15.2W fan power for the 150 CFM and 300CFM flow rates respectively and can be considered low power compared to the generated energy as will be seen in the following chapter. With the 600 CFM flow the main duct air velocity increases up to 15.5m/s and corresponds to a 344Pa pressure loss and 122W fan power. The fan power is still relatively low however the high air velocities in the main duct could result in vibrations and excess noise or whistling in the system. When using an air flow in the range of supplying a heat pump such as 1500CFM, the air velocity is seen to be much higher at 38.8 m/s in the main duct. The pressure losses are 2,145Pa for the 1500CFM air flow resulting in a high fan power of 1900W. As demonstrated by these extremely high values the duct system would need to be re-sized to reduce the air velocity and pressure losses if higher flow rates are required such as in cases to supply a heat pump. For this study the pre-heated air is intended to be used to reduce the frosting of the ERV and thus requires a higher outlet temperature, which will be demonstrated in the following chapter to be achieved with lower air flow rates, therefore it can be assumed that

the ducting system is sized properly for the intended purpose and the corresponding fan power for the 150CFM and 300CFM are reasonable.

3.8 Methodology Conclusion

As was seen in the methodology, a finite difference model of the BIPV/T cavity was established and was validated with BIPV/T experimental data resulting in a CV-RSME of 5.3% and a NMBE of -1.8%. Local weather data for the small northern village of Quaqtaq, QC 61°N was obtained from ECCC except for solar irradiance. The surface irradiance was therefore determined using interpolated CWEEDS satellite derived irradiance from the nearby weather stations of Iqaluit, NU 63°N and Kuujuaq, QC 58°N. The surface irradiance was determined for three tilt angles of 10°, 80° and 90° and was seen that the 80° & 90° surface tilt provided the highest surface irradiance during the colder months of the year when ERV frosting will be most problematic. As well, the 80° & 90° surface tilts were able to take advantage of the highly reflective snow during the months that the ground was covered. The fresh air requirements of the building were determined using the ASHRAE 62.2 standard for a typical overcrowded dwelling and resulted in 150CFM (70.8 L/s) of fresh air flow. Building integration of the PV was kept simple by using a 90° tilt angle, which allowed for the standard cladding installed on vertical wood furring strips to be replaced by PV modules, which will act as the UV and rain barriers while generating clean energy. A 19mm cavity depth was seen to provide the highest outlet temperature over a range of air flow rates. The pressure losses of the five 19 mm cavities and proposed ducting system was determined and the corresponding fan power was determined for the 150CFM air flow rate to be 1.9W and 15.2W for a 300CFM flow rate.

This validated model along with the compiled local weather data will be used in the upcoming chapters. The outlet temperature increases from the BIPV/T, will be analyzed to verify the effectiveness of ERV frosting mitigation, throughout the months of the year. As well, the electricity and thermal energy will be analyzed and compared with monitored energy usage data from a residential duplex located in the northern village of Quaqtq, QC.

4. Simulation Results

As was seen in the Methodology of Chapter 3, an air-based open loop, south facing, façade integrated, BIPV/T was modeled. Keeping the same south facade window to wall ratio as used in the Northern Housing Prototype (NHP), twenty 1m X 2m PV panels, attached to 1x3 (19mmX57mm) vertical wood furring strips created a 40 m² BIPV/T array, with five 19mm X 1936mm cavities 4m in vertical length. An air velocity of 0.38m/s is obtained in the cavities when using the ASHRAE 62.2 determined 150CFM (70.8L/s) of fresh air to supply occupants through an ERV. As was seen in section 2.9 of the literature review, ERV core frosting typically starts at a supply air temperature below -10°C (Beattie et al., 2018). Surface irradiance values were determined using the CWEEDS interpolated values between Kuujuaq, QC and Iqaluit, NU for the location of the NHP in Quaqtaq, QC. Both 0.70 reflectance and the 0.95 reflectance values for the snow cover were used in the surface irradiance calculation to provide a range of values that could be expected depending on the snow conditions present. All hourly Quaqtaq, QC weather conditions were averaged for each month and were used as the simulation inputs.

Using these items developed in Chapter 3 the following parameters will be analyzed. Outlet temperature, ERV frosting reductions, BIPV/T electrical and thermal efficiency, as well as the electricity and thermal energy generation.

4.1 BIPV/T Performance Analysis

To meet the objective of mitigating ERV core frosting, pre-heating of the fresh air supplied to the ERV must be maximized. In this section the performance of the BIPV/T to increase the outlet air temperature will be analyzed.

4.1.1 Outlet Temperature

As can be seen from Figure 4.1, there were maximum outlet temperature increases of over 16.8°C at peak irradiance using the average May weather conditions, with the fresh snow reflectance value of 0.95 used. With the old snow reflectance value of 0.7 there was an outlet temperature increase of 14.8 °C. This demonstrates that there can be up to a 2°C outlet temperature increase depending on the condition of the ground snow cover. A design consideration to achieve maximum performance of the BIPV/T should take into consideration having the south facing façade adjacent to an area with prolonged periods of clean snow, as opposed to facing a driveway or road where the snow is generally plowed and mixed with sand and other contaminants that can reduce the reflective coefficient to values much less than the 0.7 assumed for old snow.

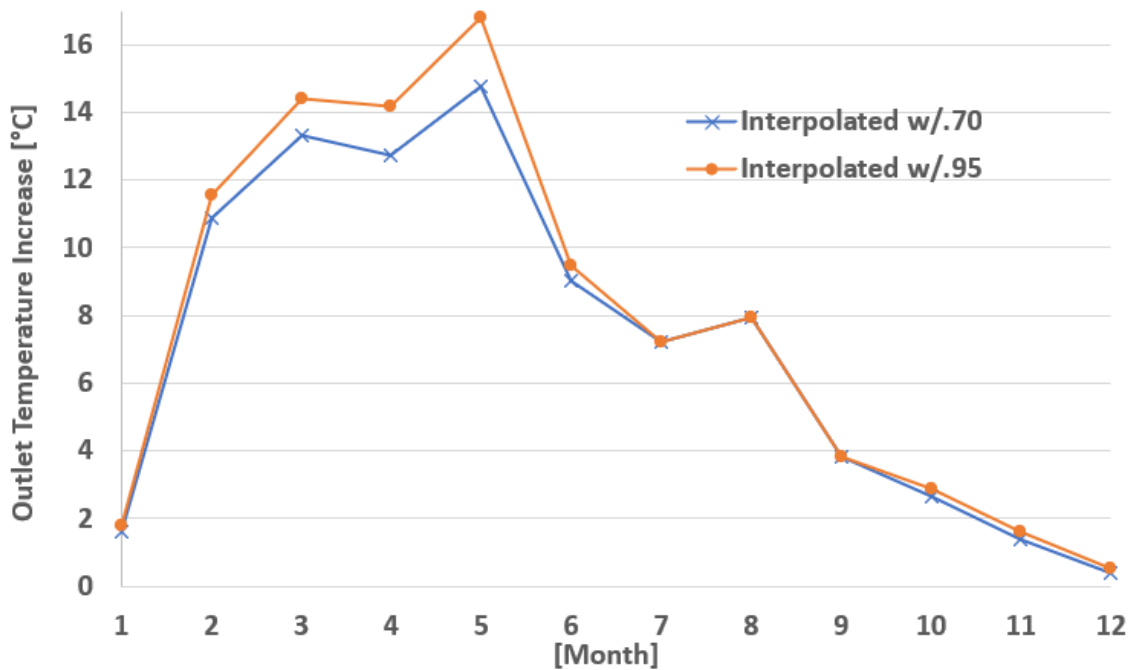


Figure 4.1 Maximum outlet temperature increase at peak irradiance using 0.70 and 0.95 snow reflectance values.

The maximum outlet temperature at peak irradiance is observed in Figure 4.2, along with the ERV frosting threshold of -10°C indicated by the red line. The BIPV/T outlet temperature is substantially increased above the ambient temperature for most months and can bring the outlet temperature above the -10°C frosting threshold at times in February, March, and April when it is seen that there is frosting risk.

It is also noted that the maximum outlet temperature never rises above 18°C for the entire year of 2017, demonstrating that preheated air can be utilized by the ERV year-round, when the outlet temperature is above ambient temperature.

However, extreme cases do exist, which will be discussed in the following section.

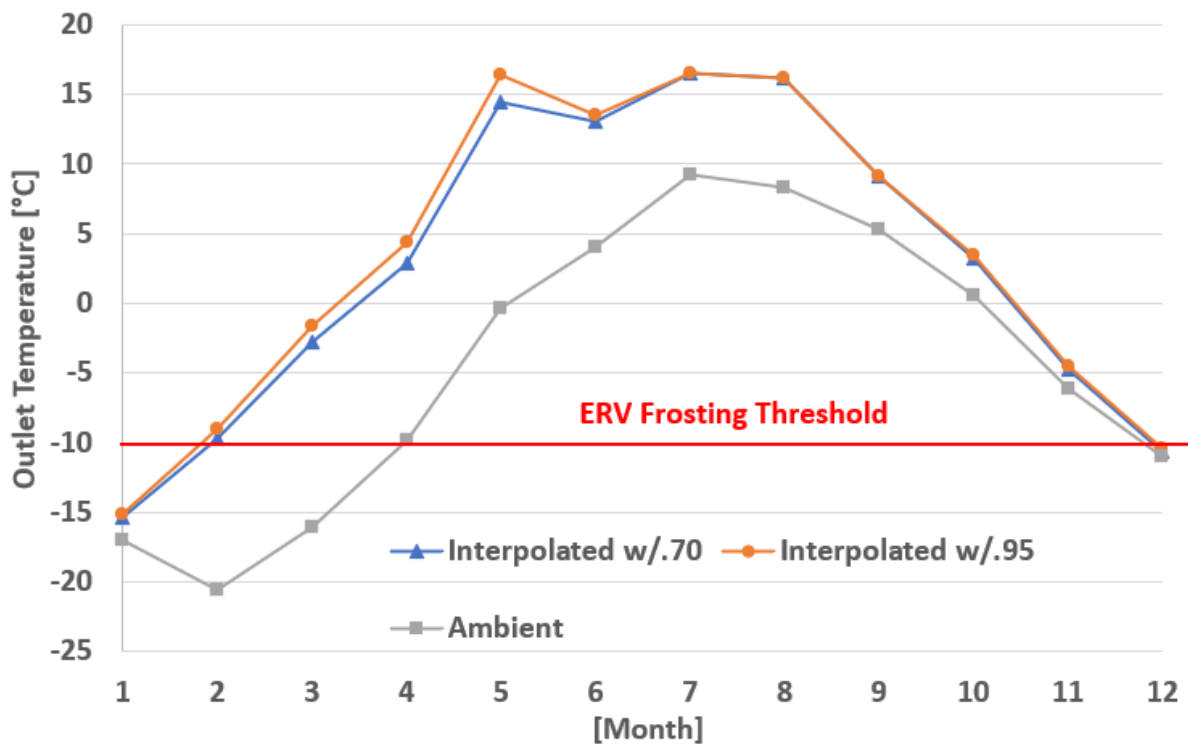


Figure 4.2 Outlet temperature at peak irradiance using 0.70 and 0.95 snow reflectance values along with the monthly average ambient temperature at peak irradiance.

4.1.2 Maximum Outlet Temperatures with Extreme Ambient Temperatures

The maximum ambient temperature in each month over a 20-year period from 2000 to 2019 were obtained from the ECCC historical weather data and can be seen in Table 4.1 for the warmer months. These maximum monthly ambient temperatures were used at average peak irradiance times of each month to determine the upper bound of the outlet temperatures, as seen in Figure 4.3, that could possibly be encountered over the design life.

Table 4.1 Absolute maximum hourly Quaqtac ambient temperature [°C] over past 20 years.

Month	Maximum Temperature [°C]
April	8
May	15
June	21
July	26
August	25.5
September	22
October	17

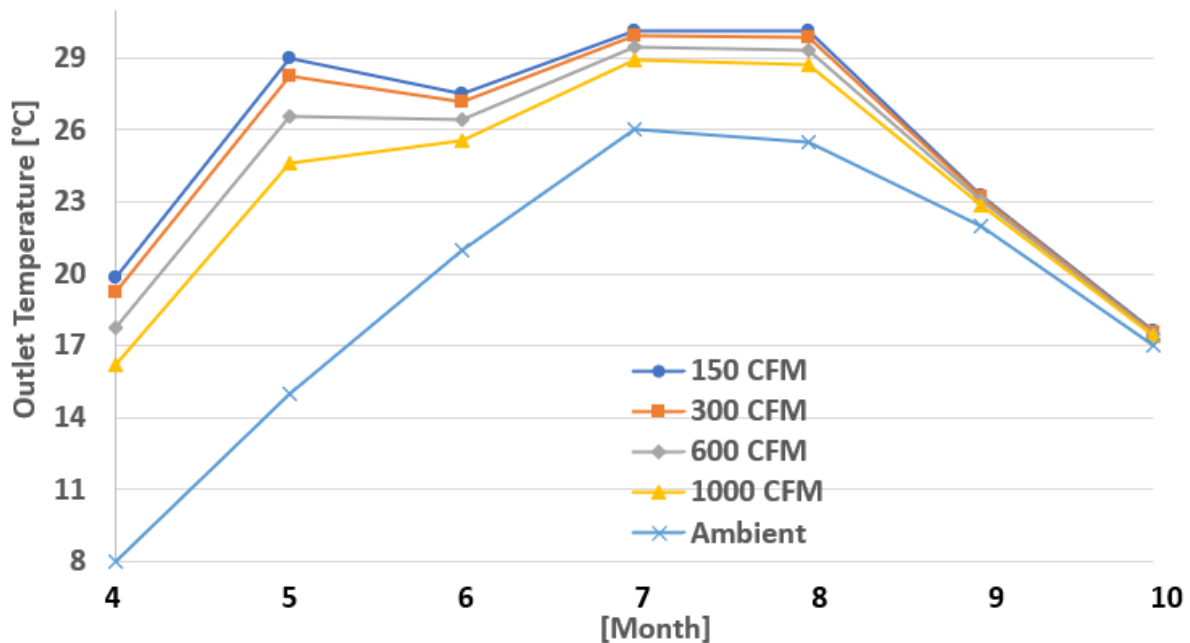


Figure 4.3 Outlet temperatures for 20 year monthly maximum ambient temperature at monthly averaged peak irradiance.

As seen in Figure 4.3, when using a 20-year maximum ambient temperature of 26°C at the average peak irradiance for July the resulting outlet temperature reaches 30.1 °C for an air flow rate of 150CFM. During such times without a heating demand the fresh air should be brought indoors directly, bypassing the BIPV/T.

While times when the ambient temperature is slightly above the seasonal norms or there is lower irradiance, it would be possible to boost the air flow rate, reducing the outlet temperature as seen from the curves using 300, 600 and 1000CFM.

For times such as the case seen in May when the outlet temperature is above the set point and there is a heating need, the ERV could be bypassed, and the preheated air can be supplied to the living space directly.

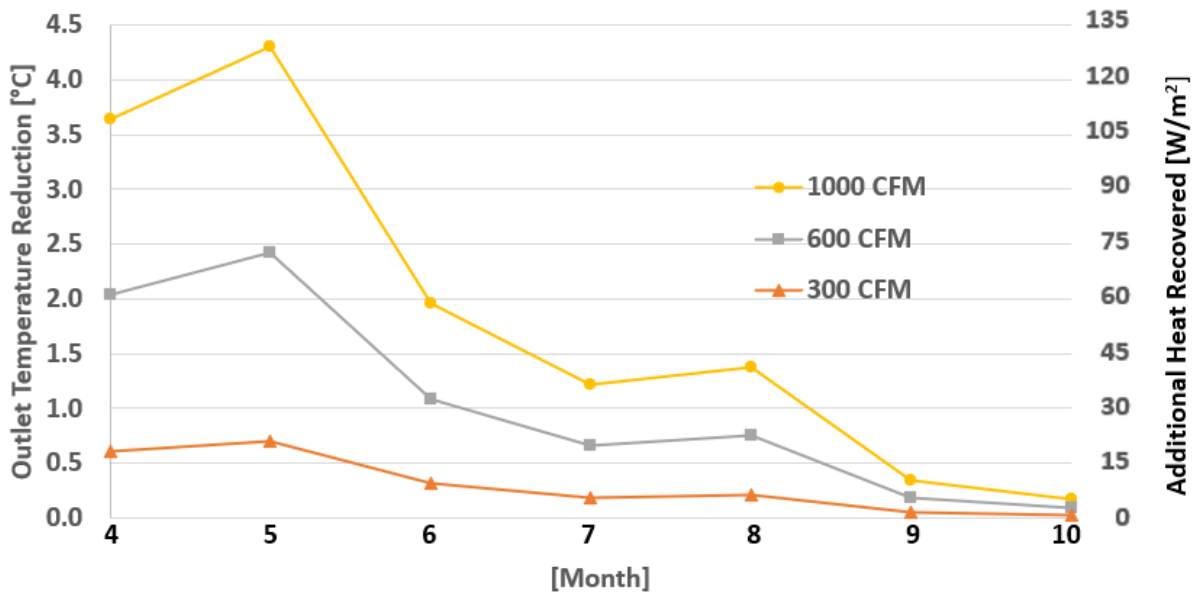


Figure 4.4 Outlet temp. reduction & additional heat recovered with increased air flow compared to 150CFM flow rate, for 20 year monthly maximum ambient temperature at monthly averaged peak irradiance.

Figure 4.4 presents the reductions in the outlet temperature as well as the additional heat recovered when the flow rates are increased from the designed rate of 150CFM to 300, 600 and 1000CFM. It can be seen when the air flow is increased as do the reductions in outlet temperature and increases in heat recovered.

For the 300CFM series, the outlet air temperature is reduced up to 0.7°C in May, while recovering up to 22 W/m² of thermal energy per BIPV/T surface area, which is equivalent to 4.5 kWh for the 40m² BIPV/T. The 600CFM flow reduces the outlet temperature by up to 2.4°C and recovering 62W/m² (12.5kWh) in May.

When using a higher air flow rate such as 1000CFM, the outlet temperature is reduced by 4.3°C and recovers 124 W/m² (25kWh). As discussed previously the duct and channels would need to

be resized accordingly if maximum heat recovery is the objective, however the same trends mentioned would be observed.

For the case shown in Figure 4.3 with the July maximum high of 26°C the increased air flow to 300CFM would not be sufficient to reduce the outlet temperature to be brought indoors, however this is the worst-case scenario and boosting the air flow could be an option throughout the months of May, June, July, and August during less extreme high temperatures and away from peak irradiance to be able to provide additional fresh while remaining energy efficient.

4.2 ERV Frosting Reductions

One of the main objectives of this study is to view the performance of the BIPV/T to mitigate ERV frosting in the extreme cold climate of Nunavik. As seen section 2.9 of the literature review, ERVs can reduce the core frosting threshold to -10°C. This freezing point will be used in the analysis of the simulated data.

The BIPV/T thermal performance to pre-heat supply air to an ERV can be viewed in Table 4.2, using the snow reflectance coefficient ρ of 0.95, and averaged monthly weather data for each hour of the day. It can be seen in Column 2 that the ERV frosting risk without pre-heated BIPV/T is 100% of the time from January to March, 75% of the time in March and 92% of the time in December. The frost reduction time, which are the hours per day that the BIPV/T outlet temperature was above -10°C while the ambient temperature was below -10°C can be seen in Column 3, where the frost reduction is up to seven hours per day in March and five hours per day in April with one hour per day in February. The frosting time is shown in Column 4 as a percent of the day where the ERV frosting time is reduced directly from the BIPV/T pre-heated air 29% and 21% for March and April respectively and 4% for February. In Column 5 the extra fresh air supplied to the

living space due to the ERV frosting time reduction is seen to provide up to an additional 2,226L/Day, 1,590L/Day and 318 L/Day in March, April, and February respectively.

Table 4.2 ERV frosting reductions with BIPV/T pre-heated air.

Month	Frosting Risk with out BIPV/T (%/Day)	BIPV/T Toutlet > -10°C & Tambient < -10°C (Hours/Day)	Frost Reduction with BIPV/T (%/Day)	Extra Fresh Air with BIPV/T (L/Day)
Jan	100	0	0	0
Feb	100	1	4	318
Mar	100	7	29	2226
Apr	75	5	21	1590
May	0	0	0	0
Jun	0	0	0	0
Jul	0	0	0	0
Aug	0	0	0	0
Sep	0	0	0	0
Oct	0	0	0	0
Nov	0	0	0	0
Dec	92	0	0	0

The duration of the pre-heated airtime supplied to the ERV from the BIPV/T was determined by using the hours per day that the pre-heated outlet air had a higher temperature than the ambient air. The values in Table 4.3 were determined using the snow reflectance coefficient ρ of 0.95. As seen in Column 2, pre-heated fresh is available for several hours per day in every month with the best performing months seen to be in May with 13 hours per day followed by April, and June with 11 hours per day. Column 3 presents the percent of time per day that the ERV is supplied with pre-heated air, with the corresponding maximum in May having pre-heated air for 54% of the day. Column 4 and 5 of Table 4.3 presents the volume of heated fresh air supplied from the BIPV/T with the May peak of 4,134 L/Day which is equivalent to 20 L/Day per square meter of floor area for the entire duplex.

Table 4.3 BIPV/T pre-heated fresh air supplied to ERV.

Month	Toutlet> Toutdoor (Hours/Day)	Pre-heated air with BIPV/T (%/Day)	Pre-heated air with BIPV/T (L/Day)	Pre-heated air with BIPV/T (L/Day/m ²)
Jan	4	17	1272	6
Feb	8	33	2544	12
Mar	9	38	2862	14
Apr	11	46	3498	17
May	13	54	4134	20
Jun	11	46	3498	17
Jul	10	42	3180	15
Aug	9	38	2862	14
Sep	8	33	2544	12
Oct	6	25	1908	9
Nov	3	13	954	5
Dec	2	8	636	3

Figure 4.5 presents the pre-heated air times and normalized volume of air per floor area, using two values of snow reflectance. There is up to 13 hours of preheated air in May which is equivalent to 20L/day/m² (4,134L/Day) of fresh air that is pre-heated.

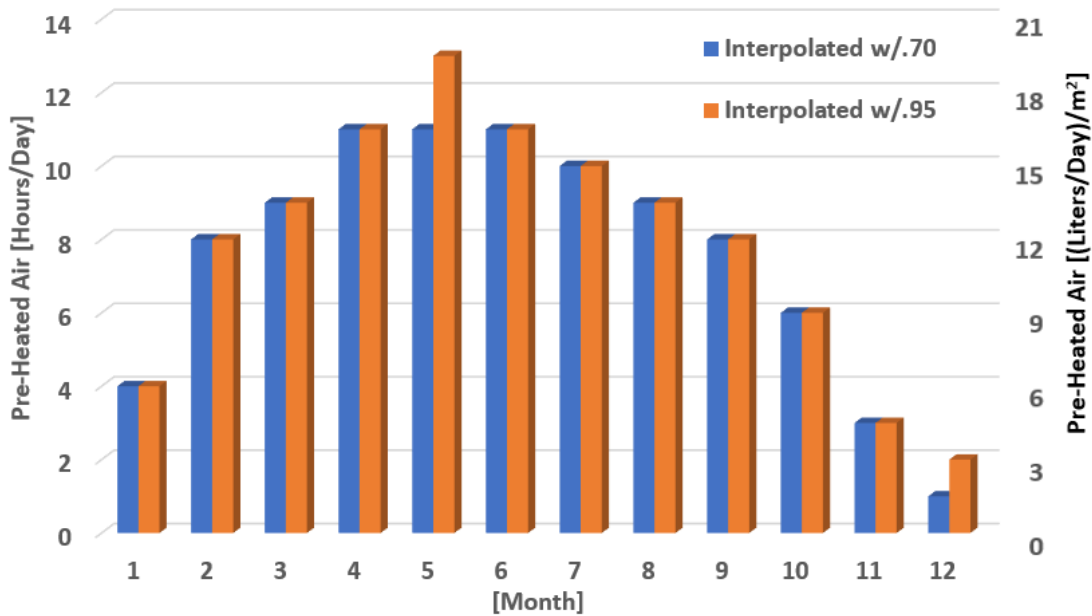


Figure 4.5 Hours/Day outlet temperature higher than ambient temperature and volume of pre-heated fresh air per m² of floor area.

4.3 PV Efficiency Improvements

4.3.1 Electrical Efficiency

The following section focuses on the PV electrical efficiency η_{PV} improvements from the forced air heat transfer behind the BIPV/T in the wall cavity, thus reducing the PV temperature.

Simulations were run with a base line air flow rate of 0 CFM in the BIPV/T cavity to obtain the η_{PV} values without forced air flow. This baseline efficiency was then compared with the efficiencies obtained when using 150, and 1500CFM. The PV electrical efficiency was determined assuming poly crystalline silicon panels and using the following standard test conditions (STC) correlation, which is a function of the PV temperature (Kayello et al 2017a).

$$\eta_{PV} = \eta_{STC} + (1 - \beta * (T_{PV} - T_{STC})) \quad (4.1)$$

$$\eta_{STC} = 15\%$$

$$T_{STC} = 20^{\circ}\text{C}$$

$$\beta = 0.0045$$

The η_{PV} obtained at peak solar irradiance can be seen in Figure 4.6 using the three air flow rates. It is observed the η_{PV} trend for all data series is the inverse of the ambient temperature which is what is expected from using the η_{PV} STC correlation. It is seen that efficiency improves when the air flow rate is increased as the cooler ambient air is drawn into the cavity reducing the PV temperature. Improvements are barely discernable between the 0 CFM and 150 CFM, except for a slight improvement during the warmer months. The range of η_{PV} can be seen to be between 17.4% in January to 15.2% in both May and July. Noticeable improvements can be seen though

with the 1500CFM series compared to the baseline values in the warmer months. With the 1500 CFM series ranging from 17.4% in January down to 15.4% in July and August.

It is worth noting though, that for all flow rates the η_{PV} was above the η_{STC} of 15% for all months of the year, with up to a 2.4% η_{PV} increase over the η_{STC} when using the 150CFM flow rate, demonstrating the advantage of generating PV energy in the extreme cold climate of Nunavik.

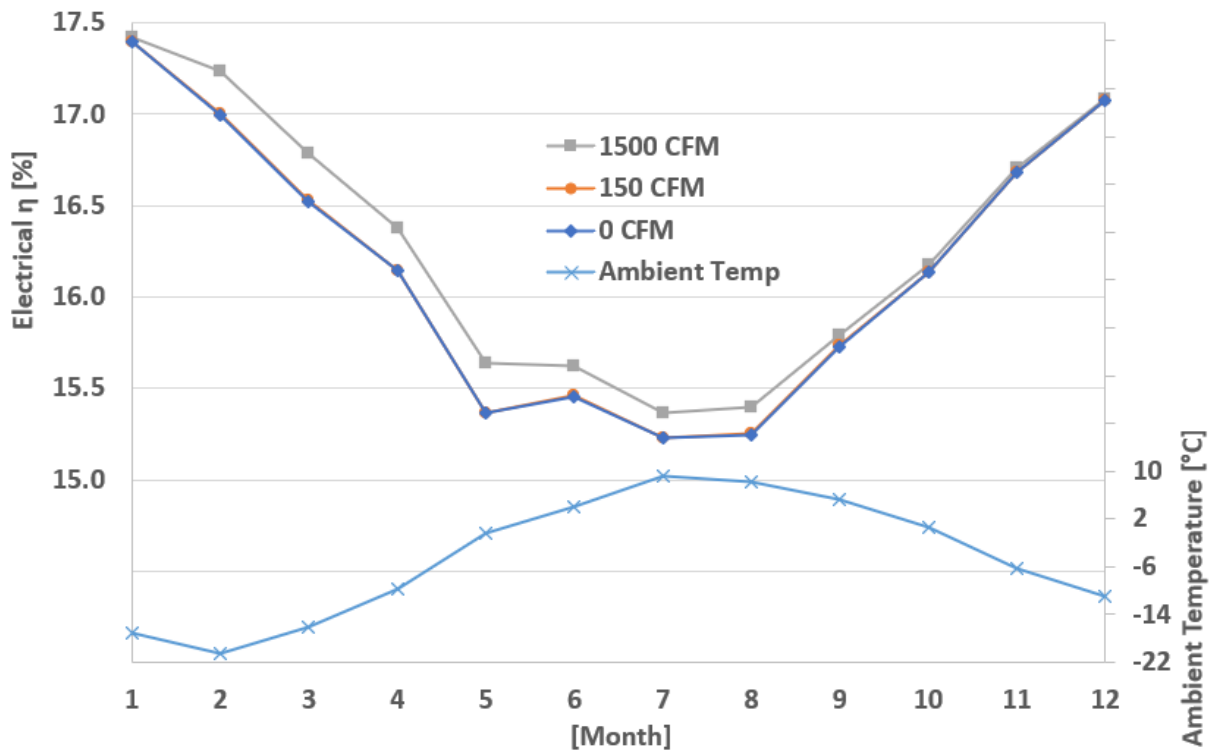


Figure 4.6 Electrical efficiencies with range of air flow rates at peak irradiance with corresponding ambient temperature using averaged monthly weather data for each hour of day.

As seen in Figure 4.7 there was little improvement in the η_{PV} when using 150 CFM. Comparing the 0 CFM to 150CFM gave at best an absolute efficiency increase of 0.01%. This small improvement can be attributed to the low air flow in the system with only 30 CFM of air flow in

each of the five cavities when using the fresh air supply air flow rate of 150 CFM. However, if the objective is to recover an increased amount thermal energy, then a higher air flow rate is desirable, and would result in noticeable PV efficiency increases as seen from the other data series. When the simulation was run using 1500 CFM the η_{PV} results improved noticeably from February until May with a peak improvement of 0.27%. The peak irradiance values are plotted as well in Figure 4.7 and can be seen that the greatest efficiency improvements occur during the months with higher surface irradiance.

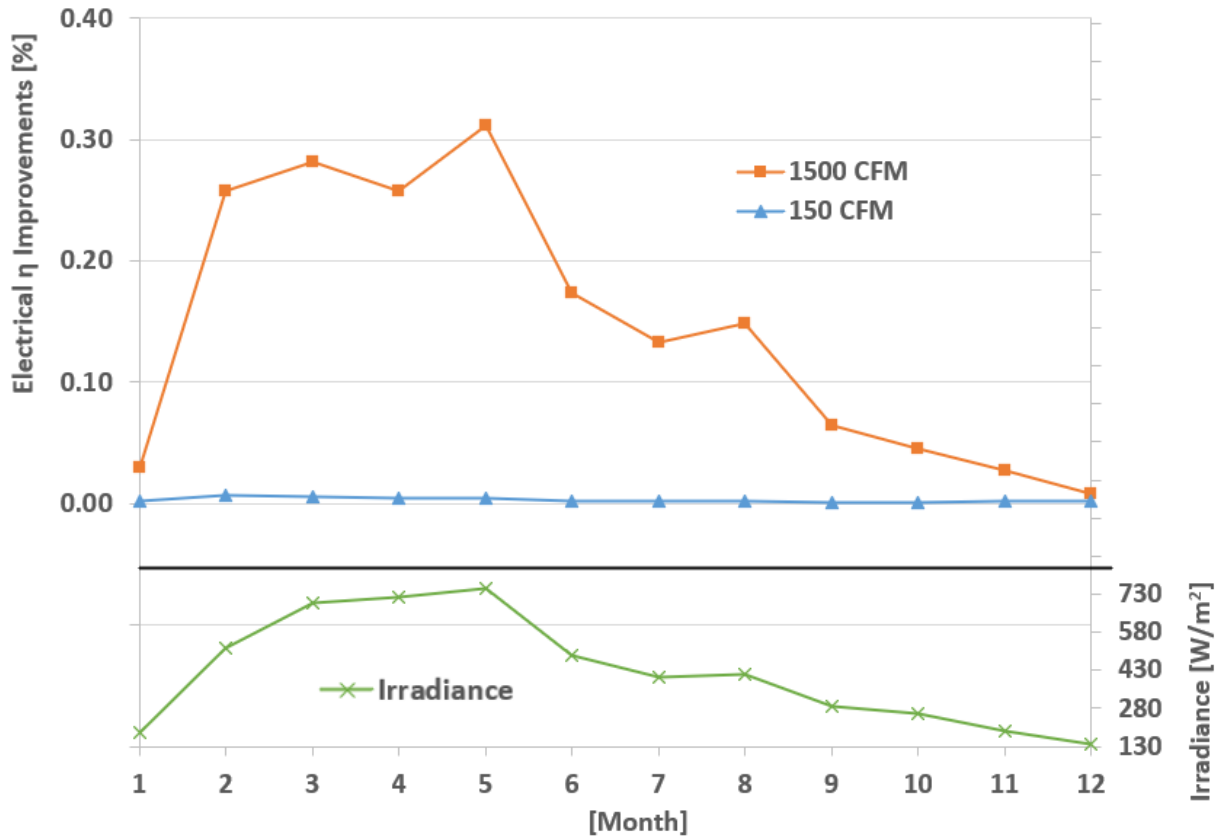


Figure 4.7 PV electrical efficiency improvements at peak irradiance with 2 air flow rates.

4.3.2 Thermal Efficiency

The comparison of the $\eta_{thermal}$ for the two flow rates can be seen in Figure 4.8. Considerable improvements can be seen when using the higher flow rate, with the 1500CFM series reaching 24.2%. Thermal efficiencies in December are very low for both flow rates with values of 1.1%, and 1.3% for the 150, and 1500CFM air flow rates respectively. These low values of thermal efficiency can be attributed to the lowest solar surface irradiance values of the year.

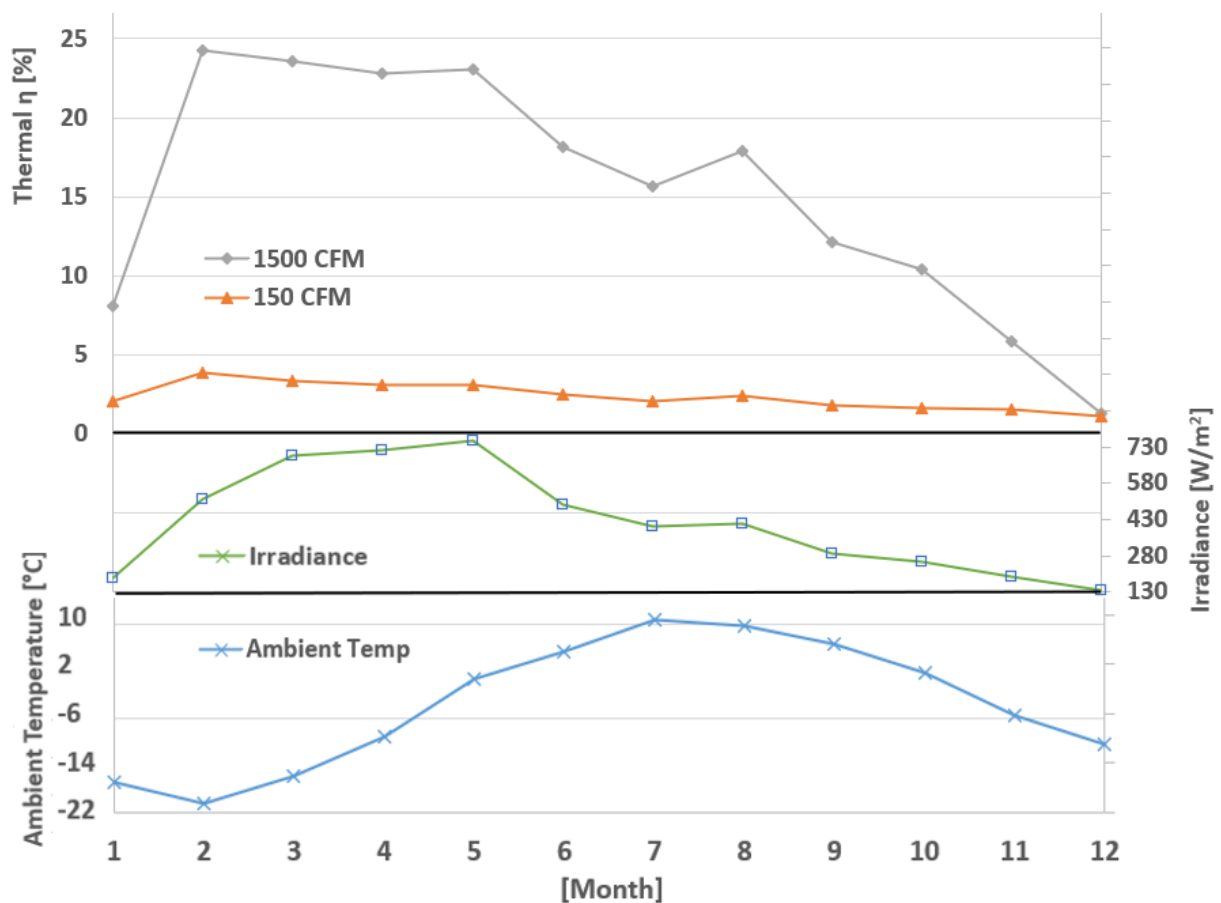


Figure 4.8 Thermal efficiency for range of flow rates with peak surface irradiance and corresponding ambient temperature.

Of interest is the spike in thermal efficiency improvement in the month of August which can be attributed to the small increase of peak irradiance to 413 W/Day compared to the 402 W/Day in

July along with the decrease of peak ambient temperature in August with a value of 8.3 °C compared to the value of 9.2 °C in July. These two factors result in a higher ΔT between the $T_{outlet} - T_{extr}$ for August which provide more heat recovered and a high thermal efficiency.

$$Q_{rec} = \dot{m} * C_{p,air} * (T_{outlet} - T_{extr})$$

4.3.3 BIPV/T Efficiency

The electrical, thermal, and total BIPV/T efficiencies for the 150CFM flow rate can be seen in Figure 4.9.

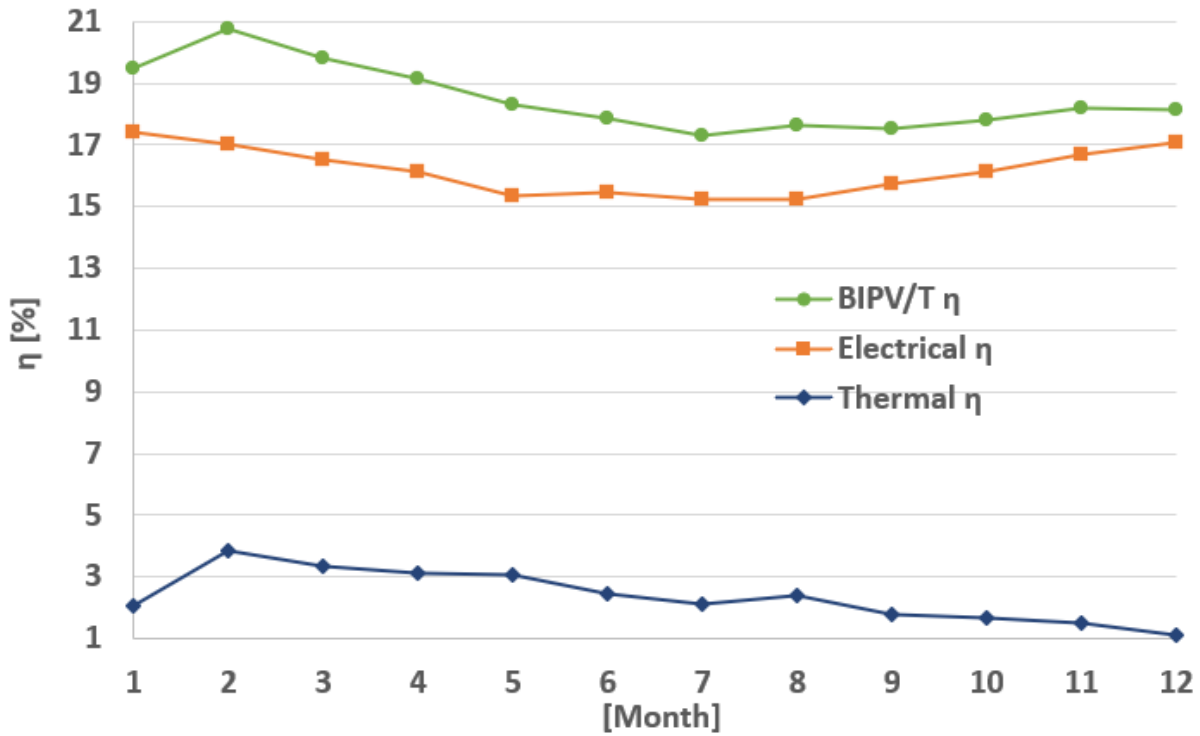


Figure 4.9 BIPV/T efficiencies using 150 CFM air flow rate.

It is noted that the thermal efficiency is much less than the electrical efficiency, which is due to the low air flow rate used to maximize the outlet temperature for ERV pre-heating. The average monthly thermal efficiency $\eta_{thermal}$ is determined by equation (4.2).

$$\eta_{thermal} = \left(\frac{Q_{rec}}{G \cdot A_{BIPV/T}} \right) \cdot 100\% \quad (4.2)$$

where

Q_{rec} = Total daily heat recovered in [W]

G =Incident solar irradiance in [W/m²]

$A_{BIPV/T}$ = Surface area of the BIPV/T collector in [m²]

$$\eta_{BIPV/T} = \eta_{thermal} + \eta_{PV}$$

Peak $\eta_{thermal}$ for the 150 CFM air flow rate occurs during February with a value of 3.8%, and a corresponding $\eta_{BIPV/T}$ value of 20.8%. The lowest $\eta_{thermal}$ value for the 150 CFM flow rate occurs during December with a value of 1.1%, however the lowest $\eta_{BIPV/T}$ occurs in July with a value of 17.3%, this can be attributed to the low η_{PV} which is connected to the highest ambient temperature of the year occurring during this month.

Figure 4.10 presents the total efficiency of the BIPV/T which is the sum of the electrical and thermal efficiencies, for the two air flow rates.

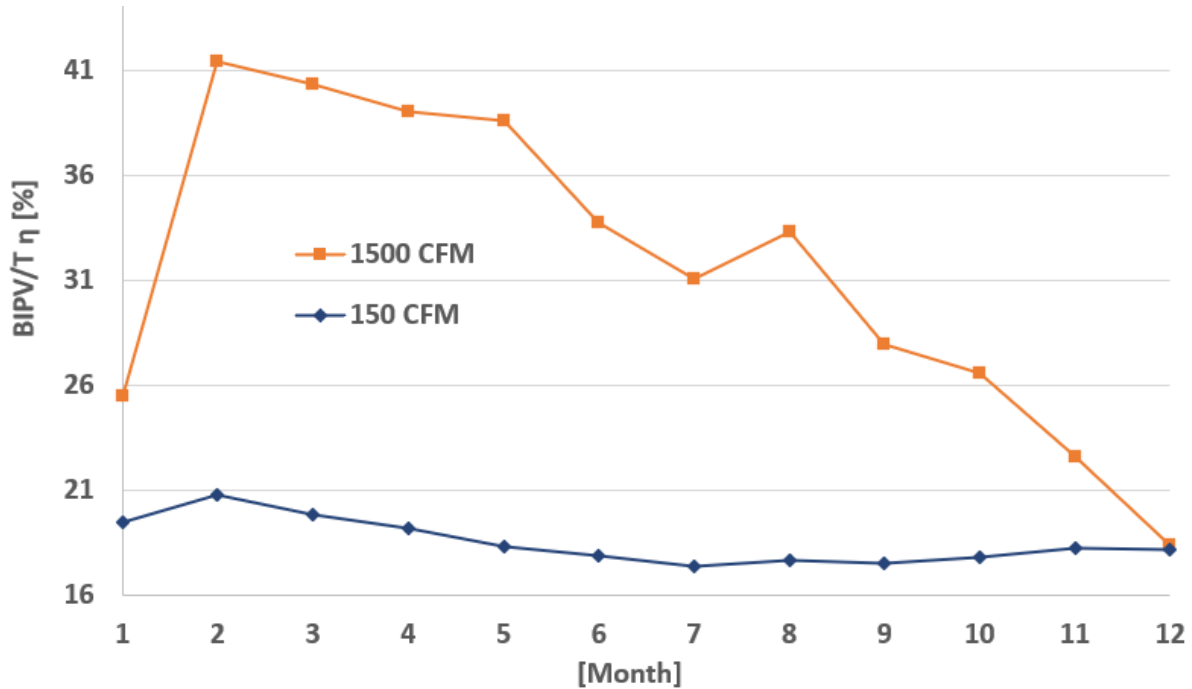


Figure 4.10 BIPV/T efficiency for range of flow rates.

The $\eta_{BIPV/T}$ for the 150CFM flow rate is seen to peak in February at 20.8%, while the 1500 CFM series is seen to be considerably improved compared to the 150 CFM series with a peak $\eta_{BIPV/T}$ of 41.4% in February. The $\eta_{BIPV/T}$ is the lowest in December for both flow rates and have very similar values of 18.2%, and 18.4% for the 150, and 1500CFM air flow rates respectively. As seen from Figure 4.8 the relatively low $\eta_{BIPV/T}$ can be attributed to the low $\eta_{thermal}$ in December for both air flow rates.

4.4 Energy Generation

The daily electrical, thermal, and combined energy generated from the BIPV/T using a total air flow rate of 150CFM are presented in this section. Two data series are shown using the two values of snow reflectance ρ to provide an upper and lower bound of expected values. A DC to AC inverter

efficiency of 0.97% is assumed based on the specifications of a 6.0kWac SMA residential inverter (SMA, 2021). As well, the fan power was determined to be 1.9W as seen in section 3.7. These losses have been applied to the electrical energy generated.

4.4.1 Electrical Energy Generation

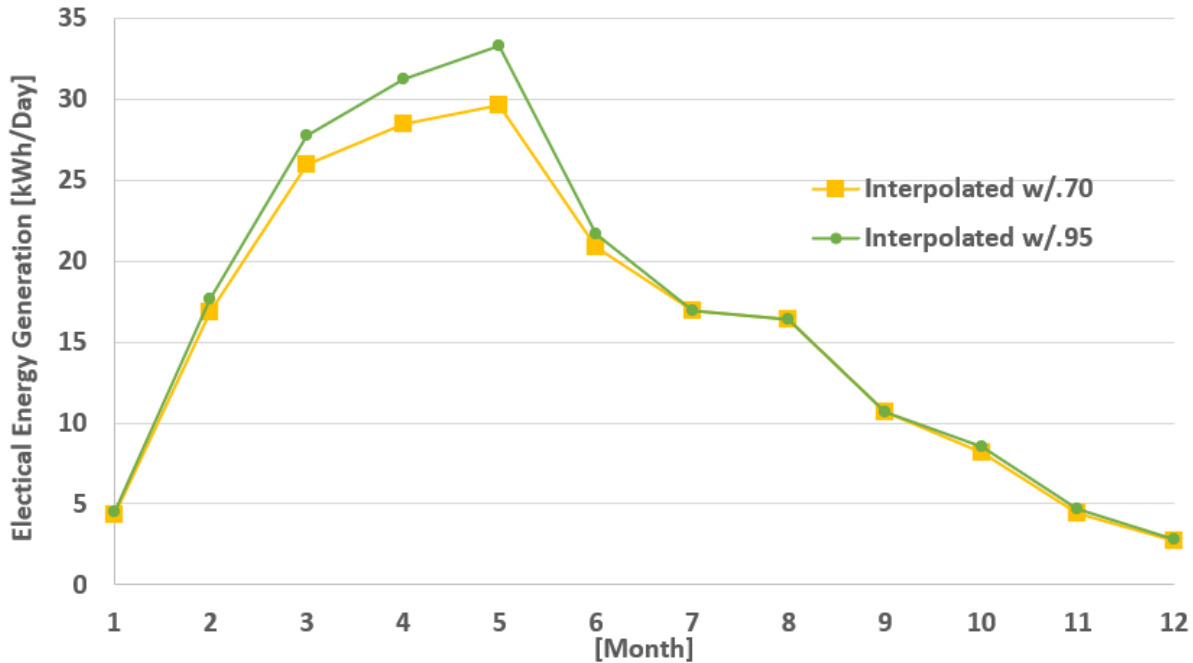


Figure 4.11 Monthly average electrical energy generated per day using 150 CFM air flow rate.

The daily electrical energy generated from the BIPV/T can be seen in Figure 4.11. The peak generation can be seen during May with the ground reflectance of 0.95 having a value of 33 kWh/Day and the ground reflectance of 0.7 having a value of 30 kWh/Day. There is a dip in the curve between May and June which can be attributed to the snow melting changing the ground reflectance from 0.7-0.95 to 0.2. As was seen when analyzing the outlet temperature, the increased reflectance from the new snow resulted in an improved electrical energy generation of up to 3.7kWh/day.

4.4.2 Thermal Energy Generation

The monthly average thermal energy generation can be seen in Figure 4.12 with the highest heat recovery during the month of May with the ground reflectance of 0.95 providing a value of 7.5 kWh/Day and the ground reflectance of 0.7 providing a value of 6.5 kWh/Day, with similar improvements seen from the increased reflectance resulting in a 1kWh increase with new snow assumed. As well, the same drop from May to June can be seen when the snow ground cover is assumed to be melted and now has the reflectance of 0.2 for tundra.

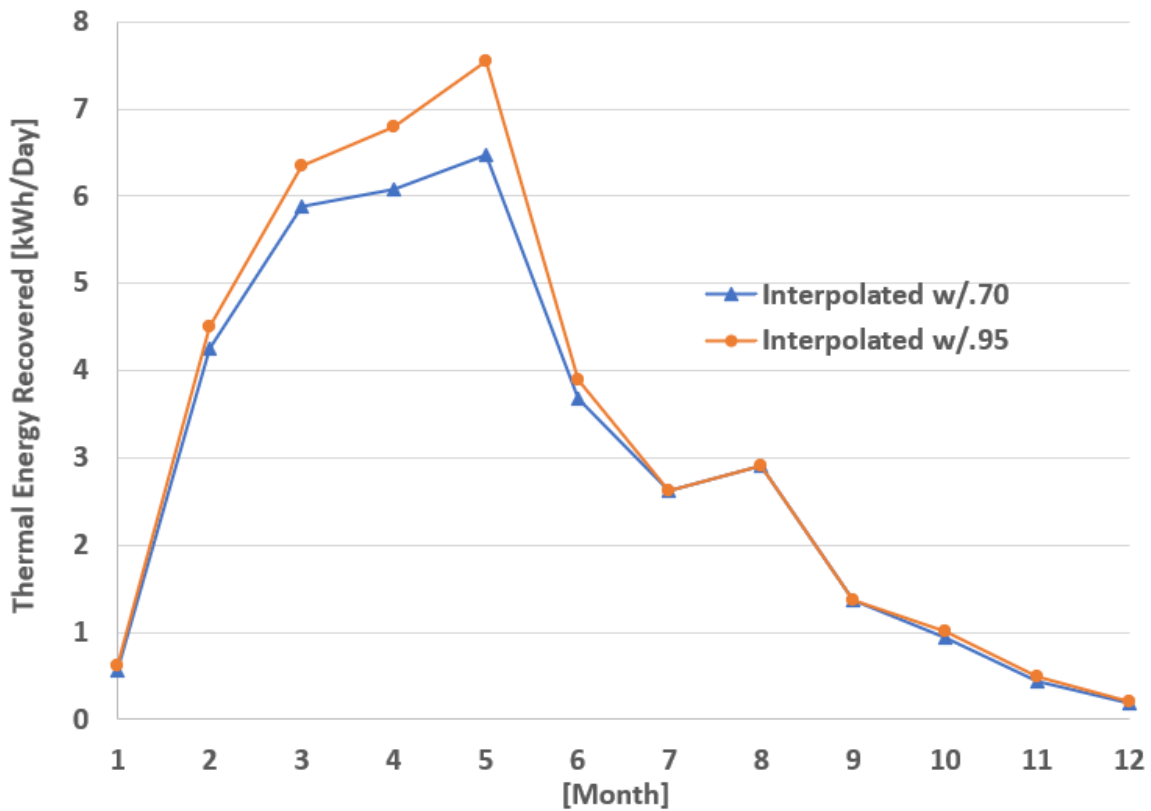


Figure 4.12 Monthly average thermal energy recovered per day using 150 CFM air flow rate.

Figure 4.13 presents the increased amount of air flow that would be in the expected range to supply a heat pump, or a building with higher fresh air requirements. When the air flow rate is increases from 150CFM to 1500CFM that heat recovery is greatly increased for several months of the year. With May having over 56kWh/day of heat recovered compared to the 7.5kWh/day recovered when using 150CFM. It is observed that little improvements were made during the low irradiance months of January, December, and November though.

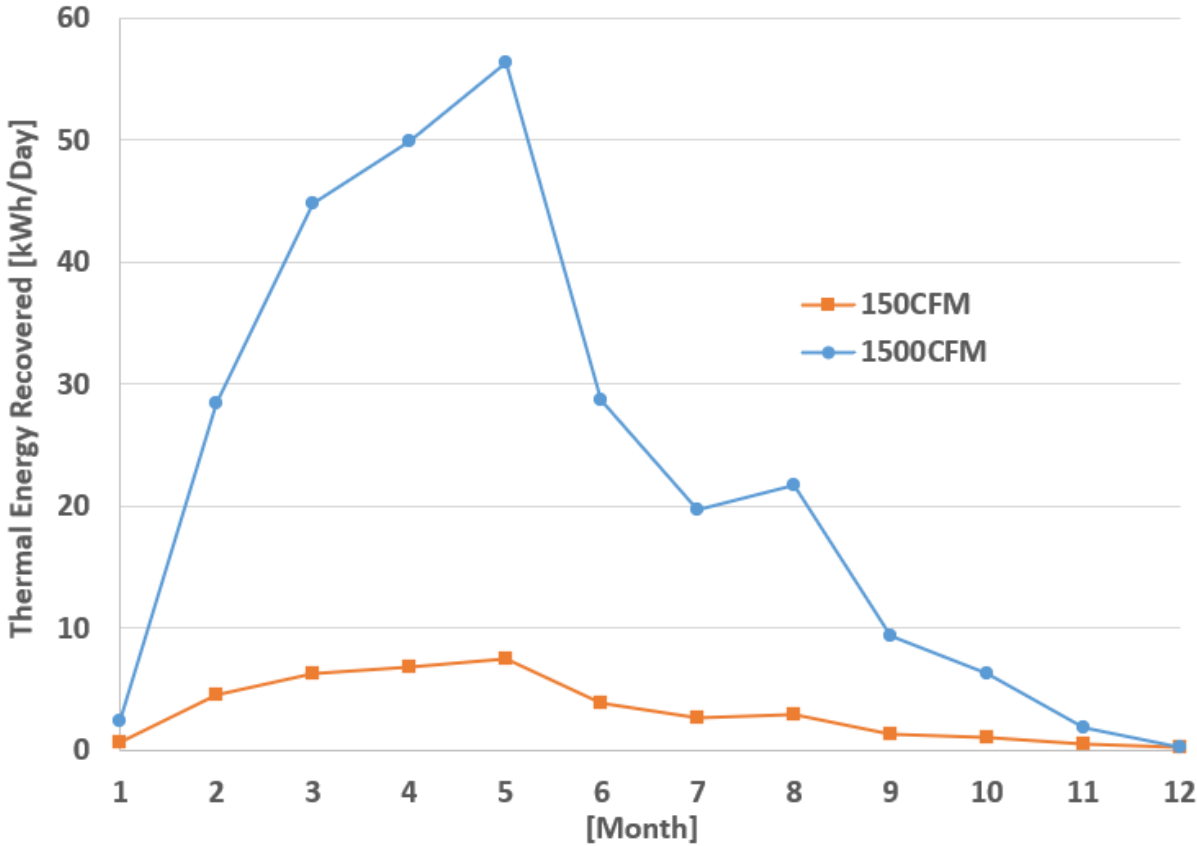


Figure 4.13 Monthly average thermal energy recovered per day using 150CFM and 1500CFM airflow rates.

4.4.3 Total Energy Generation

The total energy recovered is shown in Figure 4.14 and can be seen to be considerable amounts of electricity and heat that will be valuable to reduce daily peak electrical loads and the amount of fossil fuel used to heat the building. The best performing months can be seen to occur in March, April, and May where the system took advantage of snow cover to reflect solar radiation with the 0.95 ρ providing a value of 41 kWh/day and the 0.7 ρ providing a value 36 kWh/day. Once again it can be seen that the fresh snow was able to increase the total energy production by up to 4.7 kWh/day, demonstrating one of the advantages of using a façade integrated BIPV/T in a cold climate with long period of snow cover.

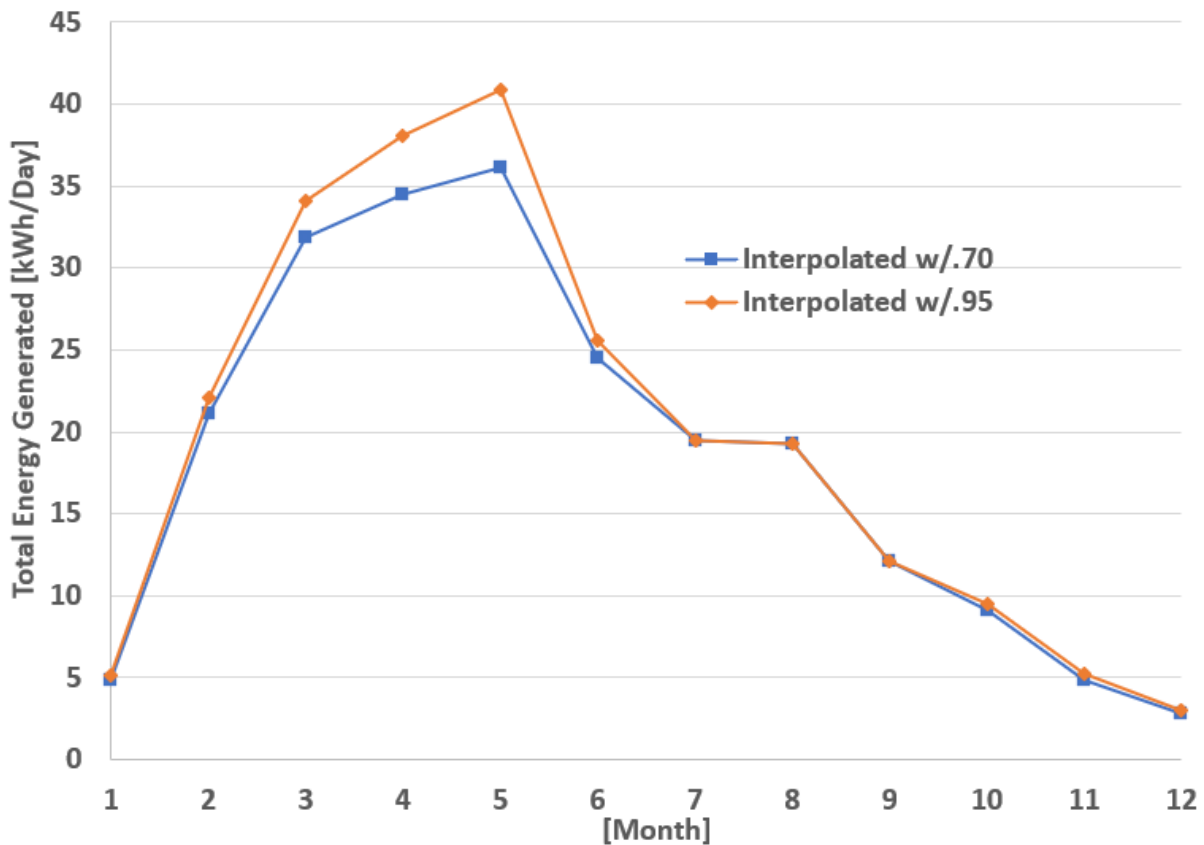


Figure 4.14 Total energy generated per day using 150 CFM air flow rate.

4.5 Discussion

As was seen in Figure 4.8 the thermal efficiency was very low when using an air flow rate of 150CFM and resulted in a low amount of heat recovered as seen in Figure 4.12. The thermal efficiency using 1500 CFM was seen in Figure 4.8 to be much higher, however, to take advantage of the additional heat recovered the installation of a heat pump, and a separate ducting system would be required. This would add to the initial costs of the installation and increases the complexity of the project. Since heat pumps are not presently used in the Arctic communities, repair of the system would require a costly trip for a technician to be flown in from the south. As well, Hydro-Quebec does not permit the usage of heat pumps in any of the off-grid Arctic communities, therefore an exemption would need to be requested, demonstrating that the heat pump could be powered by solar generated electricity. For these reasons the use of a heat pump does not meet the objective of a simple design for the north.

The potential for the BIPV/T studied, to maximize the electricity generation was shown to have limitations maximizing the heat recovered due to the low make up air flow, used in the system. However, if used on a building with higher fresh air requirements, the thermal efficiency can be increased, when the cavity dimensions are sized accordingly to achieve a high outlet temperature and sufficiently high heat recovered, resulting in a cost-effective way to reduce the heating and electricity loads while mitigating ERV frosting, increasing the indoor air quality.

5. Northern Housing Prototype Data Analysis

This study takes advantage of the monitored data collected from the Northern Housing Prototype (NHP) duplex presented in section 2.6.1 and will use this building located in the low Arctic community of Quaqtaq, QC as an archetype Arctic residential building. The BIPV/T simulated performance has been matched with the field data to obtain the expected benefits, as will be seen in the upcoming Chapter.

5.1 Hydro Quebec Domestic Rates for Off-Grid Systems

Since the communities of Nunavik are not connected to the hydro electric grid of Quebec and depend on an off-grid Arctic diesel generator to supply the local electrical energy, electricity costs in Nunavik are subject Hydro Quebec's Off-Grid System's DN Rates. From the electrical rates effective April 01, 2021, a base rate of \$0.06159/kWh for the first 40kWh/day and a second-tier rate of \$0.41969/kWh for electrical energy consumption over 40kWh/day is applicable. In the case when a building has multiple dwelling units, a multiplier equal to the number of dwelling units is multiplied by the 40kWh/day. In the case studied for the Northern House Prototype (NHP) there are two dwelling units giving a multiplier of two, resulting in a first-tier base consumption rate applied to the first 80 kWh/day and the second-tier rate for energy usage above 80kWh/day. As well, there is a charge of \$6.21/kW for an excess billing demand over the base billing demand of 50kW. The billing demand is determined by taking the greater value of either the maximum power used during the consumption period, or 65% of the maximum power usage that occurs entirely in the winter period of December 01 to March 31 in the previous 12 months. A system access charge of \$0.41168 per day times the multiplier, is charged as well. A net metering option is also available

where on-site electrical energy production that is injected into the Hydro-Quebec system is paid at the rate of \$0.48624/kWh into the customer's surplus bank.

It is also mentioned that electricity delivered in an off-grid system cannot be used for space heating, water heating or for any other thermal applications (Hydro Quebec, 2021). Since the electricity is generated in these off-grid power stations by diesel generators, it is more efficient for each building to cover their own heating needs with oil fired burners, thus the dependence on fossil fuels.

It is worth noting the 2021 DN rates were recently re-negotiated and changes to the 2019 DN rates were made increasing the base rate limit from 30kWh/day to 40kWh/day. As well, small increases were made to the 2019 rates, changing the base rate from \$0.0608/kWh to \$0.06159/kWh and the 2nd tier rate from \$0.4143/kWh to \$0.41969/kWh for the remaining daily consumption. The increasing of the base rate limit will provide substantial savings since the time spent in the second tier will be reduced. However, as will be seen in the following sections there is still potential for further savings and net energy reductions with renewable energy generation from the BIPV/T.

5.2 Daily Energy Usage

As part of the NHP pilot project, introduced in section 2.6.1, a field monitoring study was established to collect important data from the building (SHQ, 2020).

Three years of daily electrical and thermal energy data has been collected from the NHP duplex in the northern village of Quaataq, QC. Continuous data collection for 365 days occurred for 2017, however there were 28 days of missing data in 2018 and three days missing in 2019. The daily electrical and thermal energy loads normalized with the floor area in kWh/m² and in total kWh consumed can be seen in Figure 5.1 for the period between December 2016 and January 2020.

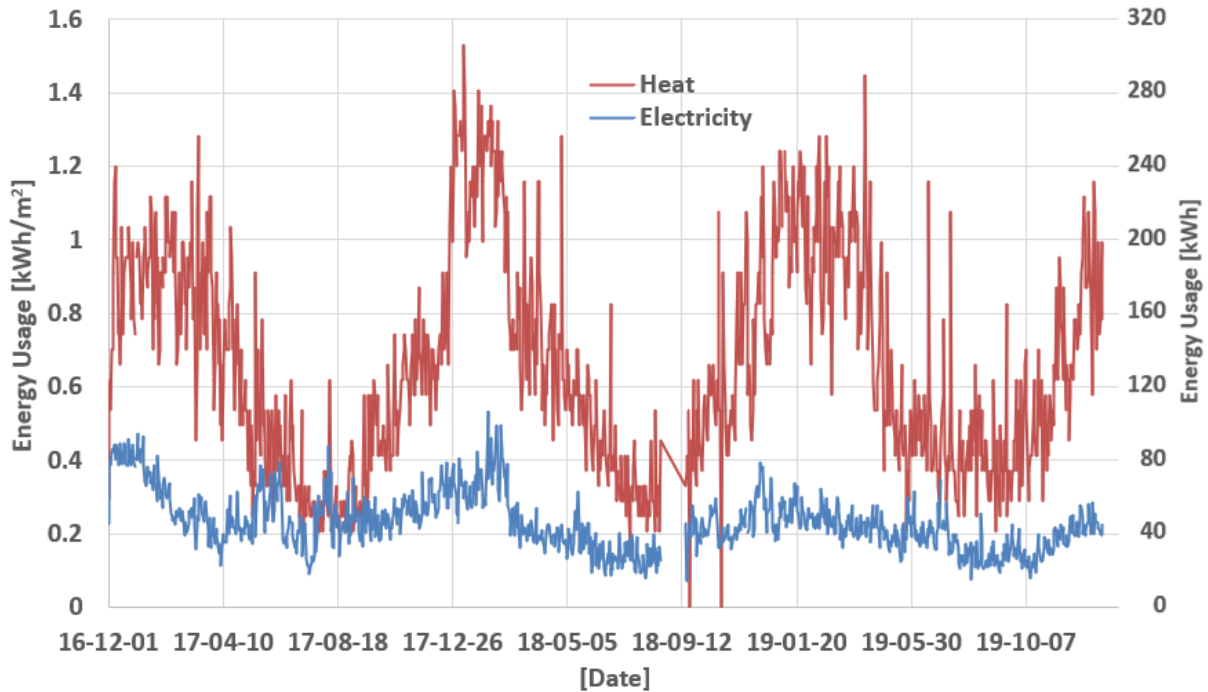


Figure 5.1 Daily energy usage normalized with living area and total usage.

Peak daily thermal energy usage of 1.53 kWh/m² and electrical energy loads of 0.53 kWh/m² occurred during the monitoring period. As mentioned in section 5.1, it is prohibited to use electricity for heating, therefore all space and domestic hot water heating are provided by the oil-fired boiler. Electrical loads for the housing units are lighting, appliances and plug loads only. While the shared mechanical room uses electricity for the non-heating devices such as water pumps, circulators and the ERV.

Because of the reasons mentioned, the heating loads are seen to be substantially greater than the electrical energy consumption, especially during the heating season. This results in the heating load taking up over 70% of the total building energy consumption in 2017, 75% in 2018 and 77% in 2019.

5.2.1 Electrical Energy

The duplex electrical energy load was determined by using the monitored daily electrical energy consumption from both housing units and the mechanical room.

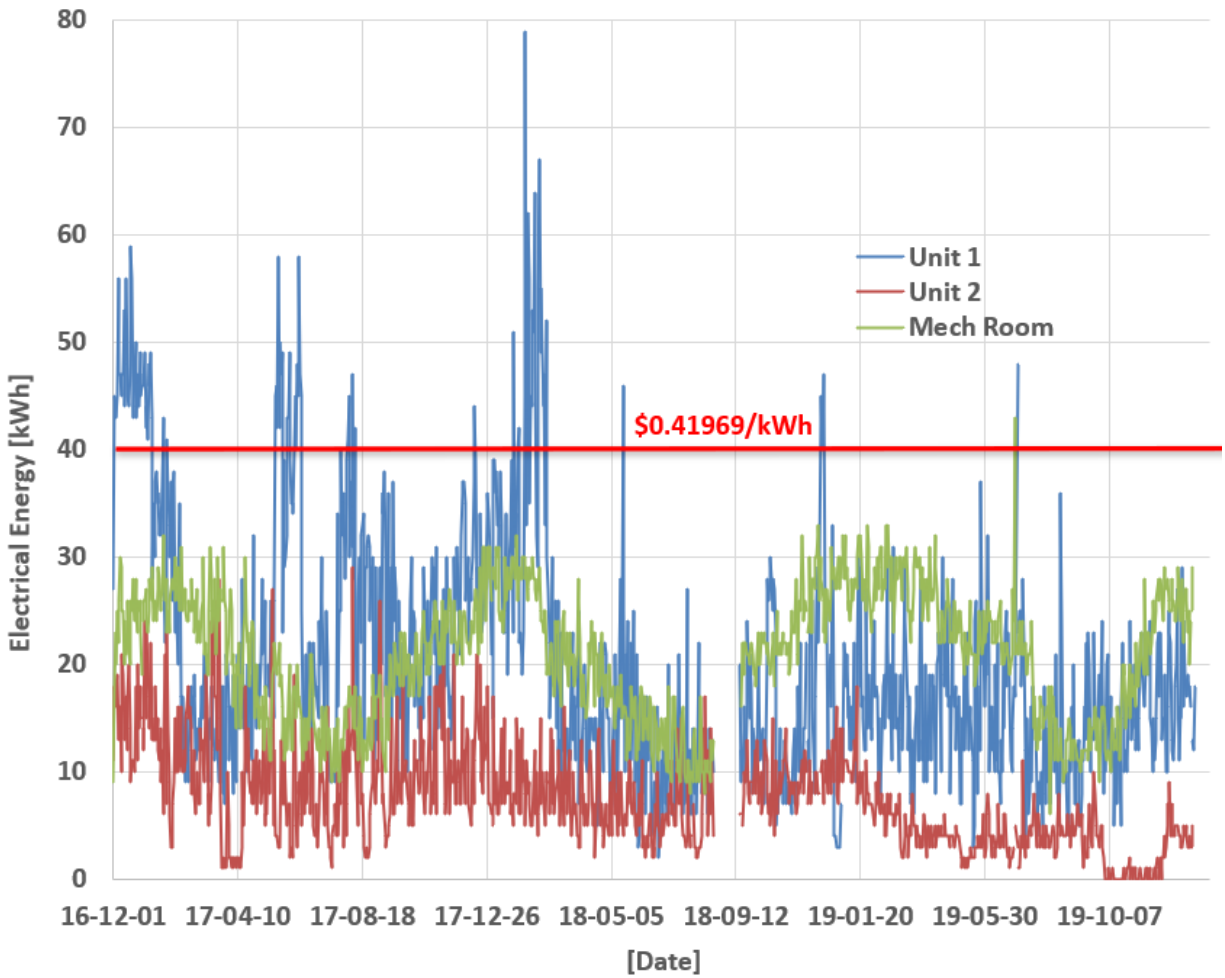


Figure 5.2 Daily electrical energy breakdown by housing unit.

The breakdown of the daily electrical energy usage per dwelling unit and mechanical room are seen in Figure 5.2. The units are viewed individually in this figure to highlight the differences in occupants' behaviours. Where, as will be seen, the combined electrical energy usage from the two units and mechanical room are billed together as one building. For this figure the base line billing

rate is set to the one housing unit rate of 40 kWh. Unit 1 had large peaks well above the 2nd tier pricing rate line while Unit 2 was under the 2nd tier pricing line for the entire monitoring period. It is noted that Unit 1 is occupied by a young couple with one small child, while Unit 2 is occupied by an older mother with an adult daughter. The mechanical room is shared between both housing units and its energy usage comes from the building's mechanical equipment such as the HVAC fans, domestic water pumps and hydronic circulation pumps etc. Large differences in electrical energy usage can be seen between both housing units and demonstrates the great differences that can occur from the occupants' behaviors, which is consistent in what was observed by Rouleau et al. (2018).

Since the duplex was equipped with one boiler to meet the heating needs of both units and mechanical room, the fuel usage could not be broken down per unit, therefore a similar analysis could not be conducted for the thermal energy usage.

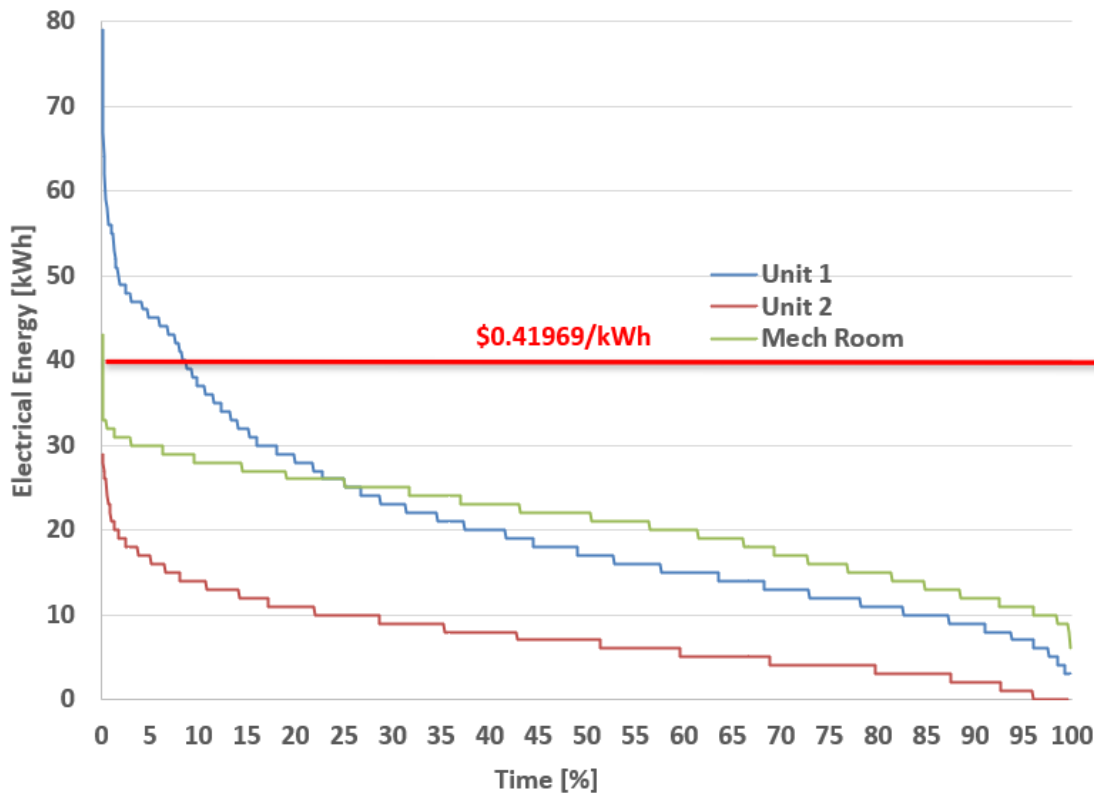


Figure 5.3 Daily electrical energy usage duration curves per housing unit.

In Figure 5.3 the daily electrical energy duration curves can be seen and shows the small percent of time that the peak loads occur. Unit 2 does not have peak electrical energy usage above the red 2nd tier pricing line and that its peaks above 20kWh/day only account for approximately 2% of the time. For the mechanical room the peak usage rises above the red line for less than 1% of the time. For housing Unit 1 the peaks are much higher crossing the red line close to 9% of the time with a maximum value reaching close to 80kWh/day. However, most of the peak values for Unit 1 are under 50kWh/Day and only rises above the red line for approximately 2% of the time. This demonstrates that the costly peaks are occurring for only a small percent of time and that the peak reductions can be achieved relatively easy by having the occupants aware of when energy usage is approaching the 2nd tier pricing range, prompting the users to turn off unnecessary devices or lighting to shed loads, waiting to use high energy consuming appliances such as clothes

washer/dryers or cooking with the oven, to the following day, shifting the loads to when the aggregated energy usage is still being charged at the base rate. Another way to reduce the daily peaks is from renewable energy production from the BIPV/T system and can lead to substantial savings by avoiding the \$0.41969/kWh rate.

5.3 NHP Coupled with BIPV/T

As discussed in more detail in Chapter 3, CWEEDS irradiance data was only available up to the end of 2017, therefore only the 2017 weather data was used in the BIPV/T simulation to obtain the electrical and thermal energy generated. A reflectance value of 0.95 was used during the periods of assumed snow cover, which gives the best-case scenario for the generated energy.

The results presented in Figure 5.4 provide a good approximation of the energy generated BIPV/T by for 2017 and the corresponding net energy usage when combined with the onsite monitored energy data from 2017. A DC to AC inverter efficiency of 97% has been assumed based on the specifications of a 6.0kWac SMA residential inverter (SMA, 2021) and has been applied to the generated electrical energy along with the fan power usage of 1.9W for a volume air flow rate of 150CFM.

5.3.1 Gross and Net Electrical Energy

The daily monitored and net electrical energy load for the entire building using the simulated energy generation from the BIPV/T are plotted in Figure 5.4. Reductions are seen helping to reduce the amount of time spent in the 2nd tier pricing range, indicated by the red line at 80kWh. As well, the net electrical energy approaches the green net zero line and dips below 0kWh for a portion of time in April 2017.

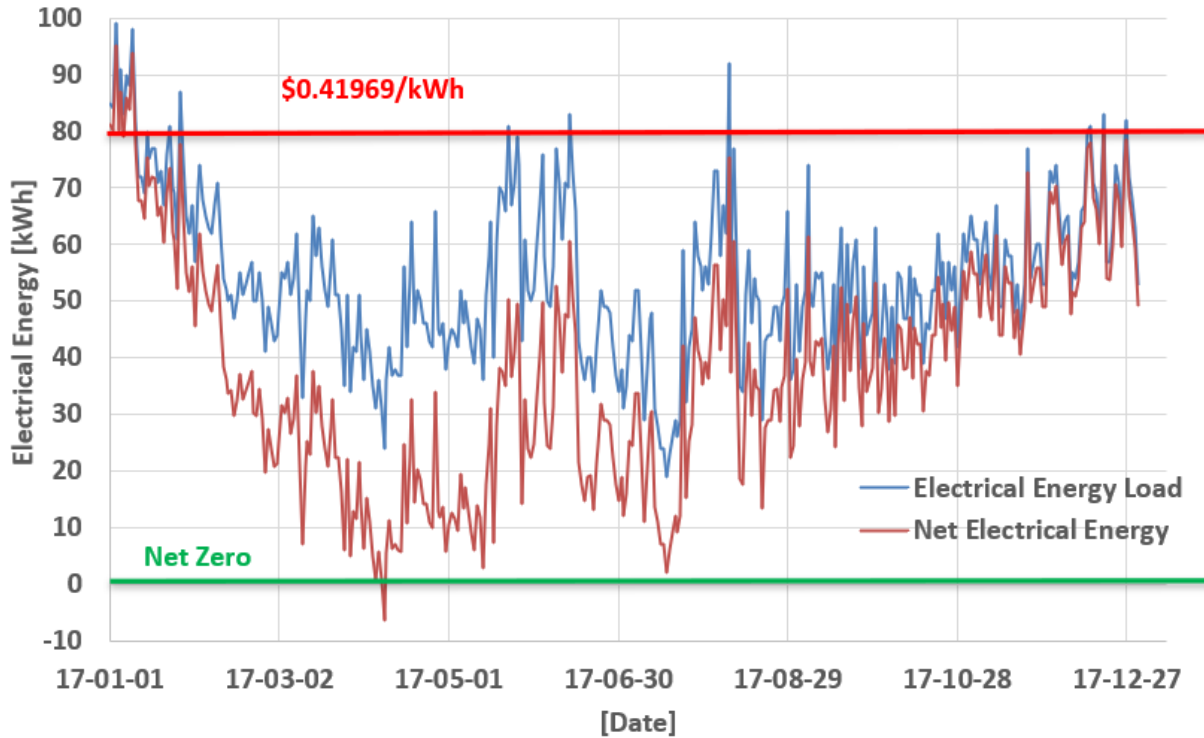


Figure 5.4 2017 daily gross and net electrical loads using BIPV/T simulated electrical energy generation.

The total duplex daily electrical energy loads collected from December 01, 2016, to December 31, 2019, are plotted in Figure 5.5 along with the simulated BIPV/T electrical energy generation and the 80kWh/day 2nd tier pricing rate line in red. The results for 2018 and 2019 are presented as well with the 2017 simulated energy production being considered the typical year generation and provides an approximate representation of the net electrical energy usage with a BIPV/T system over the entire monitoring period. Several electrical energy peaks above the red line can be seen in the \$0.41969/kWh region. As seen from Figure 5.2 these peaks can be accredited to Unit 1's high usage.

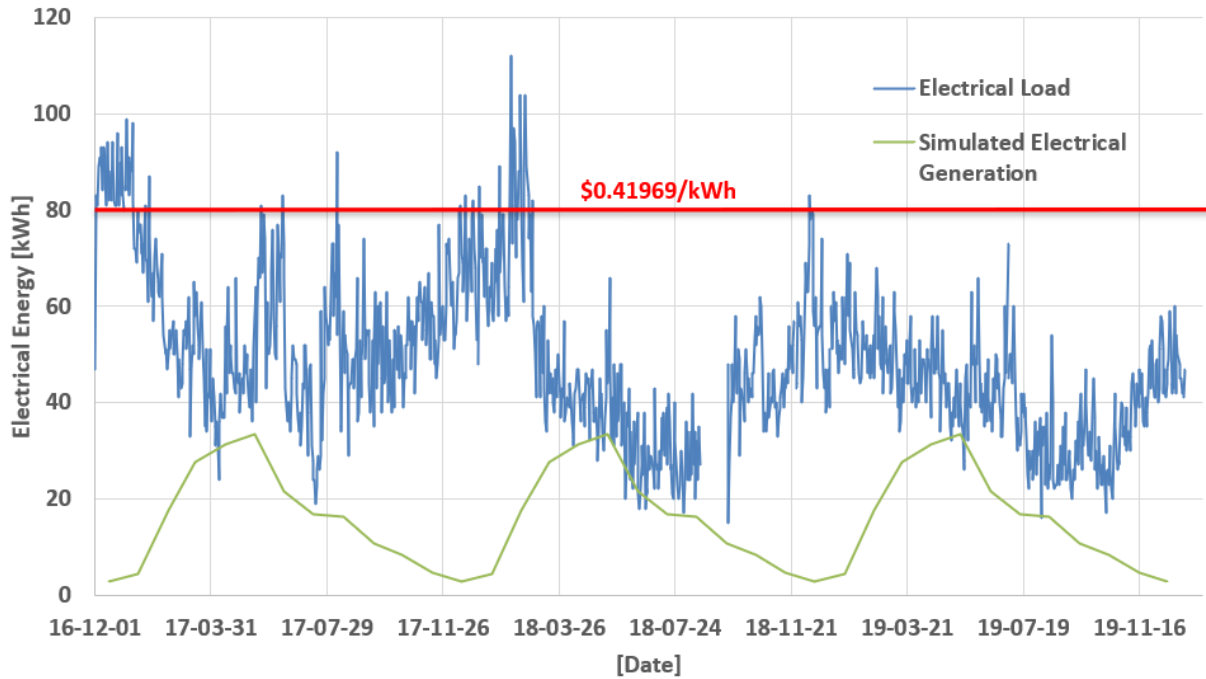


Figure 5.5 Total building electrical load and simulated PV generation.

Figure 5.6 presents the monitored gross electrical energy load from December 2016 until December 2019 along with the net electrical energy which was determined by subtracting the simulated 2017 electrical energy generation. The net energy usage can be seen to dip below the green net zero line for more periods in 2018 and 2019. As well there are reductions of peak electrical energy usage above the red 2nd tier pricing line reducing the amount of time in this costly price range. The same yearly trend of reduced net energy can be observed with the largest reductions happening during the peak irradiance months of February until September.

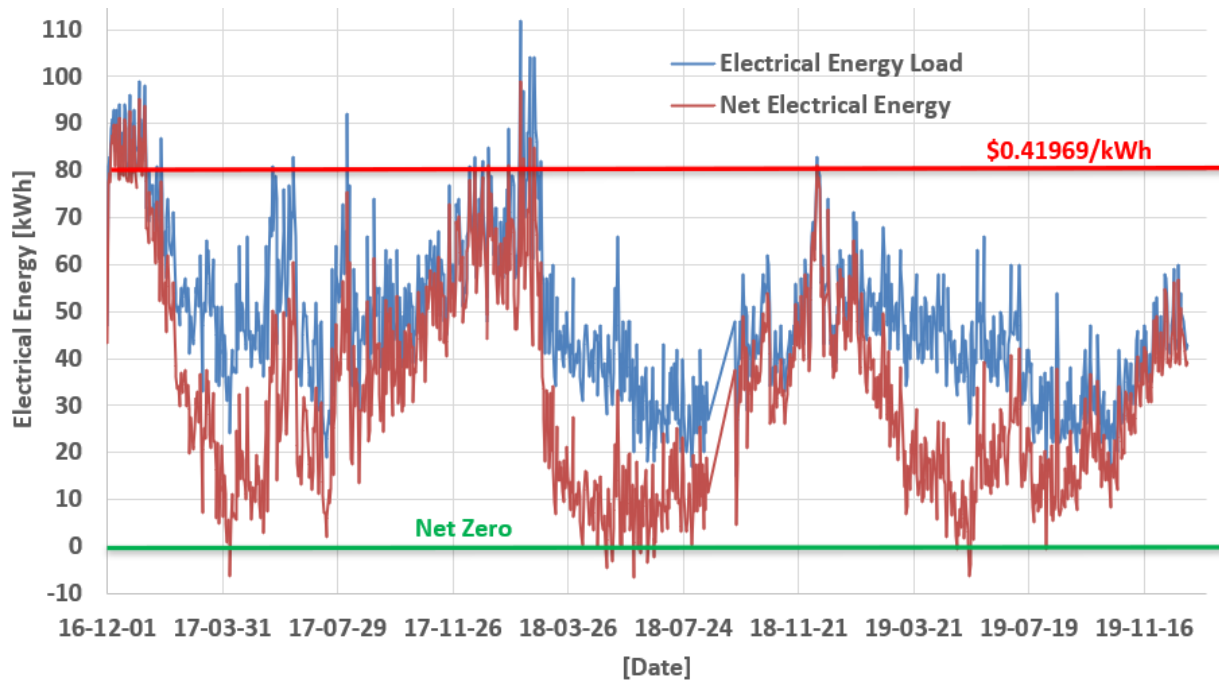


Figure 5.6 Gross and net electrical loads with BIPV/T generation.

The gross and net electrical energy time duration curve can be seen in Figure 5.7. The highest gross energy usage value of 112kWh has been reduced to the net energy amount of 99kWh and the percent of time above the red 80kWh line was reduced to approximately 2.5% for the net energy compared to the 5% for the gross energy. The net energy was approximately 2.5% of the time below the green net zero energy line as well.

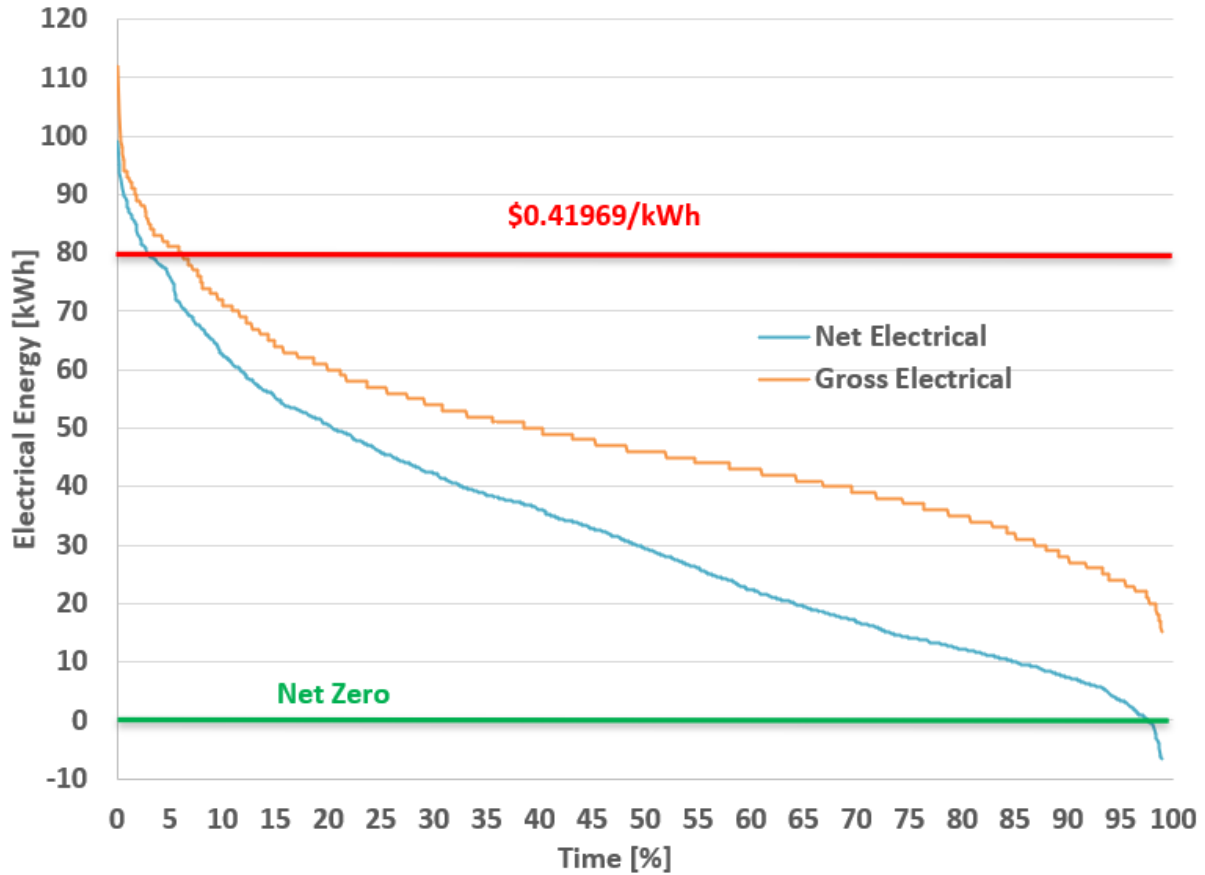


Figure 5.7 Daily gross and net electrical energy duration curves.

5.3.2 Electrical Energy Costs and Savings

A summary of the electrical energy usage and costs can be seen in Table 5.1. As mentioned previously the DN rates were updated in April 2021 and these new rates were used in the determination of the electrical energy costs and savings. It is observed that there is a \$390 savings obtained from the BIPV/T electrical energy generation for 2017. There are similar amounts seen for the other two years as well. It is worth noting that if the former pricing rates were applied there would have been even larger savings specifically from the lower base rate limit of 60kWh instead of the 2021 limit of 80kWh. Days where the 2nd tier pricing rate is avoided specifically from the BIPV/T generation can be seen, with 10 days avoided in 2017 and similar amounts in 2018, while

2019 has 0 days avoided. Taking the electrical energy generated divided by the total building electrical energy load, an electrical energy solar fraction of 30% is obtained for 2017 and up to 40% for 2019. Since power usage has not been monitored the electricity costs do not include the maximum monthly power demand charges over 50kW. If these charges were included, then there would be increased opportunities to further reduce peak charges with generated electricity.

The amount of net electrical energy available for exporting can be seen in Table 5.1 as well. These values were summed for the year and are available for net metering with the corresponding energy and dollar amounts determined to be 6kWh and \$3 for 2017, 24kWh and \$11 for 2018 and 11kWh and \$5 for 2019.

Annual normalized gross electrical energy loads are seen in Table 5.3 to be between 70-94kWh/m² with the normalized net electrical energy load seen to be between 42 -66kWh/m².

Table 5.1 Annual gross and net electrical loads with corresponding costs.

Year	2017	2018	2019
Days Data Collected	365	337	363
Annual Electrical Energy [kWh]	19,829	15,649	14,859
Generated Electrical Energy [kWh]	5,953	5,536	5,903
Net Electrical Energy [kWh]	13,876	10,113	8,956
Gross Electrical Energy Cost [\$]	1,262	1,027	915
Net Electrical Energy Cost [\$]	872	638	552
Savings [\$]	390	390	363
2nd Tier Avoided [Days]	10	11	0
Net Electrical Energy Exported [kWh]	6	24	11
Net Electrical Energy Exported [\$]	3	11	5

5.3.3 Thermal Energy

The building is equipped with one heating oil fired 47kW boiler with a thermal efficiency of 86.8%. The boiler is used to heat a water/glycol mixture for space heating, through a hydronic system, and is also used to heat the domestic hot water.

The heating load was determined using equation 5.1, with the monitored daily fuel usage F of the building in liters used. A heating value H of 10kWh/L for fuel oil was assumed and a boiler efficiency η_{boiler} of 86.8% was used based on the mechanical specifications of the building.

$$Q_{heat} = H \cdot F \cdot \eta_{boiler} \quad (5.1)$$

H = heating value of fuel

F = fuel consumption in Liters

5.3.4 Gross and Net Thermal Energy

Annual gross thermal energy loads, normalized to the living space floor area, are seen in Table 5.2 to be between 222-239kWh/m² with the net thermal energy load seen to be between 216 - 234kWh/m². Fuel savings in liters from the thermal energy recovered by the BIPV/T were determined to be 133L in 2017, 125L in 2018, and 132L in 2019. With an estimated heating oil cost of \$2/L the corresponding savings of \$267 for 2017, \$251 for 2018 and \$265 for 2019 were achieved.

Table 5.2 Gross and net thermal loads with correspond costs.

Year	Gross Thermal Energy [kWh/m²/yr]	Net Thermal Energy [kWh/m²/yr]	Fuel Savings/Year [L]	Fuel Savings/Year [\$]
2017	222.2	216.7	133.7	267
2018	232.9	227.6	125.8	252
2019	239.5	234.0	132.8	266

One of the original objectives of the NHP project was to reduce the thermal energy usage of the typical residential duplex by 60%, decreasing the amount from a baseline of 310 kWh/m² to 128 kWh/m².

It can be seen from the monitored thermal energy data that gross thermal energy usage was below the baseline value of 310 kWh/m² usage for each year, with the lowest value of 222.2kWh/m² occurring in 2017 for a 28% reduction below the baseline, however this value was well above the 128 kWh/m² target.

As was seen in the SHQ2020 report the final ACH50 was 3.05ACH which is well above the Passive House Standard of 0.6ACH50. With this level of air infiltration in the extreme cold Artic climate it was shown to be difficult to achieve substantial thermal energy reductions. In order to reduce the heating demand for future iterations of the duplex, locating the unintentional air leakage points and investigating methods to successfully seal and design against them will be an important first step to achieving the energy efficiency standard set forth.

The net thermal energy usage including the heat recovered from the BIPV/T brought the amount down to 216.7 kWh/m², which is a 30% reduction from the baseline. The 60% thermal energy reduction was not achieved with the prototype housing design coupled with the simulated BIPV/T heat recovery. However, the objective for the BIPV/T in this simulation was to pre-heat the fresh

air supply to prevent ERV frosting therefore, the heat recovered, and corresponding fuel savings were supplementary to the ERV frosting reductions.

5.3.5 Total Energy

The total annual gross energy loads, normalized to the living space floor area, which includes the electrical and thermal energy are totaled for the entire year, and can be seen in Table 5.3 to be between 307-316kWh/m². With the simulated electrical and thermal energy generation taken into consideration the total normalized annual net energy usage is reduced to 275-282kWh/m². Resulting in approximately a 10% reduction in the total usage for each year.

Table 5.3 Breakdown of annual gross and net energy.

Year	2017	2018	2019
Gross Total Energy [kWh/m²/year]	317	307	310
Net Total Energy [kWh/m²/year]	283	276	277
Gross Electrical Energy [kWh/m²/year]	94	75	71
Net Electrical Energy [kWh/m²/year]	66	48	43
Gross Thermal Energy [kWh/m²/year]	222	233	239
Net Thermal Energy [kWh/m²/year]	217	228	234

With the gross heating loads accounting for 70% to 77% of the total energy load while the net heating load accounted for 76% to 84% of the total net energy load. This demonstrates the high percentage that the heating loads account for in the total building energy usage in the Arctic and that ways to reduce the heating loads while generating thermal energy will be vital to achieve lower net energy usage.

5.4 Indoor Air Quality CO₂

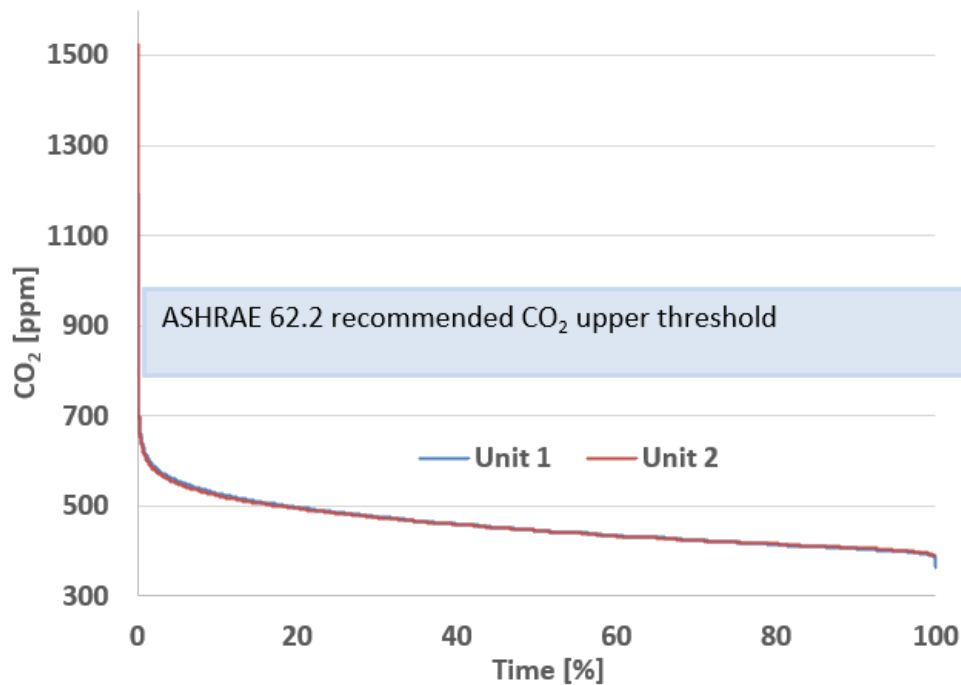


Figure 5.8 Indoor air CO₂ levels duration curve.

ASHRAE 62.2 recommends maintaining indoor CO₂ levels below 800-1000 ppm. It can be seen in Figure 5.8 that levels are below the recommended amounts approximately 99% of the time. This would indicate that both units are achieving a high level of indoor air quality.

It is recommended that for the short periods when the CO₂ levels rise above 1000ppm a booster mode can be used on the ERV/HRV to increase the volume air flow rate to provide additional fresh air. As discussed in Chapter 4, increasing the air flow through the BIPV/T decreases the outlet temperature while increasing the heat recovered. For the short portion of time when there are elevated CO₂ levels, boosting the airflow can be an option to provide an energy efficient alternative to opening a window to provide additional fresh air. However, the BIPV/T outlet temperature should be monitored and available for the occupants to observed if it is below -10°C, to verify if

there is an ERV frosting risk. Where increasing the air flow rate would further increase frosting, causing the ERV to enter recycled air mode to defrost the core. This would result in the occupants not achieving their objective of receiving additional fresh air and reducing CO₂ levels. Therefore, it is recommended for ERV usage in extreme cold climates to have an indicator to let occupants know not to use the air flow boost during such times for the reasons mentioned.

6. Conclusions

This investigation explored the simulated energy performance of a BIPV/T built into the façade of an archetypical duplex commonly used in the Nunavik territory of Northern Quebec.

A finite difference model of the air-based open loop BIPV/T was created and used hourly weather data as the inputs. Irradiance values for the small northern village of Quaqtaq, QC were created using satellite derived data from the nearby locations of Kuujjuaq, QC and Iqaluit, NU interpolated for Quaqtaq.

An easily built wood framed, façade integrated, 40m² BIPV/T collector was designed using common building materials and nominal lumber sizes, to create a series of cavities behind the PV modules to heat fresh air, in an open loop system. The ducting system was designed to be used with 150CFM to provide a high level of indoor air quality for an overcrowded household and resulted in a cavity air velocity of 0.38m/s and a main duct velocity of 3.9m/s that helped reduce the possibilities of noise and vibrations. Duct system lengths were kept to a minimum to reduce heat and pressure losses and resulted in a required fan power below 2 Watts.

The system was configured to obtain the maximum outlet temperatures to reduce the frosting times of the ERV and was seen that the cavity depth of 19mm along with a cavity width of 2m provided the highest outlet temperature compared to other larger nominal sized lumber and PV panel orientations. The 90° tilt was used for ease of construction and to match the energy production with heating needs, by taking advantage of the low solar altitude and ground reflected solar radiation during the many months of snow cover. It was seen that the snow condition had a noticeable effect on the performance of the BIPV/T, increasing the outlet air temperature up to 2°C as well as generating an additional 4.7 kWh/day, when new snow was assumed.

The simulation results showed that the BIPV/T façade was able to preheat ERV supply air all year round for several hours per day with the greatest increases occurring in April and May with temperature rises over 16°C. Defrosting time reduction was achieved up to 7 hours per day in March, supplying an additional 2,200 L of fresh air to the occupants daily.

Maximum simulated daily energy generation occurred in May with 33kWh/Day of electrical energy and 7.5 kWh/Day of thermal energy being produced. Electrical efficiency improvements of the PV were barely noticeable when using an air flow of 150CFM in the cavity, compared to a flow of 0CFM. However, electrical efficiencies improved when higher flow rates were used, with an absolute improvement of 0.27% when using a 1500CFM air flow rate. It was also noted that the electrical efficiency was above the standard test condition efficiency of 15% throughout the entire year for all flow rates, demonstrating one of the benefits of using PV in the extreme cold climate of Nunavik.

Thermal efficiencies were seen to be low with the 150CFM air flow as well, with an annual peak of 3.8%, however the thermal efficiency increased substantially with increased air flow as the 1500CFM air flow resulted in a peak thermal efficiency of 24.2% in February and peak thermal energy production of 56kWh daily in May. This demonstrated that the BIPV/T has a greater potential of recovering an increased amount of heat, when used with a building with a larger requirement of fresh air, such as a multi-unit residential building or school, without the need of a heat pump.

The total BIPV/T efficiency at converting solar radiation to useful thermal and electrical energy was seen to reach its peak using the 150CFM air flow in February with a value of 20.8%, with the lowest BIPV/T efficiency seen in July at 17.3%. When a higher flow rate of 1500 CFM was used

the resulting total BIPV/T efficiency peaked in February at 41.4% and peak total energy production of 89kWh (0.43kWh/m²) daily occurred in May.

Coupling of the simulated BIPV/T performance with collected field monitored energy data from a prototype housing duplex in Nunavik was conducted. It was seen that there was great potential for electrical loads reductions, specifically the avoidance of the high second-tier electricity rates, which resulted in substantial cost savings each year of close to \$400. As well it was shown that there were possibilities to have net electrical energy days.

Using the configuration of the BIPV/T to pre-heat 150CFM of fresh air led to modest reductions in the net thermal energy usage, but still resulted in direct fuel oil savings of approximately 130 liters per year, which is equivalent to \$260 per year when assuming a \$2 per liter fuel price in Quaqtaq. Total duplex net energy was seen to have been reduced by 10% per year with the renewable energy produced by the BIPV/T. With the gross heating loads accounting for approximately 75% of the total energy load while the net heating load accounted for 80% of the total net energy load.

In summary, the BIPV/T system has shown to assist in the reduction of net electrical energy loads, avoiding high peak electricity rates as well as pre-heating air reducing ERV frosting, helping to provide additional fresh air to the occupants while bringing down heating loads. The energy reductions from the BIPV/T also led to a direct decrease in the diesel consumption of the local Arctic diesel power plant used for local electricity generation, as well as helping to reduce the home heating fuel consumption.

In addition, the BIPV/T also demonstrated to be a renewable auxiliary energy source, not only helping to reduce the peak loads on the electrical and heating systems but also improving the

energy resilience during emergency situations, such as heating system failure, loss of fuel supply, or power failures, which is important for the energy security and a sustainable future in the remote Arctic communities of the World.

6.1 Contributions

An in-depth study of a simulated air based BIPV/T collector using local weather data was coupled with the monitored energy data from a high-performance residential duplex in Quaqtuaq, QC. This study helped to provide insight into the system's onsite performance, for validation of the appropriateness of BIPV/T for Arctic residential applications.

Contributions for the study include:

- The creation of a finite difference simulation model of an open loop air based BIPV/T system, developed to input local hourly weather data to obtain the system's electrical and thermal energy generation capabilities along with the corresponding outlet temperatures.
- Data sets of the local weather were collected, and local irradiance data was created by interpolating satellite derived values from nearby stations.
- Three years of monitored energy data from a high-performance prototype Arctic duplex was obtained and analyzed with the simulation data.
- A design for an easily built and maintained, wood framed BIPV/T system installed on the façade of an archetype, overcrowded, housing duplex in Nunavik, was created, assuming readily available building materials on the market today.

- The BIPV/T system was configured to maximize the outlet temperature during the heating season, to mitigating ERV frosting in extreme cold Arctic climate.

6.1.1 Publications

Baril, D. Athienitis, A. Ge, H. (2021). BIPV/T for Arctic Residential Applications. *International Building Physics Conference 2021*. Copenhagen, Denmark

Xie, Z. Shu, C. Reich, B. Wang, L. **Baril, D.** Ji, L. Yang, S. Bai, X. Zmeureanu, R. Lacasse, M. Wang, L. Ge, H. (2021). A field study on summer overheating of six schools in Montreal Canada. *International Building Physics Conference 2021*. Copenhagen, Denmark

Wang, R.L., H. Ge and **D. Baril.** (2020). Moisture-safe attic design in extremely cold climate: hygrothermal simulations. *Building and Environment*. 182, September 2020, 107166

Ge, H. R.L. Wang, and **D. Baril.** (2018). Field measurements of hygrothermal performance of attics in extreme cold climates. *Building and Environment* 134C: 114-130.

Baril, D., Fazio, P., & Rao, J. (2013). Field Study of Hygrothermal Performance of Housing in Canadian North. In *EIC Climate Change Technology Conference 2013*. Montreal, QC.

6.2 Future Additional Work

The following points are additional items that can be analyzed through simulations or studied experimentally to further develop the performance of BIPV/T for usage in the Arctic.

- The envelope drying potential from the increased cavity air flow and temperature created by the BIPV/T.
- The improved thermal performance of the building envelope from the heat recovered by forced air flow in the BIPV/T cavity.

- Analyzing the effect of changing the cavity surface material to increase convective and radiative heat transfer to the recovered air.
- Investigation methods for decreasing sky losses such as low-e coatings on PV surface or the addition of glazing material.
 - Search for a more accurate sky temperature correlations to be utilized for cloud covered skies.
- Developing a low order building model of the NHP to be used for model based predictive controls with weather forecasts used as inputs, for ventilation controls, energy management, and grid interaction.
- Analysis of the building's thermal energy savings when using two heating coils, one to prevent ERV frosting and the other to heat supply air from ERV to living space.
- Control of the ventilation rate to optimize outlet temperature and heat recovered to obtain high COP and maximum thermal energy from a heat pump.
- Cost analysis of energy savings over time along with envelope material savings and BIPV/T system costs.
- Creating of wood framed BIPV/T façade for experimental testing for further model calibration and validation.
- Improving the Quaqtq irradiance model using diffused irradiance correlations for cloud covered skies.
- Field trip to the NHP in Quaqtq to investigate air leakage locations and the installation of pyranometers to obtain surface irradiance values.

References

- Abouleish, M., & Yehia, Z., (2020) Indoor air quality and COVID-19. *Public Health*. 191 doi: 10.1016/j.puhe.2020.04.047.
- AMAP (1998). *AMAP Assessment Report: Arctic Pollution Issues*. Arctic Monitoring and Assessment Programme (AMAP), Oslo, Norway.
- AMAP (2017). *Snow, Water, Ice and Permafrost in the Arctic (SWIPA)*. Arctic Monitoring and Assessment Programme (AMAP), Oslo, Norway. xiv + 269 pp
- Arctic and Northern Policy Framework (2019). Available online: <https://www.rcaanc-cirnac.gc.ca/eng/1560523306861/1560523330587>
- Arctic Monitoring and Assessment Programme (AMAP 2019). *Amap Arctic Climate Change Update 2019: An Update to Key Findings of Snow, Water, Ice and Permafrost in the Arctic (Swipa) 2017*; Arctic Monitoring and Assessment Programme (AMAP): Oslo, Norway, 2019.
- Armstrong, J. (2011). "Northern SIP Building System." *K. N. D. Kott Group, ed*
- American Society of Heating, Ventilating, and Air Conditioning Engineers ASHRAE (2014). *Guideline 14-2014, Measurement of Energy and Demand Savings*; Technical Report; American Society of Heating, Ventilating, and Air Conditioning Engineers: Atlanta, GA, USA.
- Athienitis, A. K., Tzempelikos, A., Poissant, Y. (2004). Investigation of the Performance of a Double Skin Façade with Integrated Photovoltaic Panels. *In EuroSun2004 Proceedings*. Freiburg, Germany.
- Aubin D., et al (2019) *IOP Conf. Ser.: Mater. Sci. Eng.* 609 042055
- Bambara, J., Athienitis, A.K., O'Neill, B., (2011) Design and performance of a photovoltaic/thermal system integrated with transpired collector, *Build. Eng.* 117 403e410.
- Baril, D., Fazio, P., & Rao, J. (2013). Field Study of Hygrothermal Performance of Housing in Canadian North. *In EIC Climate Change Technology Conference 2013*. Montreal, QC.
- Beattie C., Fazio P., Zmeureanu R., and Rao J., (2018) experimental study of air-to-air heat/energy exchangers for use in arctic housing, *Applied Thermal Engineering* 129 p 1281-91
- Berquist, J., Banister, C., & Pellissier, M., (2021). Comparison of Heat Recovery Ventilator Frost Control Techniques in the Canadian Arctic: Preheat and Recirculation. *E3S Web of Conferences*. 246. 11010. 10.1051/e3sconf/202124611010.

- Bolton K., Lougheed M., Ford J., Nickels S., Grable C., Shirley J.,(2011) “What we know, don’t know, and need to know about climate change in Inuit Nunangat”, *Department of Indian and Northern Affairs Canada, Climate Change Adaption Program (CCAP)*, pp.15.
- Buryachenko, S., et al (2020) IOP Conf. Ser.: *Earth Environ. Sci.* 539 012024
- Candanedo, L. M., Athienitis, A. K., & Park K., (2011) convective heat transfer coefficients in a building- integrated photovoltaic/thermal system. *ASME. J. Sol. Energy Eng.* 133
- Candanedo, L. M., Athienitis, A. K., Candanedo, J. A., O'Brien, W., & Chen. Y., (2010) transient and steady state models for open-loop air-based BIPV/T systems *ASHRAE Transaction* **116** p 600-12.
- Çengel, Y.A., and Ghajar, A.J., (2011) *Heat and Mass Transfer: Fundamentals & Applications. McGraw-Hill*, New York, 924.
- Chemisana D., Lopez-Villada, J., Coronas, A., Rosell,J., Lodi, C., (2013)Building integration of concentrating systems for solar cooling applications. *ApplThermEng*; 50:1472–9.
- Chen Y., (2012) Design and Evaluation of Facade-Integrated Solar Technologies Suitable for High-Latitude Applications. *Master’s Thesis*. Concordia University, Montréal, Canada
- Chen, Y., Fazio, P., Athienitis, A. K., & Rao, J. (2012a). Sustainable Building Design in Cold Regions: High Performance Envelope and Façade-Integrated Photovoltaic/Solar Thermal Systems at High Latitudes. In *Cold Regions Engineering 2012* (pp. 199–209). Quebec, QC: American Society of Civil Engineers. doi:10.1061/9780784412473.020
- Daigle, Q., & O’Brien, P.G., (2020) Heat Generated Using Luminescent Solar Concentrators for Building Energy Applications. *Energies*. 13(21):5574. <https://doi.org/10.3390/en13215574>
- Davies, J.A., M. Abdel-Wahab, and D.C. McKay, (1984): Estimating Solar Irradiation on Horizontal Surfaces. *Int. J. Solar Energy*, Vol. 2, pp. 405-424.
- Dehlin, S., Heincke, C., Redman, Koskinen, P.,(2017) huset – ett lågenergiaparhusi Kiruna. Projekt – *Energimyndigheten*.
- Dermardiros, V., Athienitis, A., & Bucking, S., (2019) "Energy Performance, Comfort, and Lessons Learned from an Institutional Building Designed for Net Zero Energy." *ASHRAE Transactions*, vol. 125, no. 1, Jan. 2019, pp. 682+..
- Ding, W.X., Zhao, Y.H., Ji, X., (2013) *App. Mec. Mat. J.*, 368, 1135-1138
- Dow (2021), DOWFROST Heat Transfer Fluid Technical Data Sheet. <https://www.dow.com/en-us/pdp.dowfrost-heat-transfer-fluid.23545z.html> Retrieved October 26, 2021
- Duffie, J. A., & Beckman, W. A., (2013), *Solar Engineering of Thermal Processes*, Willey, Hoboken, NJ

- Environment Canada (2020) Historical Climate Data. Retrieved May 26, 2020, from <http://climate.weather.gc.ca/>
- EVLO (2018) Projects: Integrating renewable energies. Retrieved July 31, 2021 <https://www.evloenergy.com/en/projects/>
- Garber-Slaght, R., & Stevens, V., (2016) energy recovery ventilators in cold climates. *Cold Climate Housing Research Center* Fairbanks, Alaska, USA
- Ge, H., Wang, R.L., & Baril, D., (2018) Field measurements of hygrothermal performance of attics in extreme cold climates. *Building and Environment* 134C: 114-130.
- Ge, H. & Y. Ye (2007). Investigation of ventilation drying of rainscreen walls in the coastal climate of British Columbia. *Proceedings of Thermal Performance of the Exterior Envelopes of Buildings X*. ASHRAE, Florida.
- George, J., (2020). Plans to replace Kugluktuk's new power plant delayed. Nunatsiaq News, May 20, 2020
- Giordano, N., & Raymond, J., (2020) Field report and monitoring plan of the groundsource heat pump system for the community swimming pool in Kuujuaq (Nunavik, Canada). Rapport de recherche (R2007). *INRS, Centre Eau, Terre et Environnement*, Québec.
- Gordon, A., (2017). Solar panel pilot in Kuujuaq may be the future for Nunavik communities. *CBC News*, December 03, 2017
- Hottel, H. C., (1976) a simple model for estimating the transmittance of direct solar radiation through clear atmospheres *Sol. Energy*, 18 p 129-134
- Hydro Quebec, (2021) 2021 Electricity Rates
- Impact Canada, (2021) Off-Diesel Initiative <https://impact.canada.ca/en/challenges/off-diesel> Retrieved November 05, 2021
- Indigenous Clean Energy, (2021) 20/20 Catalysts https://indigenouscleanenergy.com/2020-catalysts-program/about-the-program/#program_goals Retrieved November 05, 2021
- International Energy Agency (2019) Photovoltaic Power Systems Programme, Trends in Photovoltaic Applications.
- Joshi, S.S., & Dhoble, A.S., (2018) Photovoltaic -Thermal systems (PVT): technology review and future trends, *Renew. Sustain. Energy Rev.* 92 848e882.
- Josien, A.J.C., Buizje, & A., Wright, J., (2021) The potential for the Passive House standard in Longyearbyen-the High Arctic Building *Serv. Eng. Res. Technol.* Vol. 42(3) 307–325
- Kayello, A., Athienitis, A., & Ge, H. (2016). Natural Ventilation of Attics Coupled with BIPV/T in Arctic Climates. In *Proceedings of the eSim Building 148 Performance Simulation Conference* (pp. 433–443). Hamilton, ON: McMaster University.

Kayello, A., Ge, H., & Athienitis, A., (2017a) Attic ventilation in Northern Canadian climates, in 15th *Canadian Conference on Building Science and Technology*, Vancouver, British Columbia, Canada, pp. 1–16

Kayello, A., Ge, H., Athienitis, A., & Rao, J. (2017b). Experimental study of thermal and airtightness performance of structural insulated panel joints in cold climates. *Building and Environment*, 115, 345–357. <http://doi.org/10.1016/j.buildenv.2017.01.031>

Knight, F., (1950s) Igloo. *Avataq Cultural institute*

Last, J., (2020) Kugaaruk takes small step toward sustainable energy with new solar panels. *CBC News*, October 08, 2020

Li, J., Zmeureanu, R., & Ge, Hua., (2021). Simulation of energy impact of an energy recovery ventilator in Northern housing. *E3S Web of Conferences*. 246. 10005. 10.1051/e3sconf/202124610005

Liu, B. Y. H., & Jordan, R. C., (1960) the interrelationship and characteristic distribution of direct, diffuse and total solar radiation *Sol. Energy*, 4 p 1-19

Liu, B. Y. H. & Jordan, R. C., (1963) ‘‘The Long-Term Average Performance of Flat-Plate Solar Energy Collectors.’’ *Solar Energy*, 7, 53.

Ma, L., Ge, H., Thirunavukarasu, & A., Athienitis, A., (2019) *IOP Conf. Ser.: Mater. Sci. Eng.* 609 072056

Ma, L., Ge, H., Wang, L. et al. (2021) Optimization of passive solar design and integration of building integrated photovoltaic/thermal (BIPV/T) system in northern housing. *Build. Simul.* 14, 1467–1486. <https://doi.org/10.1007/s12273-021-0763-1>

Matrix Energy (2007) Projects: Kuujuaq Airport Terminal. Retrieved June 21, 2021, from <http://www.matrixenergy.ca/stand-alone-systems/grid-tie-kuujuaq-airport.html>

Matrix Energy (2011) Projects: Northern Community Science Centre. Retrieved October 22, 2021

McAdams, W. H., (1954) Heat Transmission _Series in Chemical Engineering, *McGraw-Hill*, New York, NY

McKay, J., (2019). Town in Canadian central Arctic to get hybrid solar-diesel power plant. *CBC News*, May 23, 2019

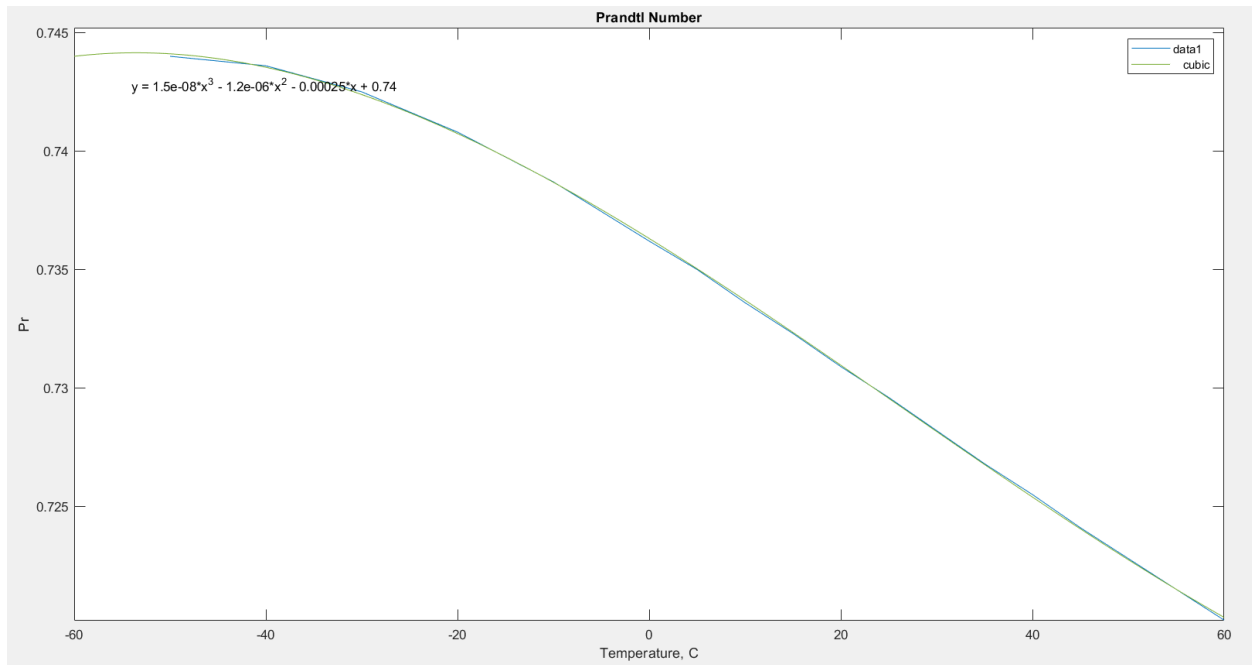
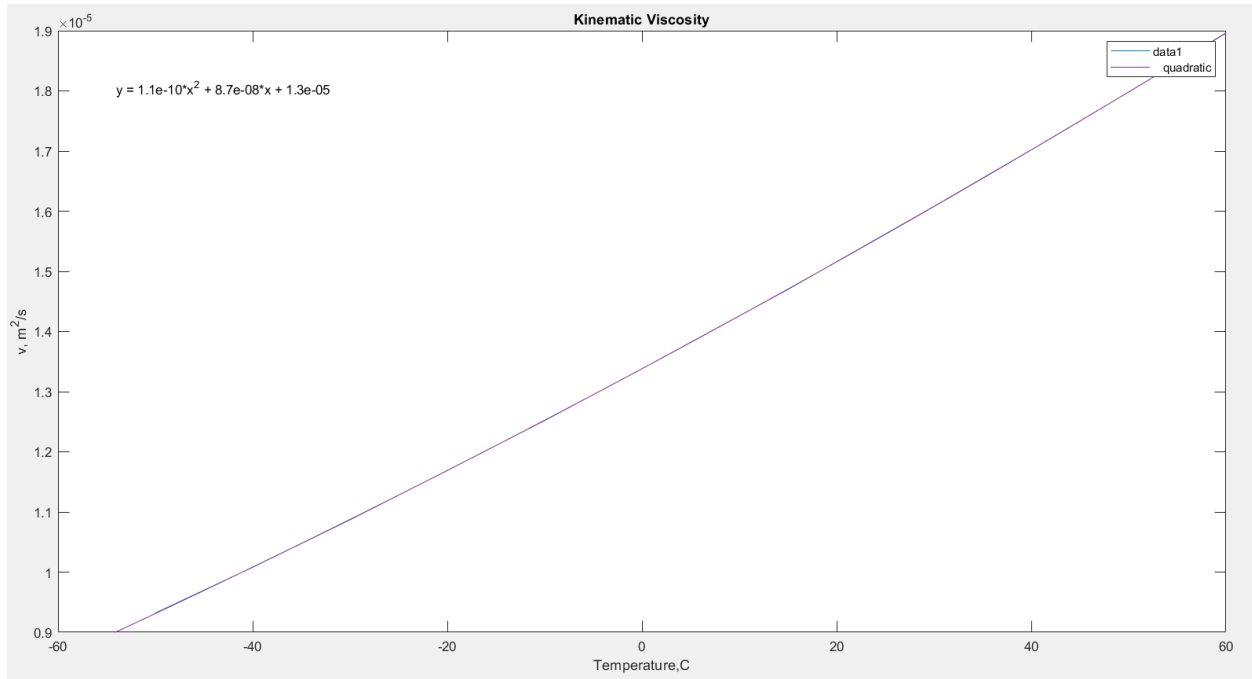
McQuiston, F. C., Parker, J. D., & Spitler, J. D. (2000). Heating, ventilating, and air conditioning: Analysis and design. New York: *John Wiley & Sons*.

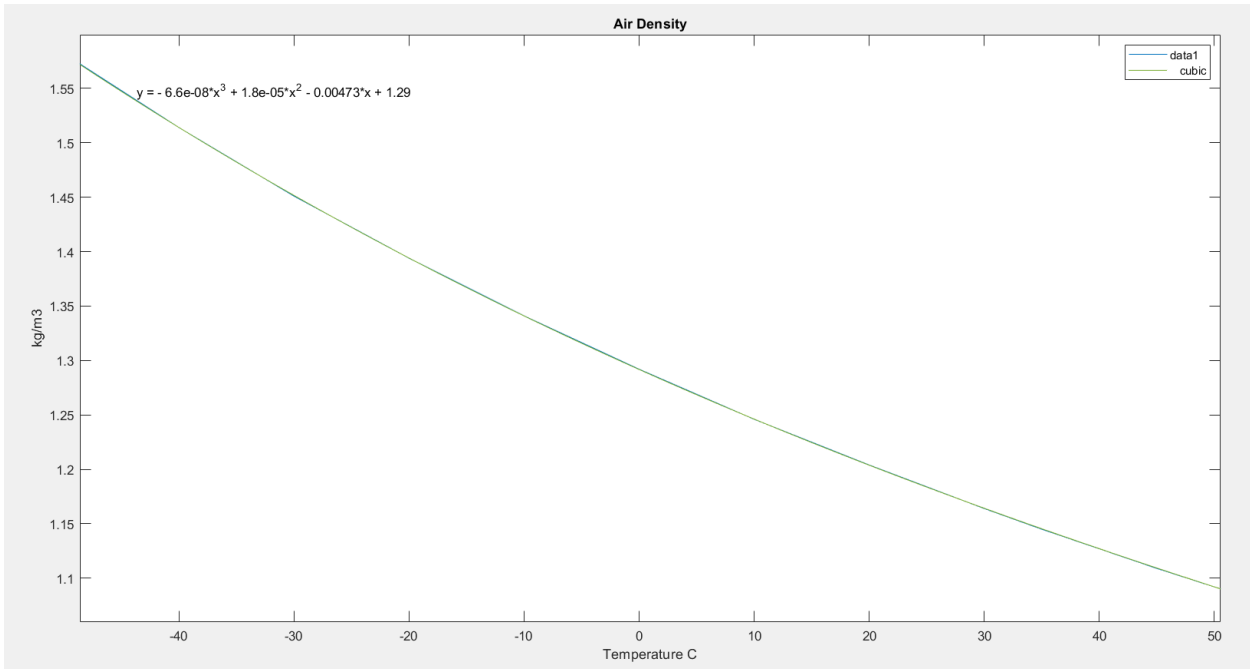
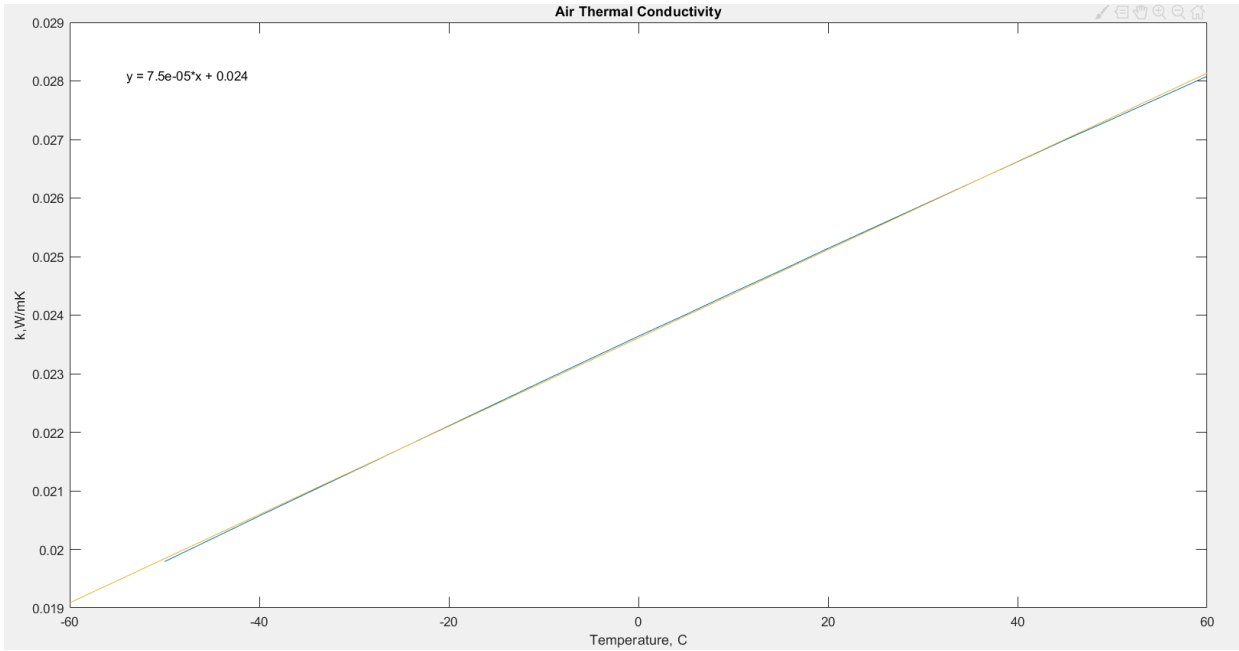
Natural resources Canada (NRCAN 2011). Survey of household energy use—summary report. Available from: <http://oee.nrcan.gc.ca/Publications/statistics/sheu-summary/pdf/sheusummary>

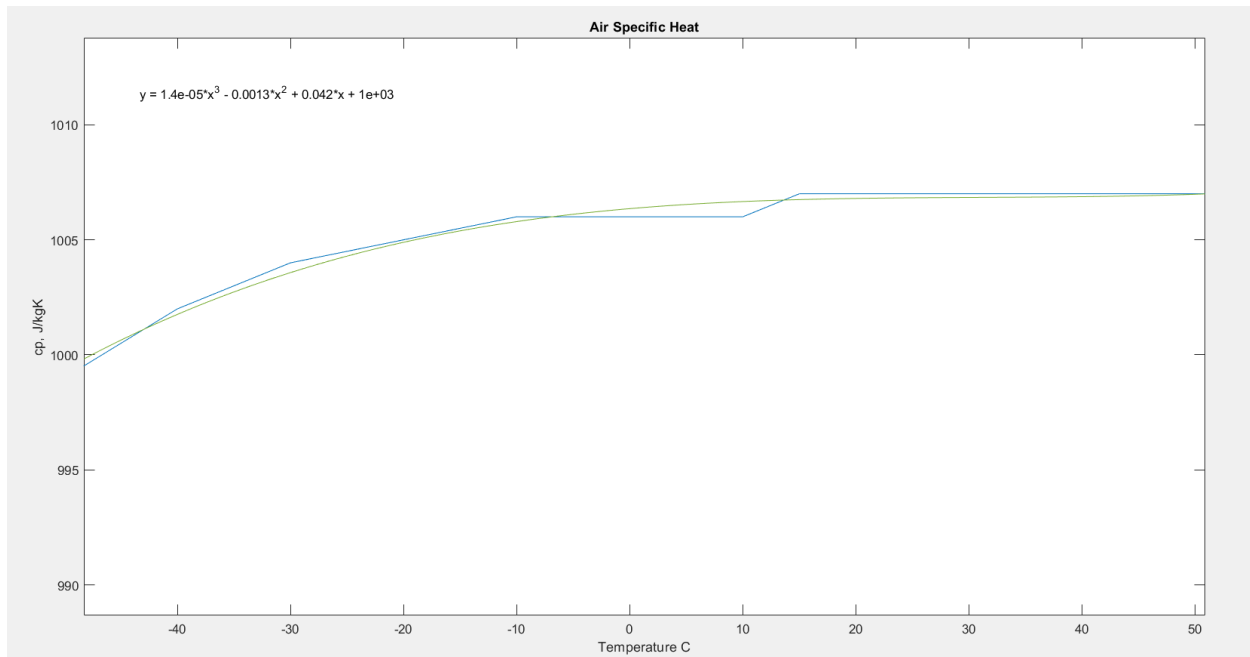
- Ouazia, B., et al (2019) *IOP Conf. Ser.: Mater. Sci. Eng.* 609 052017
- Pearson, V., (1965) Caroline preparing sealskin. *Avataq Cultural Institute*
- Perreault, K., Riva, M., Dufresne, P., & Fletcher, C., (2020) Overcrowding and sense of home in the Canadian Arctic, *Housing Studies*, 35:2, 353-375, DOI: 10.1080/02673037.2019.1602720
- PikeResearch (2012). Building Integrated Photovoltaics - BIPV and BAPV: Market Drivers and Challenges, Technology Issues, Competitive Landscape, and Global Market Forecasts (Boulder: Navigant).
- Pinel, P., Cruickshank, C., Beausoleil-Morrison, I., & Wills, A. (2011). A review of available methods for seasonal storage of solar thermal energy in residential applications. *Renewable and Sustainable Energy Reviews* 15, 3341-3359.
- Plan Nunavik, (2011) Kativik Regional Government, Makivik Corporation “*Plan Nunavik*” *Avataq*, Westmount
- Ravasio, L., Sveen, S.E., Riise, R., (2020) Green Building in the Arctic Region: State-of-the-Art and Future Research Opportunities. *Sustainability* 2020, 12, 9325.
<https://doi.org/10.3390/su12229325>
- Reijenga, T., (2000) Photovoltaic building integration concepts – what do architects need? *IEA PVPS Task7 workshop*
- Rogers, S., (2018) Nunavut community’s solar panels target for vandalism. *Nunatsiaq News*, March 22, 2018
- Rouleau, J., & Gosselin L., (2021) Impacts of the COVID-19 lockdown on energy consumption in a Canadian social housing building *Appl. Energy*, 287 p. 116565 Apr 1
- Rouleau, J., Gosselin, L., & Blanchet, P., (2018) Understanding energy consumption in high-performance social housing buildings: A case study from Canada, *Energy, Elsevier*, vol. 145(C), pages 677-690.
- Rounis, E.D., Athienitis, A., & Stathopoulos, T., (2020) Review of air-based PV/T and BIPV/T systems-Performance and modeling. *Renewable Energy* 163 (2021) 1729-1753
- Sharples, S., & Charlesworth, P. S., (1998), Full-Scale Measurements of Wind-Induced Convective Heat Transfer From a Roof-Mounted Flat Plate Solar Collector, *Sol. Energy*, 62_2, pp. 69–77.
- Sigounis, A., Rounis, E D., Athienitis, A., & Vallianos, C., (2021) Control-oriented model for air-based BIPV/T systems. International Building Physics Conference 2021. Copenhagen, Denmark

- SMA. (2021). Service & Support Downloads. Retrieved October 01, 2021, from <https://www.sma-america.com/service-support/downloads.html>
- Société d'habitation du Québec SHQ (2020) rapport – prototype d'habitation nordique à Quaqtaq Québec, Québec, Canada
- Société d'habitation du Québec SHQ (2018) Housing construction in Nunavik-Guide to good practices. Québec, Canada
- Société d'habitation du Québec SHQ (2014) Housing in Nunavik. Québec, Canada
- Stull, R.B., (2000) Meteorology for Scientists and Engineers. 2nd Edition, *Brooks/Cole Thomson Learning*, Pacific Grove.
- Sultan, S.M., & Efsan, M.N.E., (2018) Review on recent Photovoltaic/Thermal (PV/T) technology advances and applications, *Sol. Energy* 173 (2018) 939e954.
- Test, F. L., Lessmann, R. C., & Johary, A., (1981), "Heat Transfer During Wind Flow Over Rectangular Bodies in the Natural Environment," *ASME Trans. J. Heat Transfer*, 103, pp. 262–267.
- Toffanin, R., Ge, H., & Athienitis, A., (2018) Integration of building integrated photovoltaic/thermal (BIPV/T) system with heat recovery ventilators for improved performance under extreme cold climates *Cold Climate HVAC 2018*
- Tranter, E., (2020). Wind–and solar-powered greenhouse takes off in Gjoa Haven. *Nunatsiaq News*, February 03, 2020
- Vladykova, P., Rode, C., Kragh, J., & Kotol, M., Low-energy house in arctic climate: five years of experience, *J. Cold Reg. Eng.* 26 (2012) 79–100.
- Winfield, E.C., Rader, R., Zhivov, A., Dyrelund, A., Fredeen, C., et al. (2021) *ES3 Web of Conferences*; Les Ulis, Vol. 246, DOI:10.1051/e3sconf/202124608004
- Yang, T., & Athienitis, A., (2016) a review of research and developments of building-integrated photovoltaic/thermal (BIPV/T) systems *Renewable Sustainable Energy Rev.* 66 p 886-912
- Yang, T., & Athienitis, A., (2014) a study of design options for a building integrated photovoltaic/thermal (BIPV/T) system with glazed air collector and multiple inlets *Sol. Energy* 104 p 82-92

Appendix A Air Properties







Appendix B ASHRAE standard 62.2 Fresh Air Requirements Calculations

Total Ventilation Rate

SI

$$Q_{\text{tot}} = 0.15A_{\text{floor}} + 3.5(N_{\text{br}} + 1)$$

Q_{tot} = total required ventilation rate, L/s

IMP

$$Q_{\text{tot}} = 0.03A_{\text{floor}} + 7.5(N_{\text{br}} + 1)$$

Infiltration Credit

$$Q_{\text{fan}} = Q_{\text{tot}} - \Phi(Q_{\text{inf}} * A_{\text{ext}})$$

$\Phi = 1$ for balanced ventilation

$A_{ext}=1$ for a detached house, or for horizontally attached units, the amount of area not attached to the other unit divided by the entire envelope surface area.

Effective Annual Infiltration Rate (Q_{inf})

wsf=weather and shielding factor

wsf assumed to be 1 for Quaqtq

$$Q_{inf}=0.052*Q_{50}*wsf*(H/H_r)^z$$

H= vertical distance between the lowest and highest above-grade points within the pressure boundary, ft (m)=2.44m for Pilot House

H_r =reference height, 8.2' (2.5m)

$z=0.4$

Different Occupant Density

Assumed to have 2 people living in a 1 bedroom dwelling and an additional person for each bedroom. Each additional person adds 7.5 cfm or 3.5L/s.

Appendix C MATLAB Code BIPV/T

```
clearvars;
load('MonthlyWeatherData.mat');
%Environmental Conditions Inputs

G=DecCloud90TotalRad70; %incident irradiance W/m2

Textr=DecTEextrAvgHour; %Exterior air temperature in Celcuis From
Environment and Climate Change Canada

Vwind=DecWindSpeedAvgHour; %Velocity of wind in m/s From
Environment and Climate Change Canada

Tsky=DecTSkyAvgHour; % Correlation from Duffie&Beckman 2013

Tin=20; %Indoor air temperature in Celcuis

%-----
%-----
%BIPV/T Cavity Properties
```

```

Hch=0.019; %channel height in m 19X64 wood strapping For
Validation 0.04m

Wch=1.936; %channel width in m 19X64 For Validation 0.38m

Lch=4; %channel length in m For Validation 0.06 to 2.89m

nCV=200; %number of control volumes

Lcv=Lch/nCV; %Control volume length

Ach=Hch*Wch;% cross sectional area of air channel in m^2

P=2*Hch+2*Wch;%wetted area perimeter of channel in meters

Dh=4*Ach/P; %Hydraulic diameter of channel in meters

Aspect_Ratio=Wch/Hch;

Acv=Wch*Lcv;%Area of control volume in m2

ChannelAmounts=5; %Amount of channels installed on facade used
to determine flow rate in each channel

cfm=150; %48.4CFM for 1.5 m/s 8.5CFM for 0.26m/s

m3pers=cfm*0.00047194745; %meters cubed per second conversion
from cubic feet per minute

ERVFlowRate=m3pers; %m3/s High setting of Venmar EKO 1.5 ERV
(157CFM)

M=ERVFlowRate/ChannelAmounts;%Volume Flow rate in each channel
in m3/s

Vch=ERVFlowRate/(Ach*ChannelAmounts); %average velocity of air
in channel in m/s

Rins=9.55/Acv; %Equavalent Wall thermal resistance RSI of
Quaqtaq House wall=9.55
%1.6RSI used for 2" of XPS in Tingting experimental work
F=1; %View factor of cavity walls

E1=0.95; % PV top surface emisivity (0.95 Tefzel) (Glass 0.95)

E2=0.95;% PV bottom surface emisivity (steel plate 0.8)

```

```
E3=0.2;% Channel back surface emisivity (XPS)
```

```
%-----  
-----
```

```
%Initial values
```

```
% QskyTotalCV=(1:48);
```

```
for i=1:24
```

```
TPV(1,i)=Textr(i);
```

```
% TPV=(1:20)';
```

```
% qsky=(1:20)';
```

```
qsky(1,i)=1;
```

```
% Tma=(1:20)';
```

```
Tma(1,i)=Textr(i);
```

```
% TB=(1:20)';
```

```
TB(1,i)=Textr(i);
```

```
% Toutlet=(1:20)';
```

```
Toutlet(1,i)=-5;
```

```
% hr=(1:20)';
```

```
hr(1,i)=2.6;
```

```
% Qrec=(1:20)';
```

```
QrecCV(1,i)=0;
```

```
QrecTotal(1,i)=0;
```

```
% eff_PV=(1:20)';
```

```
eff_PV(1,i)=0.17;
```

```
% Pelec=(1:20)';
```

```
Pelec(1,i)=0;
```

```
% Rhr=(1:20)';
```

```
Rhr(1,i)=1.5;
```

```
% Kin_ViscosityBM=(1:20)';
```

```
Kin_ViscosityBM(1,i)=1.338e-5;
```

```
% Re=(1:51)';
```

```
Re(1,i)=3000;
```

```
% Pr=(1:20)';
```

```
Pr(1,i)=0.7362;
```

```
% Nu_f=(1:20)';
```

```
Nu_f(1,i)=22;
```

```
% Nu_b=(1:20)';
```

```
Nu_b(1,i)=37;
```

```
% k=(1:20)';
```

```
k(1,i)=0.02364;
```

```
% hf=(1:20)';
```

```
hf(1,i)=20;
```

```
% hb=(1:20)';
```

```
hb(1,i)=20;
```

```

% Rhf=(1:20)';
Rhf(1,i)=0.06;
% Rhb=(1:20)';
Rhb(1,i)=0.04;
% air_density=(1:20)';
air_density(1,i)=1.42;
% mdot=(1:20)';
mdot(1,i)=0.0092;
% cpair=(1:20)';
cpair(1,i)=1005;
% Sgn=(1:20)';
% Sgn(1,i)=-1;
% Tsky=(1:20)';
% Tsky(1,i)=Textr(i);
% Tinlet=(1:20)';
% Tinlet(1,i)=Textr(i);
% ho=(1:20)';
ho(1,i)=18;
% Rho=(1:20)';
Rho(1,i)=0.04;
% Qins=(1:20)';
Qins(1,i)=0;

end
%-----
-----

%-----
-----
%PV Module Properties based on manufactures specifications

%specific to the PV surface construction
alphaPV=0.90;%Absorbance of PV

eff_STC=0.15;%PV module efficiency at Standard Test Conditions
written as a decimal For Validation 0.061

beta=0.0045;%PV Module Temperature coefficient %/degree C

Tstc=20;%Standard Test Condition Temperature in degree C

%-----
-----
%constants

```

```

sigma=5.67e-8;%Stefan-Boltzmann constant W/m2

%-----
%-----

%Simplified Energy Balance without PV resistance

m=1;
for j=1:24 %iteration using hourly weather data for 24 hours

    PelecTotalCV(1,j)=0;

    QrecTotalCV(1,j)=0;

    QskyTotalCV(1,j)=0;

    Qsky(1,j)=0;

    TPVTotal(1,j)=0;

    TBTotat(1,j)=0;

    TmaTotal(1,j)=0;

    GrTotal(1,j)=0;

    ReTotal(1,j)=0;

    mdotTotal(1,j)=0;

    air_densityTotal(1,j)=0;

    cpairTotal(1,j)=0;

    for y=1:nCV

p=1;

for n=1:50 %number of iterations to have results converge

```

```

%-----
%-----
%-----

if y<=1%if else loop to have Tinlet= Textr for first iteration
loop, then Tinlet= previous Toutlet for next Control volumes
iteration loops

    Tinlet(p+1,j)=Textr(m);

else
    Tinlet(p+1,j)=Toutlet(51,m); %Uses the converged Toutlet
result from the previous timestep as the Tinlet
end

TPV(p+1,j)=((Textr(m)/Rho(p,j))+(alphaPV*G(m)*Acv)-Pelec(p,j)-
Qsky(p,j)+(Tma(p,j)/Rh(p,j)))+(TB(p,j)/Rhr(p,j))/((1/Rho(p,j))+
(1/Rhf(p,j))+(1/Rhr(p,j)));%PV temperature assumed to be uniform
temperature on front and back

TB(p+1,j)=((TPV(p,j)/Rhr(p,j))+(Tin/Rins)+(Tma(p,j)/Rhb(p,j)))/((
1/Rhr(p,j))+(1/Rins)+(1/Rhb(p,j)));%Cavity back surface
temperature

Toutlet(p+1,j)=((TPV(p,j)+TB(p,j))/2)+(Tinlet(p,j)-
((TPV(p,j)+TB(p,j))/2))*exp(2*Lcv/((M*cpair(p,j)*air_density(p,j)
))/ (Wch*(hb(p,j)+hf(p,j))/2)); %From Athienitis et al 2004

%
A(p+1,j)=((M*cpair(p,j)*air_density(p,j))/(Wch*(hb(p,j)+hf(p,j))
/2));
%
% e(p+1,j)=exp(-
2*Lcv/((M*cpair(p,j)*air_density(p,j))/(Wch*(hb(p,j)+hf(p,j))/2)
));

Tma(p+1,j)=(Tinlet(p,j)+Toutlet(p,j))/2; %Bulk mean temperature
at which air properties are determined for determining Reynolds
Number and Qrec

QrecCV(p+1,j)=((TPV(p,j)-Tma(p,j))/Rh(p,j))+((TB(p,j)-
Tma(p,j))/Rhb(p,j)); % Heat recovered from control volumes in
Watts. Variable will display only the values for the final
control volume. QtotalCV used to sum all of the control volume.

```

```

eff_PV(p+1,j)=eff_STC*(1-beta*(TPV(p,j)-Tstc)); %PV electrical
efficiency, function of PV temperature

Pelec(p+1,j)=eff_PV(p,j)*alphaPV*G(m)*Acv; % Function of
incidence angle, irradiance
%and PV module efficiency

hr(p+1,j)=(4*sigma*(((TPV(p,j)+273.15)+(TB(p,j)+273.15))/2)^3)/
((1/E2)+(1/E3)-1);%Linearized Equation
%hr(p+1)=((((TPV(p+1)+273.15)^4)-
((TB(p+1)+273.15)^4))*F*sigma)/((1/E2)+(1/E3)-1); %Non-
linearized Equation

Rhr(p+1,j)=1/(hr(p,j)*Acv);

Qsky(p+1,j)=(E1*sigma*((TPV(p,j)+273.15)^4)-
((Tsky(m)+273.15)^4))*Acv;

%Convective Heat Transfer Coefficients
Kin_ViscosityBM(p+1,j)=8.7e-8*Tma(p,j)+1.338e-5; %Kinematic
viscosity at Bulk Mean temperature in m^2/s Linear approximation
function

Re(p+1,j)=Vch*Dh/Kin_ViscosityBM(p,j);%Reynolds number. For
internal flow, considered laminar if <2300, turbulent >10,000
and transitional in between.

Pr(p+1,j)=1.5e-08*(Tma(p,j))^3-1.2e-06*(Tma(p,j))^2-
0.00025*Tma(p,j)+0.7362; %Prandtl number cubic approximation
function

Nu_f(p+1,j)=0.052*(Re(p,j)^0.78)*Pr(p,j)^0.4; %Nusselt number
for the front side of the cavity from L. Candanedo 2011

Nu_b(p+1,j)=1.017*(Re(p,j)^0.471)*Pr(p,j)^0.4; %Nusselt number
for the back side of the cavity L. Candanedo 2011

%
Nu_f(p+1,j)=((0.6883*(Re(p,j)^0.70)*Pr(p,j)^0.8)*exp((Lch^0.3)/(
6.45*Dh)))+(0.0124*(Re(p,j)^0.70)*Pr(p,j)^0.8); %Nusselt number
for the front side of the cavity Laminar from Yang 2014
%
%
Nu_b(p+1,j)=((50*(Re(p,j)^0.50)*Pr(p,j)^0.2)*exp((Lch^0.3)/(1.37
*Dh)))+(0.428*(Re(p,j)^0.50)*Pr(p,j)^0.2); %Nusselt number for
the front side of the cavity Laminar from Yang 2014

```

```

%
Nu_f(p+1,j)=((8.188*(Re(p,j)^0.77)*Pr(p,j)^3.85)*exp((Lch^0.2)/(
2.8*Dh)))+(0.061*(Re(p,j)^0.77)*Pr(p,j)^3.85); %Nusselt number
for the front side of the cavity Turbulent from Yang 2014
%
%
Nu_b(p+1,j)=((4.02*(Re(p,j)^1.09)*Pr(p,j)^19.3)*exp((Lch^0.2)/(1
4*Dh)))+(0.005*(Re(p,j)^1.09)*Pr(p,j)^19.3); %Nusselt number for
the front side of the cavity Turbulent from Yang 2014

k(p+1,j)=7.5e-05*Tma(p,j)+0.02364; %Thermal Conductivity k, in
W/mK Linear approximation function

hf(p+1,j)=Nu_f(p,j)*k(p,j)/Dh; %PV bottom convective heat
transfer coefficient

hb(p+1,j)=Nu_b(p,j)*k(p,j)/Dh; %Channel back surface convective
heat transfer coefficient

Rhf(p+1,j)=1/(hf(p,j)*Acv);

Rhb(p+1,j)=1/(hb(p,j)*Acv);

air_density(p+1,j)=-6.6e-08*Tma(p,j)^3+1.8e-05*Tma(p,j)^2-
0.00473*Tma(p,j)+1.292;%cubic approximation

mdot(p+1,j)=air_density(p,j)*Vch*Ach;% mass flow rate of air in
kg/s

cpair(p+1,j)=1.4e-05*Tma(p,j)^3-
0.0013*Tma(p,j)^2+0.042*Tma(p,j)+1006;%specific heat at constant
pressure in J/kgK cubic approximation

%Grashof Number-----
-----
%representing the ratio of buoyancy force to viscous force.
%Determines whether the natural convection flow is turbulent
when Gr>10^9.

Tmean(p+1,j)=(TPV(p,j)+TB(p,j))/2; %Mean temperature of the
verticle surfaces to determine the Grashof Number for Natural
Convection characteristics

Kin_ViscosityTMean(p+1,j)=8.7e-8*Tmean(p,j)+1.338e-5; %Mean
Temperature kinematic viscosity in m^2/s

```

```

Beta(p+1,j)=1/(Tmean(p,j)+273); %Volume expansion coefficient in
1/Kelvins

g=9.81;% gravitational force m/s^2

Gr(p+1,j)=(g*Beta(p,j)*(TPV(p,j)-
TB(p,j))*Hch^3)/Kin_ViscosityTMean(p,j)^2;

BuoyancyImportance(p+1)=Gr(p,j)/Re(p,j)^2; %If <1 then buoyancy
can be neglected
%-----
-----
---

ho(p+1,j)=(11.9+2.2*Vwind(m));%PV top convective heat transfer
coefficient.
% Sharples and Charlesworth give the closest results to Tingting
Yang's measured
% data

% ho(p+1,j)=(7.4+4.0*Vwind(m)); %Palyvos windward

Rho(p+1,j)=1/(ho(p,j)*Acv);

Qins(p+1,j)=(Tin-TB(p,j))/Rins;

p=p+1;

end
PelecTotalCV(j)=Pelec(51,j)+PelecTotalCV(j);% Function to sum
the Electrical Power from each control volume

QrecTotalCV(j)=QrecCV(51,j)+QrecTotalCV(j);% Function to sum the
Heat Recovered from each control volume

QskyTotalCV(j)=Qsky(51,j)+QskyTotalCV(j);% Function to sum the
Heat lost to the sky from each control volume

%Average of TPV,TB,TMA Qsky from each Control Volume for entire
channel

TBTotal(j)=TB(51,j)+TBTotal(j);

```

```

TBAvg(j)=TBTototal(j)/nCV;
TPVTototal(j)=TPV(51,j)+TPVTototal(j);
TPVAvg(j)=TPVTototal(j)/nCV;
TmaTototal(j)=Tma(51,j)+TmaTototal(j);
TmaAvg(j)=TmaTototal(j)/nCV;
GrTotal(j)=Gr(51,j)+GrTotal(j);
GrAvg(j)=GrTotal(j)/nCV;
ReTotal(j)=Re(51,j)+ReTotal(j);
ReAvg(j)=ReTotal(j)/nCV;
BuoyancyImportanceAvg(j)=GrAvg(j)/ReAvg(j)^2;
mdotTotal(j)=mdot(51,j)+mdotTotal(j);
mdotAvg(j)=mdotTotal(j)/nCV;
air_densityTotal(j)=air_density(51,j)+air_densityTotal(j);
air_densityAvg(j)=air_densityTotal(j)/nCV;
cpairTotal(j)=cpair(51,j)+cpairTotal(j);
cpairAvg(j)=cpairTotal(j)/nCV;
QrecTotal(j)=mdotAvg(j)*cpairAvg(j)*(Toutlet(51,j)-Textr(m));

end
m=m+1;
end

%Transposing of results
PelecTotalCV=PelecTotalCV';
QrecTotalCV=QrecTotalCV';
QskyTotalCV=QskyTotalCV';
TBAvg=TBAvg';
TPVAvg=TPVAvg';
TmaAvg=TmaAvg';
Toutlet=Toutlet';

```

```
GrAvg=GrAvg';  
ReAvg=ReAvg';  
BuoyancyImportanceAvg=BuoyancyImportanceAvg';  
QrecTotal=QrecTotal';  
eff_PV=eff_PV';  
TPV=TPV';
```

